SCALABLE SENSOR LOCALIZATION ALGORITHMS FOR WIRELESS SENSOR NETWORKS

by

Holly Hui Jin

A thesis submitted in conformity with the requirements
for the degree of Doctor of Philosophy
Graduate Department of Mechanical and Industrial Engineering
University of Toronto

Abstract

SCALABLE SENSOR LOCALIZATION ALGORITHMS
FOR WIRELESS SENSOR NETWORKS

Holly Hui Jin
Doctor of Philosophy
Graduate Department of Mechanical and Industrial Engineering
University of Toronto
2005

An adaptive rule-based algorithm, SpaseLoc, is described to solve localization problems for ad hoc wireless sensor networks. A large problem is solved as a sequence of very small subproblems, each of which is solved by semidefinite programming relaxation of a geometric optimization model. The subproblems are generated according to a set of sensor/anchor selection rules and a priority list. Computational results compared with existing approaches show that the SpaseLoc algorithm scales well and provides excellent positioning accuracy.

A dynamic version of the SpaseLoc method is developed for estimating moving sensors locations in a real-time environment. The method uses dynamic distance measurement updates among sensors, and utilizes SpaseLoc for static sensor localization. Further computational results are presented, along with an application to bus transit systems.

Ways to deploy sensor localization algorithms in clustered distributed environments are also studied, permitting application to arbitrarily large networks. In addition, we extend the algorithm to solving sensor localizations in 3D space. A preprocessor is developed to enable SpaseLoc for localization of networks without absolute position information.

Joint research conducted in the Dept of Management Science and Engineering, Stanford University.

To my parents

Acknowledgements

I would like to express my greatest appreciation towards my two thesis advisors, Prof. Michael Carter and Prof. Michael Saunders, for their continuous guidance, support and friendship.

My sincere gratitude goes to Prof. Carter for accepting me into the PhD program and for keeping constant faith in me. No matter what new project I start up, he is always supportive and remarkably perceptive in advising in the right direction and correcting the vital details. Without his continuous encouragement, I would still be in my PhD dreams. He is a great mentor and I learned so much from him through this long academic journey.

I am truly blessed to have come to Stanford University, where Prof. Saunders welcomed me with open arms and my life started on a whole new course. I learn from Prof. Saunders that the world is not just about optimization, but more about true kindness. He is the epitome of professionalism and perfectionism. I could not have finished my thesis in time without his untiring help in making every sentence concise and correct. I will always be looking up to the high standard he sets.

I would like to thank Prof. Yinyu Ye for inspiring me to the exciting field of sensor network research. I am very fortunate to be able to learn from him and his class. His work with Pratik Biswas was a vital starting point for my thesis. I am grateful to Dr. Steve Benson for his advice on using the DSDP5.0 solver. I also appreciate Prof. Kenneth Holmström's help in fine-tuning the Matlab implementation of some portions of SpaseLoc.

My thesis committee members, Profs. Daniel Francis, Scott Rogers, and Henry Wolkowicz, provided invaluable feedback and advice on my thesis. I really appreciate their time and help.

Thanks to the University of Toronto for making my PhD studies there possible with the prestigious Connaught scholarships. Its outstanding learning environment helped lay a solid academic foundation. I must also thank Stanford University for two years of my PhD studies there. Its invigorating environment enabled my mind to broaden and my research to thrive.

I am grateful to Robert Bosch Corporation's support of my research at Stanford University. I feel very fortunate for the opportunity to discuss potential applications of our sensor localization algorithms with the talented Bosch team, Sharmila Ravula, Bhaskar Srinivasan, Lakshmi Venkatraman, Hauke Schmidt, and Karsten Funk. They provided inspiration and background for our algorithms to be practically useful.

I am indebted to my husband Neil for his encouragement and understanding when I devoted too many evenings and weekends to my thesis study, and he had to look after our two beautiful children Danlin and Hansen while carrying a full time workload himself. Thank you so much Neil for all the mornings when you took the kids quietly out of the house in the weekends so that I could sleep in a bit after late night studying at school. Thank you Danlin and Hansen for many nights not be able to kiss you goodnight and you still give me so much love and joy.

Finally, I give heartfelt thanks to my dearest parents, my sister and my two brothers for their unyielding love and support. They provide a constant source of motivation in my life.

Contents

List of Tables

List of Figures

Chapter 1

Introduction

Ad hoc wireless sensor networks may contain hundreds or even tens of thousands of inexpensive devices (sensors) that can communicate with their neighbors within a limited radio range. By relaying information to each other, they can transmit signals to a command post anywhere within the network. They have many practical uses in areas such as military applications [27], environment or industrial control and monitoring [11, 13], wildlife monitoring [45], and security monitoring [27]. For example, Southern California Edison's Nuclear Generating Station in San Onofre, California has deployed wireless mesh networked sensors from Dust Networks to obtain real-time trend data [13]. These data are used to predict which motors are about to fail, so they could be preemptively rebuilt or replaced during scheduled maintenance periods. The use of a wireless sensor network saves the station money and avoids potential machine shutdown. Implementation of a sensor localization algorithm would provide a service that eliminates the need to record every sensor's location and its associated ID number in the network.

Wireless sensor networks are potentially important enablers for many other advanced applications. A huge variety of applications lie ahead. By 2008, there could be 100 million wireless sensors in use, up from about 200,000 in 2005, according to the market-research company Harbor Research. The worldwide market for wireless sensors, it says, will grow from $100 million in 2005 to more than $1 billion by 2009 [36]. This is motivating great effort in academia and industry to explore effective ways to build sensor networks with feature-rich services [19].

One of the important inputs these services build upon is the exact locations of all sensors in the network. The need for *sensor localization* arises because accurate positions are known for only some of the sensors (which are called *anchors*). If the networks are to achieve their purpose, the positions of the remaining sensors must be determined. One approach to localizing these sensors with unknown positions is to use known anchor locations and distance measurements that neighboring sensors and anchors obtain among themselves. The mathematical problem is to *estimate* sensor positions using a sparse data matrix of noisy distance measurements. This leads to a large, non-convex, constrained optimization problem. Large networks may contain many thousands of sensors, whose locations should be determined accurately and quickly.

One way to localize a sensor is to rely on the satellite-based global positioning system (GPS) [9]. This may be important for at least some of the sensors in a network. (They would be anchors.) However, GPS suffers the following main drawbacks:

- GPS based system is typically more expensive to deploy because devices using it are more costly.
- GPS can be less accurate. Without the use of specialized equipment, normal GPS can pin point subject locations with 5 to 10 meter accuracy in outdoor environment.
- GPS is not applicable for indoor localization since GPS requires line of sight.
- Because of satellite communication delay, use of GPS might not be an effective method for real-time tracking of moving sensors.

Existing non-GPS-based localization methods have been applicable for only moderate-sized networks. The primary aim of this thesis is to develop non-GPS-based localization algorithms that are effective for the large-scale networks that are likely to be deployed in the coming decades, and to achieve the efficiency needed for real-time environments.

In this chapter we first describe the sensor localization problem and introduce relevant notation. A review of related research work follows. Our new solution techniques are summarized next, and finally the thesis outline is given.

1.1 Problem Definition

Sensor localization in ad hoc wireless sensor network aims to find the locations of all sensors in the network, given pair-wise distance measurements among some of the sensors, and known locations of some of the sensors. The sensors with known locations are called *anchors*. From now on, *sensor* generally means *unpositioned sensor*, excluding anchors. A *node* is any sensor or anchor in the network.

We use a constrained optimization approach to estimate the sensors' locations. The following input, output, and objectives are considered.

$$\underbrace{1 \quad \le \quad i \quad < \quad j \quad \le \quad s}_{s \text{ sensors}} \Big| \underbrace{s{+}1 \quad \le \quad k \quad \le \quad n}_{m \text{ anchors}}$$

Figure 1.1: Indexing of sensors and anchors.

Input

Total points: n, the total number of nodes in the network.

Unknown points: s sensors, whose locations $x_i \in \mathcal{R}^2$, $i = 1, \ldots, s$ are to be determined. (We assume the points are on a plane here, but the approach is extended to three dimensions in Chapter 6.)

Known points: m anchors, whose locations $a_k \in \mathcal{R}^2$, $k = s{+}1, \ldots, n$ are known. (Note that we put anchors at the end of the total points' list without loss of generality, and that $n = s + m$. Index k is specific for indexing anchors. Refer to Figure 1.1 for nodes indexing.)

Known distance measurements: The readings of certain ranging devices for estimating the distance between two points. $\widehat{d_{ij}}$ is the distance measurement between two sensors x_i and x_j $(i < j \le s)$, and $\widehat{d_{ik}}$ is the distance measurement between some sensor x_i and anchor a_k $(i \le s < k)$. The distance measurements are constant data and generally have errors.

Output

Locations: Estimated locations x_i for s sensors.

Objectives

Accuracy: Minimal errors in the estimated sensor positions.

Speed: Fast enough for real-time applications (e.g., networks with moving sensors).

Scalability: Suitable for large-scale deployment (with tens of thousands of nodes).

1.2 Notation

The Euclidean distance between two vectors v and w is defined to be $\|v - w\|$, where $\|\cdot\|$ always means the 2-norm. Nodes are said to be *connected* if the associated measurements

$\widehat{d}_{ij}$ or $\widehat{d}_{ik}$ exist. The remaining elements of $\widehat{d}$ are zero. If a measurement does exist between node i and j but it is zero (i and j are at the same spot), we do not set $\widehat{d}_{ij}$ to zero: we set it to machine precision ϵ instead to distinguish from the case of $\widehat{d}_{ij} = 0$ when two nodes' distance is beyond the sensor device's measuring range.

1.3 Related Research Work

Sensor localization in ad hoc wireless network has been a booming research area recently. Hightower and Boriello [19] give an extensive review of the area and available methods. There are many ways to solve the localization problem [2, 7, 12, 15, 20, 33, 37, 38, 39, 40], with two main ones based on triangulation and optimization.

Triangulation methods estimate node positions based on distance measurements between neighboring nodes, and some algorithms use iterative steps to localize all sensors.

Early work using optimization techniques is reported by Doherty et al. [12]. Ideally the Euclidean distance between neighboring nodes should be fitted in some near-equality sense to the distance measurements:

$$\|x_i - x_j\| \approx \widehat{d}_{ij} \quad \text{and} \quad \|x_i - a_k\| \approx \widehat{d}_{ik}. \tag{1.1}$$

Doherty et al. formulate a convex optimization model by treating the constraints as $\|x_i - x_j\| \le \widehat{d}_{ij}$ and $\|x_i - a_k\| \le \widehat{d}_{ik}$, and by including certain other convex constraints. This formulation takes advantage of available optimization algorithms, including those for convex optimization. However, the method needs sufficient anchors to be positioned on the boundary of the localization area for it to work effectively.

Biswas and Ye [4] work with the near-equality constraints (1.1), and most importantly they introduced a semidefinite programming (SDP) relaxation method in order to retain the benefits of convex optimization. They report that their method yields more accuracy under all conditions than the approach in [12].

The SDP relaxation approach can solve small problems effectively. The paper reports a few seconds of laptop execution time for a 50-node localization problem. However, the number of constraints in the SDP model is $O(n^2)$, where n is the number of nodes in the network. Even a few hundred-node problem leads to excessive memory and computation time by available SDP solvers such as DSDP (Benson, Ye, and Zhang [3]) and SeDuMi (Sturm [44]). These solvers are effective for SDP problems with dimension and number of constraints up to a few thousand.

Tseng [46] has presented a second-order cone programming (SOCP) relaxation model that permits solution for problem sizes up to a few thousand using available SOCP solvers. However, the additional relaxation of the original model usually generates larger error rates, and the run-times are high. The author reports CPU times of 330 seconds for 1000 nodes and 3 hours for 2000 nodes using SeDuMi 1.05 [44] and Matlab 6.1 on a Linux PC.

Biswas and Ye [5] propose a decomposition scheme to overcome the scalability issue with SDP solvers. The anchors in the network are first partitioned into many clusters according to their physical positions, and sensors are assigned to these clusters if they have a direct connection to one of the anchors. Each cluster formulates a subproblem, and the subproblems are solved *independently* on each cluster using the SDP relaxation of [4]. The paper reports results for randomly generated sensor networks of 4000 sensors partitioned into 100 clusters strictly according to their geographic locations. Sensors with distance connections to more than one cluster are included in multiple clusters. The final estimation of their locations is determined by the cluster that gives the least estimated errors. An execution time of about 4 minutes on a 1.2GHz Pentium laptop is reported for this sized problem. The time could be reduced by using multiple CPUs.

Although Biswas and Ye [5] make large-scale sensor network localization possible by decomposing the large-scale problem geographically, there are shortfalls in this approach that may prevent its large-scale deployment. First of all, for any real deployment of a wireless sensor network, localization algorithms should run in real-time, where minutes could be too long and multiple CPUs could be too expensive. Secondly, since the partition is strictly based on geographic locations, sensors near the border lines of a cluster may not be positioned as accurately as they would be using other approaches. This is due to the fact that each cluster may include only partial connection information for the bordering sensors if the bordering sensors have connections with multiple clusters. Furthermore, the SDP relaxation approach that their decomposition method is based on provides poor accuracy on certain topologies with low anchor density or small radio range for even medium-size networks (refer to section 3.3.2).

1.4 Solution Techniques

A basic tool that we have developed during this research is a rule-based iterative algorithm named SpaseLoc (sub-problem algorithm for sensor localization). It is effective for networks involving tens of thousands of sensors and beyond.

To solve a large localization problem (defined as the *full_problem*), SpaseLoc proceeds iteratively by estimating only a portion of the total sensors' locations at each iteration.

Some anchors and sensors are chosen according to a set of rules. They form a sensor localization *subproblem* that can be treated similarly to the basic SDP formulation of Biswas and Ye [4]. The solution from the subproblem is fed back to the *full_problem* and the algorithm iterates again until all sensors are localized.

Computational results show that SpaseLoc can solve small or large problems with excellent accuracy and scalability. It is capable of localizing 4000 nodes with great accuracy in under 20 seconds, and 10000 nodes in about a minute on a 2.4GHz laptop.

With the SpaseLoc tool in hand, we are able to develop a dynamic sensor localization algorithm to track hundreds or thousands of sensors moving within a larger network. We also develop distributed methods for deploying SpaseLoc in arbitrarily large networks. A 3D version of SpaseLoc extends its utility further. In addition, a preprocessor is designed to allow SpaseLoc to be applied to sensor localizations in anchorless networks.

1.5 Thesis Outline

The basic sensor localization concept and current methods are described in the first chapter. Chapter 2 introduces the semidefinite programming model that our SpaseLoc subproblem is based on. We present our sensor localization algorithm SpaseLoc and computational results in Chapter 3.

In Chapter 4, a dynamic version of SpaseLoc is developed for estimating moving sensors' locations in a real-time environment. The method uses dynamic distance measurement updates among sensors, and utilizes SpaseLoc for static sensor localization. Computational results for the algorithm are presented, along with an application to bus transit systems.

Chapter 5 describes ways to deploy sensor localization algorithms in clustered distributed environments for true scalability.

In Chapter 6, we extend the algorithm to solving sensor localizations in 3D space.

In order for SpaseLoc to apply to networks containing no anchors, a preprocessor is developed in Chapter 7 to obtain relative positions of all sensors in the network.

The last chapter summarizes, and points out future promising research areas.

Chapter 2

The Subproblem SDP Model

This chapter reviews the quadratic programming formulation of the sensor localization problem, and the SDP relaxation model of Biswas and Ye [4] on which the SpaseLoc subproblem is based. Error analysis is also reviewed here as a reference for later chapters.

2.1 Euclidean Distance Model

Consider a network of sensors and anchors labeled as in Figure 1.1. For any point in the network, there could be three types of distance measurements. Since we generally do not need the distance information between two anchor points, we exclude this type of measurement from now on.

The other types of distance measurements are the two we need for the localization model. First is the distance measurement between two sensors (i and j) with unknown positions; second is the distance measurement between a sensor (i) and an anchor (k) with known position. Corresponding to these two types of distances, we define sets N_1, $\overline{N}_1$, N_2 and $\overline{N}_2$ as follows:

- N_1 includes pairwise sensors (i, j) if $i < j$ and there exists a distance measurement $\widehat{d}_{ij}$:
$$N_1 = \{(i, j) \text{ with known } \widehat{d}_{ij} \text{ and } i < j\}.$$
- $\overline{N}_1$ includes pairwise sensors (i, j) with unknown measurement $\widehat{d}_{ij}$ and $i < j$:
$$\overline{N}_1 = \{(i, j) \text{ with unknown } \widehat{d}_{ij} \text{ and } i < j\}.$$

- N_2 includes pairs of sensor i and anchor k if there exists a measurement $\widehat{d}_{ik}$:
$$N_2 = \{(i,k) \text{ with known } \widehat{d}_{ik}\}.$$

- $\overline{N}_2$ includes pairs of sensor i and anchor k with unknown measurement $\widehat{d}_{ik}$:
$$\overline{N}_2 = \{(i,k) \text{ with unknown } \widehat{d}_{ik}\}.$$

The full set of nodes and pair-wise distance measurements form a graph $G = \{V, E\}$, where $V = \{1, 2, \ldots, s, s+1, \ldots, n\}$ and $E = N_1 \cup N_2$.

Introduce α_{ij} to be the difference between the measured squared distance $(\widehat{d}_{ij})^2$ and the squared Euclidean distance $\|x_i - x_j\|^2$ from sensor i to sensor j. Also, let α_{ik} be the difference between the measured squared distance $(\widehat{d}_{ik})^2$ and the squared Euclidean distance $\|x_i - a_k\|^2$ from sensor i to anchor k. Intuitively, we seek a solution for which the magnitude of these differences is small.

Lower bounds r_{ij} or r_{ik} are imposed if $(i,j) \in \overline{N}_1$ or if $(i,k) \in \overline{N}_2$. Typically each r_{ij} or r_{ik} value is the radio range (also known as *radius*) within which the associated sensors can detect each other.

Biswas and Ye [4] formulate the sensor localization problem as minimizing the ℓ_1 norm of the squared-distance errors α_{ij} and α_{ik} subject to mixed equality and inequality constraints:

$$\begin{array}{lllll}
\underset{x_i, x_j, \alpha_{ij}, \alpha_{ik}}{\text{minimize}} & \displaystyle\sum_{(i,j)\in N_1} |\alpha_{ij}| + \sum_{(i,k)\in N_2} |\alpha_{ik}| & & & \\
\text{subject to} & \|x_i - x_j\|^2 - \alpha_{ij} & = & (\widehat{d}_{ij})^2, & \forall\ (i,j) \in N_1, \\
& \|x_i - a_k\|^2 - \alpha_{ik} & = & (\widehat{d}_{ik})^2, & \forall\ (i,k) \in N_2, \\
& \|x_i - x_j\|^2 & \geq & r_{ij}^2, & \forall\ (i,j) \in \overline{N}_1, \\
& \|x_i - a_k\|^2 & \geq & r_{ik}^2, & \forall\ (i,k) \in \overline{N}_2, \\
& x_i,\ x_j \in \mathcal{R}^2, & & \alpha_{ij},\ \alpha_{ik} \in \mathcal{R}, & \\
& i, j = 1, \ldots, s, & & k = s+1, \ldots, n. &
\end{array} \tag{2.1}$$

The above model is a non-convex constrained optimization problem. As yet there is no effective solution method. In the following sections, we review Biswas and Ye's [4] relaxation method for solving this problem approximately.

2.2 The Euclidean Distance Model in Matrix Form

The distance model (2.1) is reformulated into (2.2) (refer to Biswas and Ye [4]) by introducing matrix variables as follows:

$$\begin{array}{lrcll}
\text{minimize} & \displaystyle\sum_{(i,j)\in N_1} (\alpha_{ij}^+ + \alpha_{ij}^-) \ + \sum_{(i,k)\in N_2} (\alpha_{ik}^+ + \alpha_{ik}^-) & & & \\
\text{subject to} & e_{ij}^T\, Y\, e_{ij} - \alpha_{ij}^+ + \alpha_{ij}^- & = & (\widehat{d}_{ij})^2, & \forall\ (i,j) \in N_1, \\
& \begin{pmatrix} e_i \\ -a_k \end{pmatrix}^T \begin{pmatrix} Y & X^T \\ X & I \end{pmatrix} \begin{pmatrix} e_i \\ -a_k \end{pmatrix} - \alpha_{ik}^+ + \alpha_{ik}^- & = & (\widehat{d}_{ik})^2, & \forall\ (i,k) \in N_2, \\
& e_{ij}^T\, Y\, e_{ij} & \geq & r_{ij}^2, & \forall\ (i,j) \in \overline{N}_1, \\
& \begin{pmatrix} e_i \\ -a_k \end{pmatrix}^T \begin{pmatrix} Y & X^T \\ X & I \end{pmatrix} \begin{pmatrix} e_i \\ -a_k \end{pmatrix} & \geq & r_{ik}^2, & \forall\ (i,k) \in \overline{N}_2, \\
& Y & = & X^T X, & \\
& \alpha_{ij}^+,\ \alpha_{ij}^-,\ \alpha_{ik}^+,\ \alpha_{ik}^- & \geq & 0, & \\
& i,j = 1,\ldots,s, & & k = s+1,\ldots,n, &
\end{array} \qquad (2.2)$$

where

- $X = (x_1\ x_2\ \ldots\ x_s)$ is a $2 \times s$ matrix to be determined;
- e_{ij} is a zero column vector except for 1 in position i and -1 in position j, so that
$$\|x_i - x_j\|^2 \ = \ e_{ij}^T\, X^T X\, e_{ij};$$
- e_i is a zero column vector except for 1 in position i, so that
$$\|x_i - a_k\|^2 \ = \ \begin{pmatrix} e_i \\ -a_k \end{pmatrix}^T \begin{pmatrix} X & I \end{pmatrix}^T \begin{pmatrix} X & I \end{pmatrix} \begin{pmatrix} e_i \\ -a_k \end{pmatrix};$$
- Y is defined to be $X^T X$;
- The substitutions $\alpha_{ij} = \alpha_{ij}^+ - \alpha_{ij}^-$ and $\alpha_{ik} = \alpha_{ik}^+ - \alpha_{ik}^-$ are made to deal with $|\alpha_{ij}|$ and $|\alpha_{ik}|$ in the normal way.

2.3 The SDP Relaxation Model

The approach of Biswas and Ye [4] is to relax the constraint $Y = X^T X$ to be $Y \succeq X^T X$, for which an equivalent matrix inequality is (Boyd et al. [6])

$$Z_I \equiv \begin{pmatrix} Y & X^T \\ X & I \end{pmatrix} \succeq 0. \tag{2.3}$$

With the definitions

$$A_I = \begin{pmatrix} \mathbf{0} & \mathbf{0} & \mathbf{0} \\ 1 & 0 & 1 \\ 0 & 1 & 1 \end{pmatrix}, \qquad b_I = \begin{pmatrix} 1 \\ 1 \\ 2 \end{pmatrix},$$

where $\mathbf{0}$ in A_I is a zero column vector of dimension s, problem (2.2) is relaxed to a linear SDP:

$$\begin{array}{lrcll}
\text{minimize} & \displaystyle\sum_{(i,j)\in N_1} (\alpha_{ij}^+ + \alpha_{ij}^-) + \sum_{(i,k)\in N_2} (\alpha_{ik}^+ + \alpha_{ik}^-) & & & \\
\text{subject to} & \operatorname{diag}(A_I^T\ Z\ A_I) & = & b_I, & \\
& \begin{pmatrix} e_{ij} \\ \mathbf{0} \end{pmatrix}^T Z \begin{pmatrix} e_{ij} \\ \mathbf{0} \end{pmatrix} - \alpha_{ij}^+ + \alpha_{ij}^- & = & (\widehat{d}_{ij})^2 & \forall\ (i,j) \in N_1, \\
& \begin{pmatrix} e_i \\ -a_k \end{pmatrix}^T Z \begin{pmatrix} e_i \\ -a_k \end{pmatrix} - \alpha_{ik}^+ + \alpha_{ik}^- & = & (\widehat{d}_{ik})^2 & \forall\ (i,k) \in N_2, \\
& \begin{pmatrix} e_{ij} \\ \mathbf{0} \end{pmatrix}^T Z \begin{pmatrix} e_{ij} \\ \mathbf{0} \end{pmatrix} & \geq & r_{ij}^2 & \forall\ (i,j) \in \overline{N}_1, \\
& \begin{pmatrix} e_i \\ -a_k \end{pmatrix}^T Z \begin{pmatrix} e_i \\ -a_k \end{pmatrix} & \geq & r_{ik}^2 & \forall\ (i,k) \in \overline{N}_2, \\
& Z \succeq 0, \qquad \alpha_{ij}^+,\ \alpha_{ij}^-,\ \alpha_{ik}^+,\ \alpha_{ik}^- & \geq & 0, & \\
& i,j = 1,\dots,s, & & k = s+1,\dots,n, &
\end{array} \tag{2.4}$$

where the constraint $\operatorname{diag}(A_I^T Z A_I) = b_I$ ensures that the matrix variable Z's lower right corner is a 2-dimensional identity matrix I, so that Z takes the form of Z_I in (2.3).

Initially, Biswas and Ye [5, 4] omit the $\geq$ inequalities involving r_{ij} and r_{ik}, and solve the resulting problem to obtain an initial solution Z_1. (The inequality constraints increase the problem size dramatically, and Z_1 is likely to satisfy most of them.) They then adopt an "iterative active-constraint generation technique" in which inequalities violated by Z_k are added to the problem and the resulting SDP is solved to give Z_{k+1} ($k = 1, 2, \ldots$). The process usually terminates before all constraints are included. Further study of this approach is presented in section 3.3.1.

2.4 SDP Model Analysis

Let $\bar{Z} = \begin{pmatrix} \bar{Y} & \bar{X}^T \\ \bar{X} & I \end{pmatrix}$ be a feasible solution of the relaxed SDP (2.4). Biswas and Ye [4] give conditions under which $\bar{X}$ and $\bar{Y}$ solve problem (2.2) exactly, when exact distance measurements are assumed:

- $\bar{Z}$ is the unique optimal solution of (2.4), including all inequality constraints.
- In (2.4), there are $2n + n(n+1)/2$ exact pair-wise distance measurements.

These conditions ensure that $\bar{Y} = \bar{X}^T\bar{X}$. In practice, distance measurements have noise and we only know that the SDP solution satisfies $\bar{Y} - \bar{X}^T\bar{X} \succeq 0$. This inequality can be used for error analysis of the position estimation provided by the relaxation. For example, $\text{trace}(\bar{Y} - \bar{X}^T\bar{X}) = \sum \tau_i$, where

$$\tau_i \equiv \bar{Y}_{ii} - \|\bar{x}_i\|^2 \geq 0, \tag{2.5}$$

is a measure of deviation of the SDP solution from the desired constraint $Y = X^TX$ (ignoring off-diagonal elements). The individual trace τ_i can be used to evaluate the position estimation $\bar{x}_i$ for sensor i. In particular, we interpret a smaller τ_i to mean higher accuracy in the estimated position x_i. Further explanation is given in [4].

Chapter 3

SpaseLoc: A Scalable Localization Algorithm

When the number of nodes in (2.4) is large, applying a general SDP solver such as DSDP5.0 [3] or SeDuMi [44] would not scale well. In this chapter, we present a sequential subproblem approach named SpaseLoc to solve the full localization problem iteratively.

We first explain in detail how SpaseLoc works, followed by an example to illustrate the steps of SpaseLoc. The last section presents computational results.

3.1 Adaptive Subproblem Approach

We call the overall sensor localization problem including all sensors and anchors the *full_problem*. At each iteration, SpaseLoc selects from the *full_problem* a subset of the unpositioned sensors and a subset of the anchors to form a localization *subproblem*. We call the selected sensors in the subproblem *subsensors*, and the selected anchors in the subproblem *subanchors*, These subsensors and subanchors, together with their known distance measurements and known anchors' locations, form a sub SDP relaxation model to be solved using the same formulation as in (2.4).

In our adaptive approach, the subanchors and subsensors for each subproblem are chosen dynamically according to rule sets. (Rather than using predefined data, every new iteration's subproblem generation is based on the previous iteration's results.) The resulting SDP subproblems are of varying but limited size. Currently they are solved by Benson, Ye, and Zhang's SDP solver DSDP5.0 [3].

SpaseLoc is a *greedy algorithm* in the sense that each subproblem determines the final estimate of the associated sensor positions.

3.1.1 The SpaseLoc Algorithm

The main steps of SpaseLoc are listed below, followed by explanations of the steps and definitions of new terms used therein.

A0 Set *subproblem_size*.

A1 Subproblem creation: Select subsensors and subanchors to be included in the subproblem.

A2 Formulate SDP relaxation model (2.4) based on the chosen subsensors and subanchors, together with the known distances among them and the subanchors' known positions.

A3 Call SDP solver to obtain optimal solution for the subsensors' positions.

A4 Classify positioned subsensors according to their τ_i value.

A5 If all sensors in the network become positioned or are determined to be outliers, go to step A6. Otherwise, return to step A1 for the next iteration.

A6 Output all sensor locations and report outliers if any. Stop.

In step A0, *subproblem_size* specifies a limit on the number of unpositioned sensors to be included in each subproblem. It can range from 1 to a upper limit value that is potentially solvable by the SDP solver. In our experiments, the upper limit is 150. The most effective *subproblem_size* seems to change with the *full_problem* size, the model parameters such as *radius*, and the SDP solver used. We perform an approximate line-search to find *subproblem_size* that corresponds to the minimum time, since empirically the total execution time with all other parameters fixed is essentially a convex function of *subproblem_size*.

For example, when *full_problem* size is 10000 with 100 anchors, *radius* 0.02068, and no noise, *subproblem_size* 5 seems to give the best execution time with the DSDP5.0 solver (refer to Figure 3.1). The search time for *subproblem_size* is not included as part of the SpaseLoc execution time.

Step A1 involves choosing a subset of unpositioned sensors (no more than *subproblem_size*) and an associated subset of nodes with known positions. The latter can include a subset of the original anchors and/or a subset of sensors already positioned by a previous subproblem (we define them as *acting anchors*). The rules for choosing subsensors and subanchors in this iteration are discussed in sections 3.1.3–3.1.4.

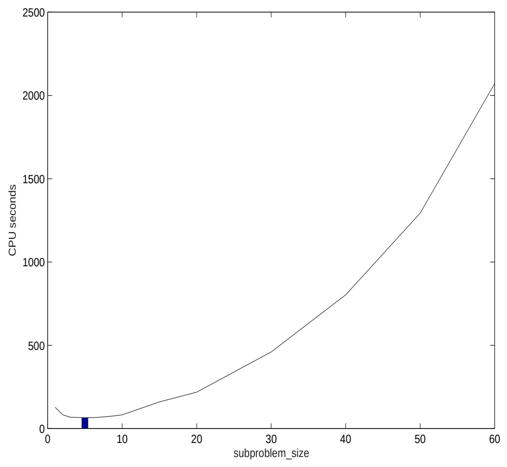

Figure 3.1: SpaseLoc execution time as a function of *subproblem_size*: total nodes = 10000, anchors = 100, *radius* = 0.02068.

In step A4, the error in sensor i's positioning is estimated by its individual trace τ_i as discussed in section 2.4. Subsensors whose τ_i value is within a given tolerance τ are labeled as positioned and treated as acting anchors for the next iteration, whereas subsensors whose positioning error is higher than the tolerance are also labeled as positioned but are not used as acting anchors in later iterations. These new acting anchors are labeled with different acting levels as explained in section 3.1.3. The value of τ has an impact on the localization accuracy. Bigger values allow more positioned sensors to be acting anchors, but with possibly greater transitive errors. Smaller values may increase the estimation accuracy for some of the sensors, but could lead to more outliers. A rule of thumb is to use a small τ for networks with high anchor density to achieve potentially more accuracy, and a bigger τ for networks with low anchor density to avoid potential outliers.

In step A5, an unpositioned sensor is called an *outlier* when it does not have any distance information for the algorithm to decide its location. If a sensor has no connection to any anchors, it is classified as an outlier. In addition, if a connected cluster of sensors has no connection to any anchors, then all sensors in the cluster will be outliers.

The next sections explain the subproblem creation procedure used by step A1 above. Section 3.1.2 lists steps S1–S9 of the creation procedure itself. Section 3.1.3 presents rules RS1–RS4 for subsensor selection in step S5. Section 3.1.4 presents rules RA1–RA3 for subanchor selection in step S8. Section 3.1.5 illustrates the method for independent subanchor selection used in rules RA2–RA3. Sections 3.1.6–3.1.7 discuss the routines used in step S7 to localize sensors that have less than 3 connected anchors.

3.1.2 Subproblem Creation Procedure

As explained, *subproblem_size* is a predetermined parameter that represents the maximum number of unpositioned sensors that can be selected as subsensors in a subproblem. When there are more than *subproblem_size* unpositioned sensors, we have a choice to make among them.

The subproblem creation procedure makes sure that the choice of subsensors is based first on the number of connected anchors they have, and second on the type of connected anchors such as original anchors and different levels of acting anchors as defined by a priority list (section 3.1.3), and the choice of subanchors is based on a set of rules (section 3.1.4). The main steps are listed below, followed by explanations of the steps and definitions of new terms used.

S1 Specify *MaxAnchorReq*.

S2 Initialize *AnchorReq* = *MaxAnchorReq*.

S3 Loop through unpositioned sensors, finding all that are connected to at least *AnchorReq* anchors. If *AnchorReq* ≥ 3, determine if there are 3 *independent* subanchors; if not, go to next sensor.[1] Enter each found sensor into a *candidate subsensor list*, and enter its connected anchors into a corresponding *candidate subanchor list*. Each sensor in the candidate subsensor list has its own candidate subanchor list (so there are as many candidate subanchor lists as the number of sensors in the candidate subsensor list). Let *sub_s_candidate* be the length of the candidate subsensor list.

S4 If *sub_s_candidate* = *subproblem_size*, the candidate subsensor list becomes the chosen subsensors list. Go to step S8.

S5 If *sub_s_candidate* > *subproblem_size*, the choice of subsensors is further based on subsensor selection rules RS1–RS4 described in section 3.1.3. After exactly *subproblem_size* subsensors are selected from the candidate list according these rules, go to step S8.

S6 If *sub_s_candidate* < *subproblem_size* and the candidate list is not null, go to step S8.

[1]See section 3.1.5 for dependency definition and independent anchor selection.

S7 Now $sub\_s\_candidate = 0$. Reduce *AnchorReq* by 1.

If $AnchorReq \geq 3$, go to step S3 for another round of subproblem creation.

If $AnchorReq = 2$, apply the procedure in section 3.1.6 then go to step S3.

If $AnchorReq = 1$, apply the procedure in section 3.1.7 then go to step S3.

Otherwise, $AnchorReq = 0$ and $sub\_s\_candidate = 0$ indicates that there are still unpositioned sensors left that are not connected to any positioned nodes. We classify them as outliers and exit this procedure to continue at step A6 of section 3.1.1.

S8 Now that we have a subsensor list and the candidate subanchor lists, choose subanchors using selection rules RA1–RA3 presented in section 3.1.4.

S9 The subsensors and subanchors are selected and the subproblem creation routine finishes here. Continue at step A2 in section 3.1.1.

In step S1, *MaxAnchorReq* determines the initial (maximum) value of *AnchorReq*. It is useful for scalability when connectivity is dense. A smaller *MaxAnchorReq* would generally cause fewer subanchors to be included in the subproblem, thus reducing the number of distance constraints in each SDP subproblem and hence reducing execution time for each iteration. For instance, under ideal conditions (where there is no noise), even if a sensor has 10 distance measurements to 10 anchors, we don't need to include all 10 anchors because we can use 3 to localize that sensor accurately.

In the presence of noise, a bigger *MaxAnchorReq* should reduce the average estimation error. For example, if there is a large distance measurement error from one particular anchor, since *MaxAnchorReq* anchors are all taken into consideration for deciding the sensor's actual position, the large error would be averaged out. Another consideration for setting *MaxAnchorReq* is the trade-off between estimation accuracy and execution speed. If we are in a static environment and would like to have sensor positioning as accurate as possible under noise conditions, we might choose a large *MaxAnchorReq*. However, in a real-time environment involving moving sensors, where speed might take priority, we would consider a smaller *MaxAnchorReq*.

In step S2, *AnchorReq* is a dynamic parameter that may decrease in later steps.

In step S6, the subproblem will contain less than *subproblem_size* subsensors, and this is perfectly acceptable. The alternative is to reduce *AnchorReq* by 1 and find more subsensor candidates that have fewer distance connections. However, this approach might reduce the accuracy of the algorithm, because we do want to localize the subsensors as accurately as possible as the iteration progresses, and the newly localized subsensors could be further used as acting anchors for the next iteration.

In step S7, *AnchorReq* is iteratively reduced by 1 from *MaxAnchorReq* to 0 eventually. This approach allows sensors with at least *AnchorReq* connections to anchors to be positioned before sensors with fewer connections to anchors. As we know, under no-noise conditions, a sensor's position can be uniquely determined by at least 3 independent distance measurements to 3 anchors. If a sensor has only 2 distance measurements to 2 anchors, there are two possible locations; and if there is only 1 distance measurement to an anchor, the sensor can be anywhere on a circle. In this situation, we use heuristic subroutines described in sections 3.1.6–3.1.7 to include the sensor's anchors' connected neighboring nodes in the subproblem in order to improve the estimation accuracy.

3.1.3 Subsensor Selection Priority List

In step S5, when the number of sensors in the candidate subsensor list is bigger than *subproblem_size*, the choice of subsensors is further based on the types of anchors each sensor is connected to.

First, we introduce the concept of *sensor priority.* We assign a priority to each sensor in the candidate subsensor list. A sensor with a smaller priority value is selected to be localized before one with a bigger priority value. A sensor's priority is based on the types of anchors the sensor is directly connected to. Next, in order to define different types of anchors, we introduce the concept of *anchor acting levels.* All anchors including acting anchors are assigned certain acting levels. Original anchors are always set to acting level 1. Every acting anchor is set to an acting level after it has been localized as a sensor. The acting level depends on the priority of the sensor that becomes this acting anchor. Essentially, acting anchors are set with acting levels depending on the levels of the anchors that localized them.

The priority rules for selecting subsensors from a candidate subsensor list are as follows:

RS1 When *AnchorReq* ≥ 3 and a sensor has at least 3 connected anchors that are independent, the sensor's priority depends on the lowest acting level among all the connected anchors and the number of anchors in this level. The lower the acting level and the larger the number of anchors in that level, the higher the sensor's priority.

RS2 If the sensor has 3 connected anchors that are dependent, it is ranked with the same priority as when the sensor is connected to only 2 anchors.

Table 3.1: An example: priority list when *MaxAnchorReq*=3.

Priority value	Level 1 anchor	Level 2 anchor	Level 3–7 anchor	Level 8–10 anchor	Resulting level
1	≥ 3	any	any	any	2
2	$= 2$	$total \geq 1$		any	3
3	$= 1$	$total \geq 2$		any	4
4	0	≥ 3	any	any	5
5	0	$= 2$	$total \geq 1$	any	6
6	0	≤ 1	$total \geq 2$ if level 2 anchor = 1, else $total \geq 3$	any	7
7	$total \geq 3$, at least one of the 3 anchors is acting level 8 or 9, or 10				8
8	$total = 2$				9
9	$total = 1$				10

RS3 Sensors with 2 anchor connections are ranked with equal priority, independent of the acting levels of the 2 connected anchors. (This can be easily expanded to be more granular according to the connected anchors' acting levels.) Sensors in this category are assigned lower priority than any sensors that have at least 3 independent anchor connections.

RS4 Sensors with 1 anchor connection are ranked with equal priority, independent of the acting level of the connected anchor. (Again, this can be more granular according to the connected anchor's acting level.) Sensors in this category are assigned lower priority than any sensors that have at least 2 anchor connections.

Table 3.1 illustrates the priority list for an example where *MaxAnchorReq* = 3 and the sensor's priority is determined by the number of its connected anchors that have the lowest acting level among all the sensor's connected anchors. We can certainly add more granularity by further classifying the sensor's second and third connected anchors' acting levels. Although more categorizations of the priorities should increase localization accuracy under most noise conditions, more computational effort is required to handle more levels of priorities. In Table 3.1, we assume we will generate only 9 levels of priorities.

Each item in the table represents the number of anchors with different acting levels that is needed at each priority. The last column represents the resulting acting anchors' acting levels for subsequent iterations. For example, if a sensor has at least three independent connections to anchors, and if 2 of the anchors are original anchors (acting level 1) and at least 1 of the connected anchors is at any acting level from 2 to 7, this sensor belongs to priority 2 as listed in row 2 of the table. Also, when this sensor is positioned, it becomes acting anchor level 3. The sensors that connect to two anchors belong to the second last priority (8 in the table), and sensors that connect to only one anchor belong to the last priority (9 in this case). In addition, if a sensor connects to at least 3 independent anchors, among which at least one anchor belongs to level 8, 9, or 10, this sensor will be classified as the third last priority as listed in row 7.

3.1.4 Subanchors Selection

In step S8, for each unpositioned subsensor, only *AnchorReq* of the connected anchors are allowed to be included in the subproblem. We use the following rules to select subanchors from a candidate subanchor list that contains more than *AnchorReq* anchors.

RA1 Original anchors are selected first, followed by acting anchors with lower acting level.

RA2 The subanchors chosen should be linearly independent.

RA3 Among independent anchors in the candidate subanchor list, we use distance scale-factors to encourage selection of the closest subanchors.

Rules RA2 and RA3 are implemented as in section 3.1.5. Rule RA3 is based on the assumption that under noise conditions, we trust the shorter distance measurements more than the longer ones. This is specially true for ranging devices based on RF (radio frequency) strength.

For certain applications, it may be beneficial to choose *MaxAnchorReq* large in order to increase the localization accuracy, though it could impact the algorithm speed.

3.1.5 Independent Subanchors Selection

Suppose sensor i is connected to K $(K > 3)$ anchors at locations a_{ik} with corresponding distance measurements $\widehat{d}_{ik}$ $(k = 1, \ldots, K)$. Define the matrices

$$A = \begin{pmatrix} 1 & 1 & \ldots & 1 \\ -a_{i1} & -a_{i2} & \ldots & -a_{iK} \end{pmatrix}, \quad D_1 = \mathrm{diag}(1/\sqrt{1 + \|a_{ik}\|^2}), \quad D_2 = \mathrm{diag}(1/\widehat{d}_{ik}).$$

We select an independent subset by a QR factorization with column interchanges [17]: $B = AD_1D_2$, $BP = QR$, where Q is orthogonal, R is upper-trapezoidal, and P is a permutation chosen to maximize the next diagonal of R at each stage of the factorization. (D_1 normalizes the columns of A, and D_2 biases them in favor of anchors that are closer to sensor i.) If the 3rd diagonal of R is larger than a predefined threshold (10^{-4} is used in our simulation), the first 3 columns of AP are regarded as independent, and the associated anchors are chosen. Otherwise, all subsets of 3 among the K anchors are regarded as dependent. (In Matlab, R and P are obtained by a command of the form `[Q,R,P] = qr(B)`.)

3.1.6 Geometric Subroutine (Two Connected Anchors)

This section illustrates the heuristic techniques used in step S7 of section 3.1.2 to localize sensors connected to only two anchors.

When a sensor's connected anchors are also connected to other anchors, this subroutine may improve the accuracy of the sensor's positioning, as illustrated by an example in Figure 3.2.

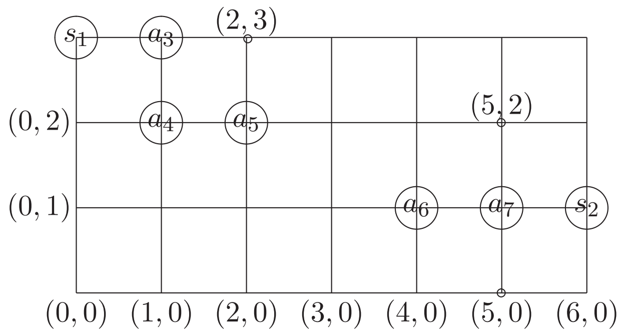

Figure 3.2: Sensors with connections to at most two anchors.

In this example, assume s_1 and s_2 are sensors with unknown locations, and $a_3(1,3)$, $a_4(1,2)$, $a_5(2,2)$, $a_6(4,1)$, $a_7(5,1)$ are anchors with known positions in brackets. Assume that the sensors' radio range is $\sqrt{2}$, and we are also given two distance measurements $\widehat{d}_{13} = 1$ and $\widehat{d}_{14} = \sqrt{2}$ for sensor s_1 and one measurement $\widehat{d}_{27} = 1$ for sensor s_2.

Given two distances $\widehat{d}_{13}$ and $\widehat{d}_{14}$ to two anchors $a_3(1,3)$ and $a_4(1,2)$, we know that s_1 should be either at $(0,3)$ or $(2,3)$. If we only use s_1, $a_3(1,3)$, $a_4(1,2)$ in an SDP subproblem, SDP relaxation will give a solution near the middle of the two possible points, which would be very close to point $(1,3)$. If there is any anchor (a_5) that is near s_1's connected anchors (a_3 and a_4) with any of the two possible sensor' points within their radio range (point $(2,3)$ is within a_5's range), that point $(2,3)$ must not be the real location of s_1, or else s_1 would be connected to this anchor (a_5) as well. Thus we can infer that s_1 must be at the other point $(0,3)$.

Inspired by the above observation, when a sensor has at most 2 connected anchors, we include these anchors' connected anchors in the subproblem (we call them the connected

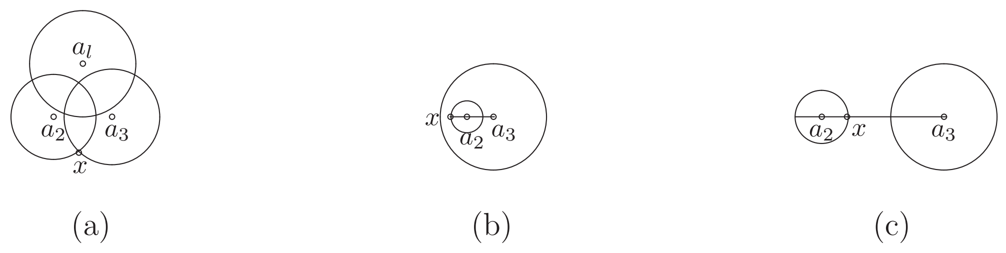

Figure 3.3: (a) Sensor with two anchors' circles intersecting. (b) Sensor with two anchors, a_2's circle in a_3's. (c) Sensor with two anchors' circles disjoint.

anchors' neighboring anchors) together with the sensor and its directly connected anchors. By including the neighboring anchors, we might hope that the inequality constraints in the SDP relaxation model (2.4) would push the estimation towards the right point. However, because of the relaxation, enforcing inequalities in (2.4) is not equivalent to enforcing them in the distance model (2.2). The added inequality constraints only push the original solution near $(1, 3)$ a tiny bit towards s_1's real location $(0, 3)$, and the solution essentially stays at around $(1, 3)$.

Given the ineffectiveness of the SDP relaxation approach under this condition, we propose instead a geometric approach as illustrated in Figure 3.3. Assume $s_1(x_x, x_y)$ has measurements $\widehat{d}_{12}$ to anchor $a_2(a_{2x}, a_{2y})$ and $\widehat{d}_{13}$ to anchor $a_3(a_{3x}, a_{3y})$. We also assume $\widehat{d}_{12} \le \widehat{d}_{13}$ (we can always swap the two indexes otherwise). Let a_l $(l = 4, \dots, k)$ be a_2 and/or a_3's neighboring anchors with radio range r_{1l} $(l = 4, \dots, k)$, and let d_{23} be the known (exact) Euclidean distance between a_2 and a_3.

- If two circles centered at a_2 and a_3 with radii $\widehat{d}_{12}$ and $\widehat{d}_{13}$ intersect each other ($\widehat{d}_{12} + \widehat{d}_{13} \ge d_{23}$ and $\widehat{d}_{13} - \widehat{d}_{12} \le d_{23}$) as in Figure 3.3(a):
  - Two possible locations of s_1 are given by solutions x^* and x^{**} of the equations

$$\|x - a_2\|^2 = \widehat{d}_{12}^2 \ , \qquad \|x - a_3\|^2 = \widehat{d}_{13}^2 \ .$$

  - Sensor s_1's position is selected from x^* and x^{**}, whichever is further away from any neighboring anchor. Thus, for $l = 4$ to k,

```
         if $\|x^* - a_l\|^2 < r_{1l}^2$,  then $x = x^{**}$ and stop
    else if $\|x^{**} - a_l\|^2 < r_{1l}^2$,  then $x = x^*$ and stop.
```

    Otherwise, $x = (x^* + x^{**})/2$ and stop.

- Under noise conditions, the a_2 circle may be inside the a_3 circle ($\widehat{d}_{12} + \widehat{d}_{13} \ge d_{23}$ and $\widehat{d}_{13} - \widehat{d}_{12} > d_{23}$) as in Figure 3.3(b).

- The solutions x^* and x^{**} of the following equations give two possible points for s_1 on the a_2 circle:

$$\begin{aligned}(x_x - a_{2x})^2 + (x_y - a_{2y})^2 &= \widehat{d}_{12}^2,\\ (a_{2x} - a_{3x})(x_y - a_{2y}) &= (a_{2y} - a_{3y})(x_x - a_{2x}),\end{aligned}$$

  where x is on the line through a_2 and a_3 represented by the second equation.

- If $\|x^* - a_3\| < \|x^{**} - a_3\|$, then $x = x^{**}$; otherwise $x = x^*$. This guarantees that the point further from a_3 is chosen. Note that we base the sensor's estimation on the closest anchor (a_2 here since $\widehat{d}_{13} \geq \widehat{d}_{12}$), assuming that a shorter measurement is generally more accurate than longer ones, given similar anchor properties.

The same approach applies when the a_3 circle is inside the a_2 circle ($\widehat{d}_{12} - \widehat{d}_{13} > d_{23}$).

- Under noise conditions, the a_2 and a_3 circles may again have no intersection ($\widehat{d}_{12} + \widehat{d}_{13} < d_{23}$) as in Figure 3.3(c).

  - The solutions x^* and x^{**} of the following equations give two possible points for s_1 on the circle for the anchor with smaller radius. Let's assume $\widehat{d}_{12} \leq \widehat{d}_{13}$:

$$\begin{aligned}(x_x - a_{2x})^2 + (x_y - a_{2y})^2 &= \widehat{d}_{12}^2,\\ (a_{2x} - a_{3x})(x_y - a_{2y}) &= (a_{2y} - a_{3y})(x_x - a_{2x}),\end{aligned}$$

    where x is on the line through a_2 and a_3 represented by the second equation.

  - If $\|x^* - a_3\| > \|x^{**} - a_3\|$, then $x = x^{**}$; otherwise $x = x^*$. This guarantees that the point closer to a_3 (in between a_2 and a_3) is chosen.

3.1.7 Geometric Subroutine (One Connected Anchor)

Similar inefficiency occurs in the SDP solution when a sensor connects to only *one* anchor. The SDP solver under this condition gives a solution for the sensor to be in the same location as the sensor's connected anchor. In reality, the sensor could be anywhere on the circle. The SDP gives an average point, at the center of the circle, and that is where the connected anchor is. Even if the anchor's neighboring anchor is included in the SDP subproblem, the inequality constraints are not active most of the time because the SDP solution may not provide optimal solutions all the time.

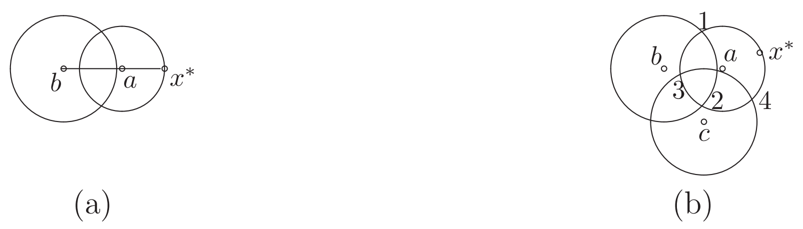

Figure 3.4: (a) Sensor with one anchor connection a and one neighboring anchor b. (b) Sensor with one anchor connection a and two neighboring anchors b, c.

We propose a heuristic for estimating a sensor's location with only one connecting anchor. The idea is to use one neighboring anchor's radio range information to eliminate the portion of the circle that the sensor would not be on, and then calculate the middle of the other portion of the circle to be the sensor's position. For the example in Figure 3.2, because we know the distance between s_2 and a_7 is 1, we know that s_2 could be anywhere on the circle surrounding a_7 with a radius of 1. Knowing a_7's neighboring anchor node a_6 is not connected to s_2, we know that s_2 would not be in the area surrounding a_6 with a radius of $\sqrt{2}$. Thus, s_2 could be anywhere around the half circle including points $(5, 2)$, $(6, 1)$, $(5, 0)$. The heuristic chooses the middle point between the two circles' intersection points $(5, 2)$ and $(5, 0)$, which happens to be $(6, 1)$ in this example. The heuristic gives better accuracy for the sensor's location than the SDP solution under most conditions. The procedure follows:

- Assume s has one distance measurement $\widehat{d}$ to anchor a, and b is the closest connected neighboring anchor to a with radio range r (refer to Figure 3.4(a)). We assume $a = (a_x, a_y)$, $b = (b_x, b_y)$, $x = (x_x, x_y)$.

- The solutions x^* and x^{**} of the following equations give two possible points s on the circle:

$$\begin{aligned}(x_x - a_x)^2 + (x_y - a_y)^2 &= \widehat{d}^2,\\ (a_x - b_x)(x_y - a_y) &= (a_y - b_y)(x_x - a_x),\end{aligned}$$

  where x is on the line through a and b represented by the second equation.

- If $\|x^* - b\| < r$, then $x = x^{**}$; otherwise $x = x^*$. This guarantees that the point further from b is chosen.

The above heuristic provides a simple way of estimating a sensor's location when the sensor connects to only one anchor. A more complicated approach can be adopted when the connected anchor has more than one neighboring anchor, which can increase the accuracy of the sensor's location. We call it an arc elimination heuristic. The idea is to loop through each of the neighboring anchors and find the portion of the circle that the sensor won't be on, and eliminate that arc as a possible location of the sensor. Eventually, when one or more plausible arcs remain, we choose the middle of the largest arc to be the sensor's location. For example, assume we add one more neighboring anchor c to sensor s's anchor a from the previous example in Figure 3.4(a). The new scenario is shown in Figure 3.4(b). First, we find the intersections (points 1 and 2) of two circles: one at a with radius $\widehat{d}$, the other at b with radius r. We know that the 1–2 portion of the arc closer to point b won't be the location of s. Second, we find the intersections (points 3 and 4) of two circles: one at a with radius $\widehat{d}$, the other at c with radius r. We know that the arc 3–4 closer to point c won't be the location of s. Thus we deduce that s must be somewhere on the arc 1–4 further away from b or c. The estimation of s is given in the middle of the arc 1–4. As we see, this method should provide more accuracy than the one-neighboring-anchor approach.

3.2 An Example

A simple example is shown in Figure 3.5 to illustrate the SpaseLoc algorithm and some of the rules of the subproblem selection process. Assume s_1, s_2, …, s_{14} are sensors with unknown locations, and a_{15}, a_{16}, …, a_{20} are original anchors. Assume that the actual locations of these nodes are all on a regular square grid structure with edge size 1, and that the sensors' radio range is $\sqrt{2}$. We also use the priority list in Table 3.1 in this example.

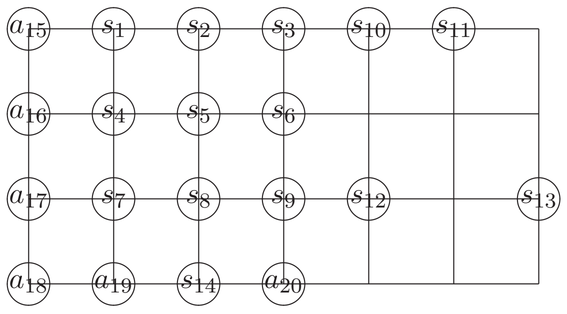

Figure 3.5: An example.

- In A0 we set *subproblem_size* = 3.

- In A1 we go through the subproblem creation procedure:
  - In S1 we set *MaxAnchorReq* = 3
  - In S2, *AnchorReq* is set to *MaxAnchorReq*, which is 3.
  - S3 goes through the unpositioned sensor list and finds that s_4 and s_7 both have at least 3 connections to anchors. However, anchors a_{15}, a_{16}, a_{17} connected to sensor s_4 are dependent, so the subsensor candidate list is only s_7 for this iteration.
  - Since the subsensor candidate list of 1 is shorter than the *subproblem_size* of 3, we are at S6. *AnchorReq* is not reduced yet because the candidate list is not empty. Continue to S8.
  - In S8, we have anchors a_{16}, a_{17}, a_{18}, a_{19} connected to sensor s_7 in the subsensor candidate list, so we follow the subanchor selection rules RA1–RA3 in section 3.1.4. Rule RA2 says to choose three independent anchors, which could be a_{16}, a_{18}, a_{19} or a_{17}, a_{18}, a_{19}. Since anchors a_{16}, a_{17}, a_{18} are dependent, they won't be chosen. Rule RA3 says that if there are multiple anchors to choose from, the closest ones should be used. Therefore a_{17}, a_{18}, a_{19} are selected instead of a_{16}, a_{18}, a_{19}.
  - In S9, the subproblem consists of subsensor s_7 and subanchors a_{17}, a_{18}, a_{19}.
- In A2, formulate the SDP subproblem from subsensor s_7 and subanchors a_{17}, a_{18}, a_{19}.
- In A3, call SDP to give s_7's position estimation.
- In A4, s_7 is positioned and becomes an acting anchor at level 2 for the next iteration.
- In A5, some sensors are still not positioned. Go back to A1.
- With s_7 as acting anchor, iterate steps A1–A5 (2nd time). s_4, s_8, s_{14} are positioned in this iteration with subanchors a_{16}, a_{17}, a_{19}, a_{20}, s_7, and all become acting anchors at level 3 for the next iteration.
- With added acting anchors s_4, s_8, s_{14}, iterate steps A1–A5 (3rd time). s_1, s_5, s_9 are positioned with subanchors a_{15}, a_{16}, s_4, s_7, s_8, s_{14}, a_{20}, and become acting anchors at levels 3, 7, 4.

- With added acting anchors s_5 and s_9, iterate steps A1–A5 (4th time). s_2 and s_6 are positioned with subanchors s_1, s_4, s_5, s_8, s_9, and both become acting anchors at level 7.

- With added acting anchors s_2 and s_6, iterate steps A1–A5 (5th time). s_3 is positioned with subanchors s_2, s_5, s_6, and becomes acting anchor at level 7.

- With s_3 positioned, iterate steps A1–A5 (6th time). Although we find unpositioned sensor s_{12} has connections to 3 anchors s_6, s_9, a_{20}, they are dependent. There is no unpositioned sensor with connections to at least 3 independent anchors, so we move to S7.

- Since the subsensor candidate list is now empty, *AnchorReq* is reduced from 3 to 2 at S7. Iterate steps A1–A5 (7th time) with a new *AnchorReq* value of 2, finding s_{12} and s_{10} with at least 2 anchor connections. Since s_{12} has connections to 3 dependent anchors s_6, s_9, a_{20}, it is effectively the same as being connected to exactly 2 anchors. s_{10} is connected to s_3 and s_6. We now follow the geometric subroutine in section 3.1.6 for sensors connected to two anchors. Subanchors s_3, s_6, s_8, a_{20} have connected neighboring anchors s_2, s_5, s_8, s_{14} and they are used to exclude the other possible points for s_{10} and s_{12}. Thus s_{10} is now positioned, and both become acting level 9.

- With s_{10} positioned, iterate steps A1–A5 (8th time). There is no unpositioned sensor with connections to at least 2 anchors, so we move to S7 again.

- Since the subsensor candidate list is now empty, *AnchorReq* is further reduced from 2 to 1 at S7. Iterate steps A1–A5 (9th time) with a new *AnchorReq* value of 1. Since s_{11} connects to only one subanchor s_{10}, follow the geometric subroutine in section 3.1.7. s_{10}'s nearest connected neighboring anchor s_3 is used to determine the position of s_{11}, and it becomes acting level 10.

- Iterate steps A1–A5 (10th time). There is no unpositioned sensor with connections to 1 or more anchors, so we move to S7 again.

- Since the subsensor candidate list is now empty, *AnchorReq* is further reduced from 1 to 0 at S7. Because *AnchorReq* $= 0$ and there is one more unpositioned sensor s_{13}, s_{13} is classified as an outlier in S7. Now we move to step A6.

- In A6, report sensor positions and outliers and stop.

3.3 Computational Results

This section explains the simulation method and the setup for experimenting with the SpaseLoc algorithm, then presents results for various parameter settings.

For the simulation, a total number of nodes n (including s sensors and m anchors) is specified in the range 50 to 10000. The positions of these nodes are assigned with a uniform random distribution on a square region of size $r \times r$ where $r = 1$, or put on the grid points of a regular topology such as a square or an equilateral triangle on the same region. *MaxAnchorReq* $= 3$ is used in the simulation. The m anchors are randomly chosen from the given n nodes. We assume all sensors have the same radio range (*radius*) for any given test case. Various radio ranges were tested in the simulation.

Euclidean distances $d_{ij} = \|x_i - x_j\|$ are calculated among all sensor pairs $(i,\ j)$ for $i < j$. We then use $\widehat{d}_{ij}$ to simulate measured distances, where $\widehat{d}_{ij}$ is d_{ij} times a random error simulated by *noise_factor* $\in [0, 1]$. For a given *radius* $\subseteq [0, 1]$ it is defined as follows:

- If $d_{ij} \leq \mathit{radius}$, then $\widehat{d}_{ij} = d_{ij}(1 + \texttt{rn} * \mathit{noise\_factor})$, where `rn` is normally distributed with mean zero and variance one. (Any numbers generated outside $(-1, 1)$ are regenerated.)

  In practical networks, depending on the technologies that are being used to obtain the distance measurements, there may be many factors that contribute to the noise level. For example, one way to obtain the distance measurement is to use the received radio signal strength between two sensors. The signal strength could be affected by media or obstacles in between the two sensors. In this study, *noise_factor* is a normally distributed random variable with mean zero and variance one. This model could be replaced by any other noise model in practice.

- If $d_{ij} > \mathit{radius}$, the bound $r_{ij} = 1.001 * \mathit{radius}$ is used in the SDP model.

In the simulation, we define the average estimation error to be $\frac{1}{s}\sum_{i=1}^{s} \|\bar{x}_i - x_i\|$, where $\bar{x}_i$ is from the SDP solution and x_i is the ith node's true position. In a practical setting, we wouldn't know the node's true location x_i. Instead, we would use the node's trace τ_i (2.5) to gauge the estimation error.

To convey the distribution of estimation errors and trace, we also give the 95% quartile.

Factors such as noise level, radio range, and anchor densities can directly impact localization accuracy. The sensors' estimated positions are derived directly from the given distance measurements. If the noise level in these measurements is high, the estimation accuracy cannot be high. We also need sufficiently large radio range to achieve accurate positioning, because too small a range could cause many sensors to be unreachable. Finally, more anchors in the network should help with the estimation accuracy because there are more reference points.

In the following subsections, we present simulation results (most results averaged over 10 runs) to show the accuracy and scalability of the SpaseLoc algorithm. We observe the impact of various radio ranges, anchor densities, and noise levels on the accuracy and performance of the algorithm. Computations were performed on a laptop computer with 2.4GHz CPU and 1GB system memory, using Matlab 6.5 [29] for SpaseLoc and a Mex interface to DSDP5.0 (Benson, Ye, and Zhang [3]) for the SDP solutions.

3.3.1 Effect of Inequality Constraints in SDP Relaxation Model

As we discussed in section 3.1.6, because of the $Y \succeq X^T X$ constraint relaxation, enforcing the r_{ij}^2 and r_{ik}^2 inequality constraints in (2.4) is not equivalent to enforcing them in the distance model (2.2). In order to observe the effectiveness of including these inequality constraints, we conduct simulations with the following three strategies, according to the number of times we check for violated inequality constraints and then include them to obtain new solution.

I2 corresponds to solving the SDP problem with all equalities (and no inequalities), and then adding violated inequality constraints and re-solving one or more times until all inequalities are satisfied. The final solution is an optimal solution to problem (2.4).

I1 corresponds to solving the SDP problem with all equalities and then adding all violated inequality constraints at most once.

I0 corresponds to solving the SDP problem with equality constraints only. (No inequality constraints are ever added.) The final solution is optimal for problem (2.4) without the inequality constraints involving r_{ij}^2 and r_{ik}^2.

Our experimental results show that the added inequality constraints do not always provide better positioning accuracy, but greatly increase the execution time. In this section, we illustrate the inequality constraints' impact through two simulation examples: one with no noise but low connectivity; the other with full connectivity but with noise.

In our first example, we run simulation results on a network of 100 randomly uniform-distributed sensors with radius 0.2275 and 10 randomly selected anchors. One of the sensors happens to be connected to only two other nodes. The sensors are localized with the full SDP and with SpaseLoc, using each of the I2, I1, I0 strategies in turn. And for SpaseLoc, we also examine each case with or without our geometric routines. The results are shown in Figure 3.6 and Table 3.2.

Figure 3.6 shows there is a sensor (s) that is connected with only 2 anchors. For full SDP shown in (a), no violated inequalities are ever found, so full SDP with I2, I1, or I0 has only one SDP call and always generates the same results. For SpaseLoc in (b) with I0 and no geometric routine, SDP is called 46 times (with no subsequent check for violated constraints). It produces the same estimation accuracy as the full SDP approach but with much improved performance. In (c), SpaseLoc with I2 or I1 produces the same results, which means violated inequalities are found only once. Comparing (b) and (c), we see that including violated inequalities does improve the estimation accuracy. Best of all in (d), SpaseLoc with I0 and our geometric routines localizes all sensors with virtually no error.

Table 3.2 shows that adding violated inequalities increases execution time slightly for SpaseLoc.

In our second example, in order to observe the effectiveness of the inequality constraints under noise conditions, we run simulations for a network of 100 nodes whose true locations are at the vertices of an equilateral triangle grid. 10 anchors are positioned along the middle grid-points of each row, and the radius is 0.25. A *noise_factor* of 0.1 is applied to the distance measurements. The sensors are localized with either full SDP or SpaseLoc using I2, I1, I0 in turn without geometric routines. (Although we do not activate the geometric routines in this experiment, they are not a factor here because the localization error is not caused by low connectivity but by the noisy measurements.) The results are shown in Figure 3.7 and Table 3.3. Figure 3.7 (b) and (c) correspond to strategy I2 for full SDP and SpaseLoc.

As we can see, adding violated inequalities for full SDP not only increases the execution times dramatically, but also increases the localization error. For SpaseLoc, adding violated inequalities improves the estimation accuracy slightly. Note that I2 had 2 more SDP calls but did not improve the accuracy over I1.

In summary, the first experiment shows that when the errors are caused by *low connectivity*, SpaseLoc with geometric routines and no inequality constraints (I0) outperforms SpaseLoc with inequalities (I1 or I2) and all of the full SDP options. Given this observation, from now on we only use SpaseLoc with geometric routines, which means the geometric routines are used instead of SDP to localize sensors connected to fewer than 3 anchors.

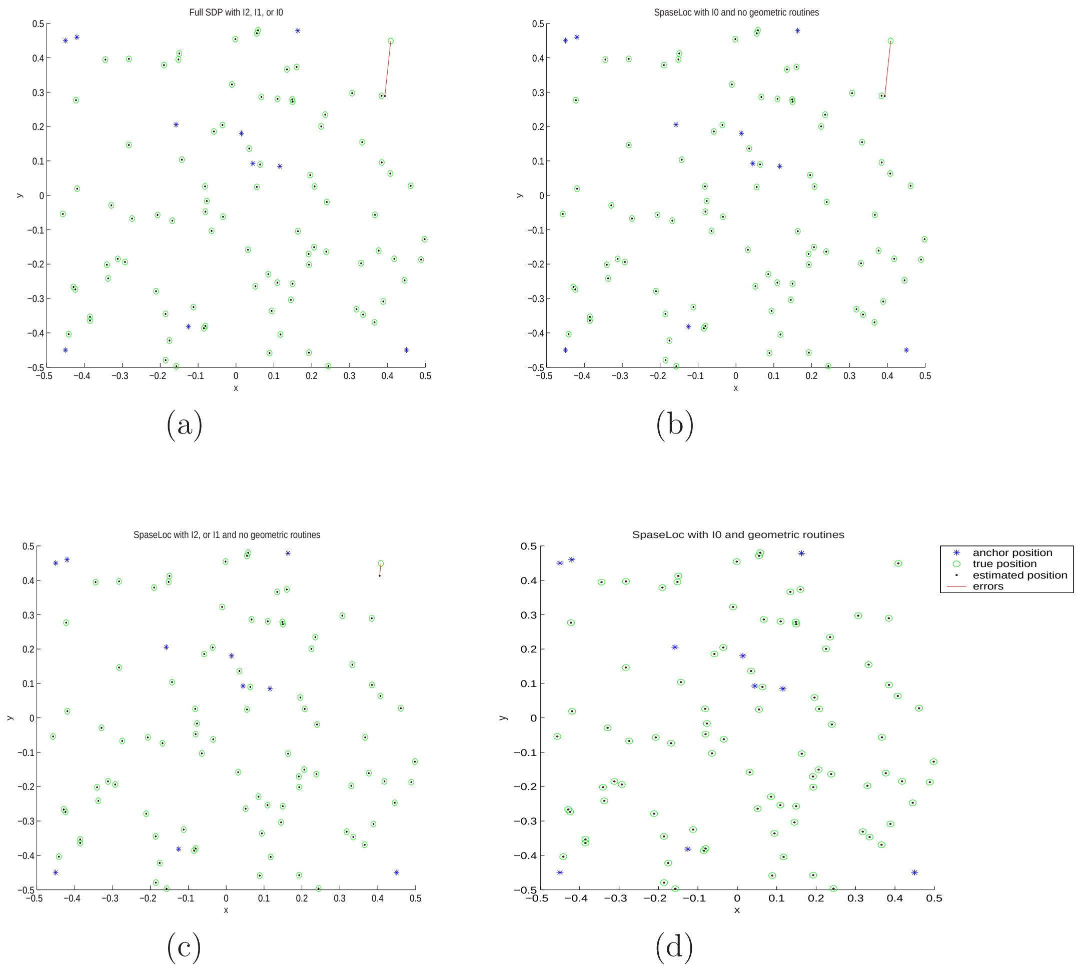

Figure 3.6: Inequality impact on accuracy: 100 nodes, 10 anchors, no noise, radius 0.2275.

Table 3.2: Inequality impact on accuracy and speed: 100 nodes, 10 anchors, no noise, radius 0.2275.

Methods	Error	95% Error	Time	SDP's
Full SDP with I2, or I1 or I0	1.80e-3	1.74e-10	11.63	1
SpaseLoc with I0 and no geometric routines	1.80e-3	1.09e-08	0.40	46
SpaseLoc with I2 or I1 and no geometric routines	4.01e-4	1.09e-08	0.44	47
SpaseLoc with I0 and geometric routines	1.28e-7	8.78e-09	0.41	45

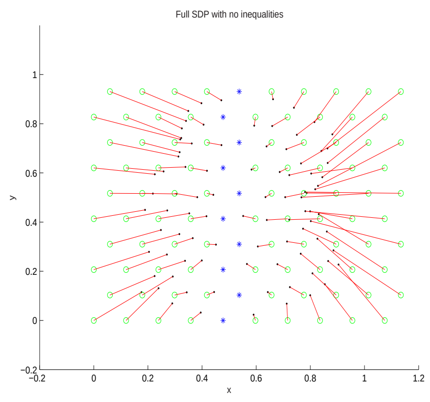

(a)

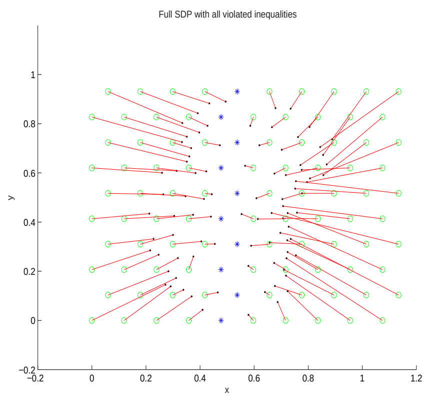

(b)

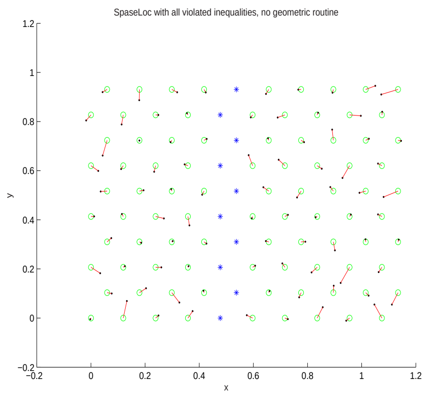

(c)

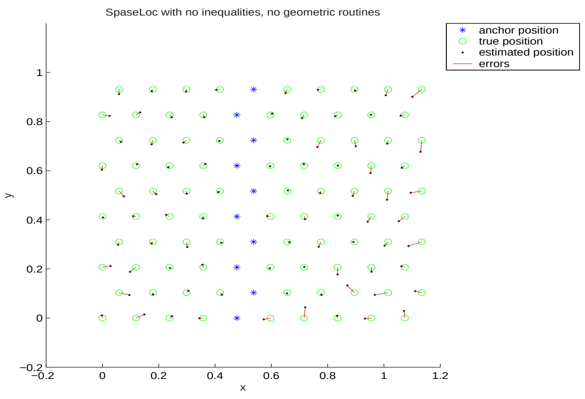

(d)

Figure 3.7: Inequality impact on accuracy: 100 nodes, 10 anchors, *noise_factor* 0.1, radius 0.25.

Table 3.3: Inequality impact on accuracy and speed: 100 nodes, 10 anchors, *noise_factor* 0.1, radius 0.25.

Methods	Error	Time	SDP's
Full SDP with I2	0.1403	134.50	4
Full SDP with I1	0.1292	34.20	2
Full SDP with I0	0.1268	13.87	1
SpaseLoc with I2	0.0154	0.71	48
SpaseLoc with I1	0.0154	0.65	46
SpaseLoc with I0	0.0165	0.42	30

The second experiment indicates that under noise conditions, although adding violated inequalities does not seem to improve the estimation accuracy for full SDP, it does improve accuracy for SpaseLoc.

In the subsequent sections, we continue to examine the inequality constraints' effects on accuracy and speed.

3.3.2 Accuracy and Speed Comparison: Full SDP vs SpaseLoc

For very small networks, the full SDP solution is both accurate and efficient. (This is vital to the performance of SpaseLoc, as many small subproblems must be solved using SDP.) However, the performance of the pure SDP approach deteriorates rapidly with network size.

Table 3.4 shows the localization results using full SDP (a) and using SpaseLoc (b) for a range of examples with various numbers of nodes whose true locations in the network are at the vertices of an equilateral triangle grid. Anchors are positioned along the middle grids of each row. A *noise_factor* of 0.1 is applied to the distance measurements.

Let's first look at the impact of I2, I1, and I0 on estimation accuracy. As we can see from Table 3.4 (a), for full SDP, 5 errors with I2 are bigger than with I1, and 8 errors with I1 are bigger than with I2. Comparing I2 with I0, we see that for each strategy, 8 errors are bigger than the errors for the other strategy. It appears that full SDP with added inequalities does not improve the estimation accuracy in this simulation. For SpaseLoc, I2 and I1 generate almost equivalent estimation accuracy, I0 has 8 errors that are bigger than with I1, and at the same time, I1 has 7 errors that are bigger than with I0. It is therefore hard to judge the effectiveness of the added inequalities.

Now let's compare full SDP with SpaseLoc. Figures 3.8–3.9 plot results for full SDP with I0 and SpaseLoc with I0 for two of these examples: 9 and 49 nodes, including 3 and 7 anchors positioned at the grid-point in the middle of each row. As we can see from these two figures and Table 3.4, for localizing 4 and 9 nodes, full SDP and SpaseLoc show comparable performance. Beyond that size, the contrast grows rapidly. For localizing 49 nodes, SpaseLoc is more than 10 times faster than the full SDP method, with more than 4 times better accuracy. For 400 nodes, SpaseLoc is about 1000 times faster and 20 times more accurate with strategy I0, about 2000 times faster with I1, and 6000 times faster with I2, with similar accuracy improvements. Thus, the full SDP model becomes less effective as problem size increases. In fact, for problem sizes above 49 nodes, the average estimation error becomes so large that the computed solution is of little value.

Table 3.4: Accuracy and speed comparison between full SDP and SpaseLoc.

(a) Full SDP

Number	Radio	Error			Time (sec)			SDP calls		
of nodes	range	I2	I1	I0	I2	I1	I0	I2	I1	I0
4	2.24	0.0317	0.0317	0.0317	0.01	0.01	0.01	1	1	1
9	1.12	0.0800	0.0800	0.0704	0.05	0.07	0.02	2	2	1
16	0.75	0.0680	0.0703	0.0837	0.35	0.21	0.10	3	2	1
25	0.56	0.1170	0.1170	0.0938	1.26	0.80	0.37	3	2	1
36	0.45	0.0561	0.0618	0.0719	3.02	1.88	0.81	3	2	1
49	0.40	0.1190	0.1190	0.1190	5.42	5.33	2.10	2	2	1
64	0.40	0.0954	0.0919	0.1218	21.60	9.21	3.43	4	2	1
81	0.40	0.0885	0.0894	0.1380	59.05	19.66	7.26	5	2	1
100	0.25	0.1403	0.1292	0.1268	140.26	34.20	13.87	4	2	1
121	0.40	0.1091	0.1088	0.1157	182.74	81.62	23.24	3	2	1
144	0.21	0.1891	0.1899	0.1480	584.23	168.43	37.76	4	2	1
169	0.40	0.1217	0.1141	0.1283	692.12	278.72	71.87	4	2	1
196	0.18	0.1286	0.1275	0.1404	1081.35	461.97	151.52	4	2	1
225	0.40	0.1571	0.1589	0.1568	2408.67	752.75	232.31	5	2	1
256	0.15	0.1370	0.1375	0.1429	3260.33	1089.52	356.86	5	2	1
324	0.14	0.1685	0.1685	0.1685	2620.20	2659.18	962.66	2	2	1
361	0.13	0.1833	0.1842	0.1734	15281.26	5051.05	1391.04	4	2	1
400	0.12	0.1968	0.1970	0.1819	20321.60	5950.34	1662.22	4	2	1

(b) SpaseLoc

Number	Radio	Error			Time (sec)			SDP calls		
of nodes	range	I2	I1	I0	I2	I1	I0	I2	I1	I0
4	2.24	0.0317	0.0317	0.0317	0.01	0.01	0.01	1	1	1
9	1.12	0.0766	0.0766	0.0670	0.11	0.32	0.03	3	3	2
16	0.75	0.0599	0.0599	0.0612	0.07	0.07	0.04	7	7	4
25	0.56	0.0495	0.0495	0.0516	0.11	0.11	0.08	10	10	7
36	0.45	0.0250	0.0250	0.0262	0.22	0.21	0.12	17	17	10
49	0.40	0.0283	0.0283	0.0282	0.21	0.21	0.19	15	15	14
64	0.40	0.0193	0.0193	0.0202	0.41	0.38	0.25	28	27	19
81	0.40	0.0186	0.0187	0.0192	0.56	0.53	0.31	41	40	24
100	0.25	0.0154	0.0154	0.0165	0.71	0.65	0.42	48	46	30
121	0.40	0.0152	0.0152	0.0143	0.86	0.82	0.51	58	57	37
144	0.21	0.0133	0.0133	0.0123	0.99	0.93	0.61	65	63	44
169	0.40	0.0108	0.0108	0.0110	1.22	1.16	0.74	81	80	52
196	0.18	0.0113	0.0112	0.0100	1.30	1.24	0.86	85	83	61
225	0.40	0.0099	0.0099	0.0097	1.88	1.68	0.96	126	118	70
256	0.15	0.0075	0.0075	0.0077	2.01	1.79	1.10	136	126	80
324	0.14	0.0075	0.0075	0.0075	1.64	1.64	1.48	102	102	102
361	0.13	0.0073	0.0073	0.0069	2.20	2.16	1.65	139	139	114
400	0.12	0.0070	0.0070	0.0064	3.31	2.98	1.78	217	204	127

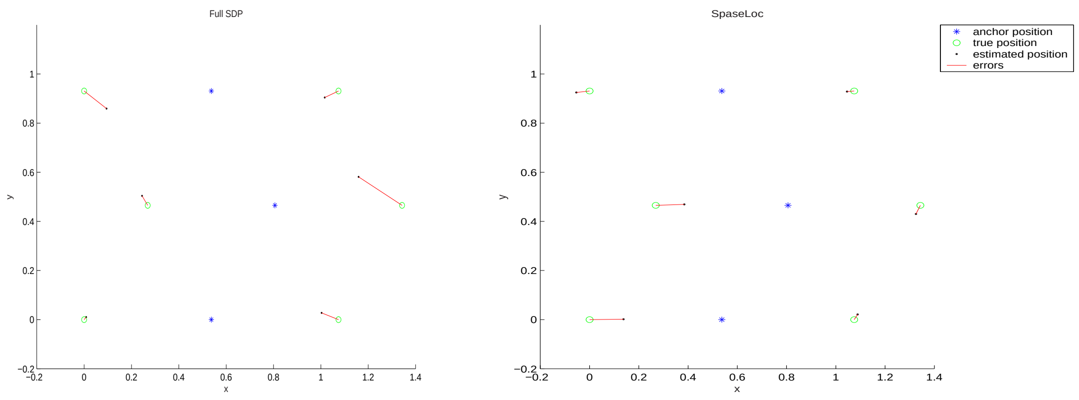

Figure 3.8: 9 nodes on equilateral-triangle grids, 3 anchors, 0.1 noise, radius 1.12.

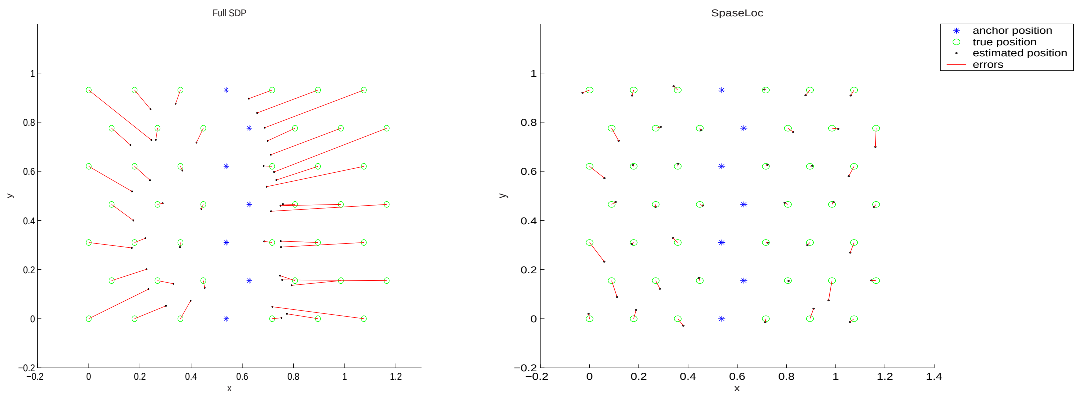

Figure 3.9: 49 nodes on equilateral-triangle grids, 7 anchors, 0.1 noise, radius 0.40.

It may seem non-intuitive that SpaseLoc's greedy approach could produce smaller errors than the full SDP method. However, all of the SDP problems and subproblems of the form (2.4) are *relaxations* of Euclidean models of the form (2.2). It shows experimentally that the relaxations are *tighter* in SpaseLoc's subproblems than in the single large SDP.

In the following sections, we run more simulations only with SpaseLoc.

Table 3.5: SpaseLoc scalability. Strategies I2, I1, and I0 generate same results.

Nodes	Anchors	*radius*	*sub_size*	Error	95% Error	Trace	95% Trace	Time	SDP's
49	7	0.3412	2	1.40e-08	9.86e-10	6.28e-09	4.10e-10	0.21	21
100	10	0.2275	2	1.28e-07	8.78e-09	2.68e-08	2.36e-09	0.45	45
225	15	0.1462	3	6.98e-07	7.74e-08	8.75e-08	1.19e-08	0.80	70
529	23	0.0931	3	2.87e-06	9.42e-08	2.68e-07	1.03e-08	1.99	169
1089	33	0.0620	3	2.50e-06	1.65e-07	1.27e-07	1.12e-08	4.12	350
2025	45	0.0451	3	2.70e-05	2.41e-07	2.28e-07	1.41e-08	8.55	658
3969	63	0.0330	3	6.32e-06	3.53e-07	1.30e-07	1.39e-08	19.51	1302
5041	71	0.0292	3	6.70e-06	5.06e-07	1.44e-07	1.80e-08	25.57	1656
6084	78	0.0266	3	6.95e-06	5.47e-07	1.50e-07	1.84e-08	33.38	2000
7056	84	0.0247	4	5.92e-06	6.43e-07	1.35e-07	1.90e-08	41.58	1743
8100	90	0.0230	5	3.92e-06	6.42e-07	8.23e-08	1.78e-08	50.34	1602
9025	95	0.0218	5	8.38e-06	6.74e-07	1.17e-07	1.74e-08	57.34	1788
10000	100	0.0207	5	4.70e-06	7.63e-07	1.12e-07	1.94e-08	65.08	1981

3.3.3 Scalability

Table 3.5 shows simulation results for 49 to 10000 randomly uniform-distributed sensors being localized using SpaseLoc with strategies I2, I1, and I0. The node numbers 49, 100, 225, ... are squares k^2, and the *radius* is the minimum value that permits localization on a regular $k \times k$ grid. The number of anchors changes with the number of sensors in order to maintain the same anchor density. Noise is not included in this simulation.

We find that the three strategies I2, I1, I0 produce the same results. This is because the inaccuracy of the positioning estimation is purely caused by low connectivity, not by noisy distance measurements. Empirically we see that the program scales well: almost linearly in the number of nodes in the network. Indeed, the computational complexity of the SpaseLoc algorithm is of order n, the number of sensors in the network, even though the full SDP approach has much greater complexity, as we now show.

We know that in the full SDP model (2.4), the number of constraints is $O(n^2)$, and in each of iteration of its interior-point algorithm the SDP solver needs to solve a *sparse* linear system of equations whose dimension is the number of constraints. Figure 3.10 plots the CPU time for strategy I0 from Table 3.4 (a) as well as three curves of the form $\textit{time} = a_p n^p$ for $p = 2, 3, 4$, where a_p is determined by a least-squares fit. It appears that the SDP complexity with strategy I0 lies somewhere between $O(n^3)$ and $O(n^4)$.

In SpaseLoc, we partition the full problem into p subproblems of size q or less, where $p \times q = n$. We generally set q to be much smaller than n, ranging from 2 to around 10 in most of our simulations. If τ represents the execution time taken by the full SDP method for a 10-node network, in the worst case the computation time for SpaseLoc is $\tau \times O(p)$.

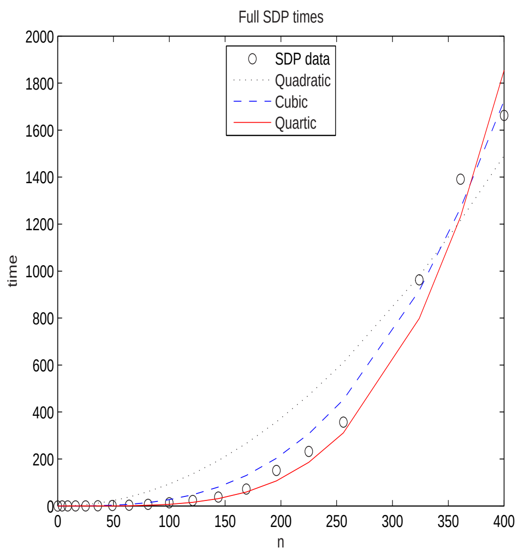

Figure 3.10: SDP computational complexity

Thus, SpaseLoc is really linear in p in theory. Since we can assume q to be a parameter ranging from 2 to 10, with worst case 2, we know that $O(p) = O(n/q) \leq O(n/2) = O(n)$. Now we can see that SpaseLoc's computation time is $O(n)$.

In the remaining subsections we choose the middle network size from Table 3.5 (nodes = 3969) to observe the effect of varying radio range, noise factor, and number of anchors.

3.3.4 Radio Range Impact

With a fixed total number of randomly uniform-distributed nodes (3969, of which 63 are anchors), Table 3.6 shows the direct impact of radio range on accuracy and performance. (Noise is not included.) When *radius* is reduced to 0.02, the number of unreachable sensors (outliers) reaches 302, which is unacceptable. Clearly, the simulation could assist sensor network designers in selecting a radio range to achieve a desired estimation error and algorithm speed.

Strategies I2 and I1 produce the same results. I2, I1, and I0 generate the same results except for radius of 0.020, 0.028, and 0.030, when I2 and I1 have more SDP calls than I0. I2 and I1 produce slightly reduced average error for radius of 0.028 and 0.030 but the same 95% error, and obviously, I2 and I1 take more time than I0.

Table 3.6: Radio range impact: nodes = 3969, anchors = 63, no noise.

radius	*sub_ size*	Out-liers	Error			95% Error			Time			SDP's		
			I2	I1	I0	I2	I1	I0	I2	I1	I0	I2	I1	I0
0.020	28	302	5.26e-3	5.26e-3	5.26e-3	3.77e-3	3.77e-3	3.77e-3	8.40	7.72	7.30	390	390	388
0.022	13	68	2.93e-3	2.93e-3	2.93e-3	1.49e-3	1.49e-3	1.49e-3	10.92	10.48	9.79	539	539	539
0.024	9	17	1.38e-3	1.38e-3	1.38e-3	2.28e-4	2.28e-4	2.28e-4	12.94	13.02	11.95	684	684	684
0.026	6	7	4.36e-4	4.36e-4	4.36e-4	1.36e-6	1.36e-6	1.36e-6	14.90	14.77	13.49	783	783	783
0.028	3	2	1.20e-4	1.20e-4	1.21e-4	1.01e-6	1.01e-6	1.01e-6	16.31	16.36	14.79	1295	1295	1294
0.030	3	0	3.04e-5	3.04e-5	3.08e-5	6.69e-7	6.69e-7	6.69e-7	18.12	18.15	16.23	1303	1303	1302
0.032	3	0	1.06e-5	1.06e-5	1.06e-5	4.10e-7	4.10e-7	4.10e-7	18.22	18.22	18.22	1302	1302	1302
0.033	3	0	6.32e-6	6.32e-6	6.32e-6	3.53e-7	3.53e-7	3.53e-7	19.51	19.51	19.51	1302	1302	1302

3.3.5 Noise Factor Impact

With constant *radius* (0.033) and the same randomly distributed nodes (3969), Table 3.7 shows the impact of noise conditions on accuracy and performance. We see that more noise in the network has a direct impact on estimation accuracy. Simulations of this kind may help designers determine the measurement noise level that will give an acceptable estimation error.

We also see that strategies I2 and I1 (with added inequality constraints) provide consistent improvement for both average and 95% error, at the price of increased execution time.

Table 3.7: Noise factor impact: nodes = 3969, anchors = 63, *radius* = 0.033, *subproblem_size* = 3.

noise_ factor	Error			95% Error			Time			SDP's		
	I2	I1	I0	I2	I1	I0	I2	I1	I0	I2	I1	I0
0.1	2.57e-3	2.58e-3	3.18e-3	1.99e-3	2.00e-3	2.23e-3	31.93	30.45	22.00	1907	1860	1303
0.2	4.55e-3	4.60e-3	5.60e-3	3.76e-3	3.79e-3	4.40e-3	43.21	37.52	22.61	2520	2310	1303
0.3	6.49e-3	6.60e-3	8.04e-3	5.49e-3	5.58e-3	6.63e-3	52.96	42.43	23.86	2879	2471	1301
0.4	8.25e-3	8.45e-3	1.01e-2	7.06e-3	7.21e-3	8.62e-3	66.46	48.19	26.07	3075	2533	1302
0.5	1.00e-2	1.03e-2	1.23e-2	8.56e-3	8.78e-3	1.07e-2	86.74	56.13	29.45	3278	2571	1302

3.3.6 Number of Anchors Impact

With constant *radius* (0.033) and the same randomly distributed nodes (3969), Table 3.8 shows the impact of the number of anchors on accuracy and performance. (Noise is not included.) As we can see, when the radio range is sufficiently large, the number of anchors in the network has a very slight impact, improving the estimation accuracy in general, with no obvious impact on algorithm speed. This analysis is beneficial for designers to avoid the cost of deploying unnecessary anchors.

Strategies I2 and I1 produce identical results. I2, I1, and I0 achieve exactly the same 95% error, although when there are fewer than 30 anchors, the added inequality constraints improve the average error consistently.

Table 3.8: Number of anchors impact: nodes = 3969, *radius* = 0.033, no noise, *subproblem_size* = 3.

Anchors	Error			95% Error			Time			SDP's		
	I2	I1	I0	I2	I1	I0	I2	I1	I0	I2	I1	I0
5	1.97e-5	1.97e-5	2.09e-5	4.06e-7	4.06e-7	4.06e-7	22.01	22.21	19.05	1320	1320	1319
10	1.98e-5	1.98e-5	2.10e-5	4.10e-7	4.10e-7	4.10e-7	21.77	21.83	19.07	1319	1319	1318
20	2.00e-5	2.00e-5	2.14e-5	3.65e-7	3.65e-7	3.65e-7	22.12	21.80	19.11	1315	1315	1314
30	5.53e-6	5.53e-6	8.24e-6	3.99e-7	3.99e-7	4.01e-7	21.93	21.87	19.30	1314	1314	1313
40	4.15e-6	4.15e-6	4.15e-6	3.62e-7	3.62e-7	3.62e-7	21.97	21.92	19.29	1309	1309	1309
50	3.64e-6	3.64e-6	3.64e-6	3.73e-7	3.73e-7	3.73e-7	22.02	22.23	19.36	1306	1306	1306
60	6.23e-6	6.23e-6	6.23e-6	3.60e-7	3.60e-7	3.60e-7	22.11	22.13	19.49	1303	1303	1303

3.3.7 Number of Anchors Impact with Noise

With the same *radius* (0.033) and the same randomly distributed nodes (3969), Table 3.9 shows the impact of the number of anchors on accuracy and performance when a *noise_factor* of 0.1 is included in the simulation. With this radio range (sufficiently large), more anchors give only slightly better estimation accuracy, with no obvious impact on algorithm speed in general. Compared with Table 3.8, the presence of noise does add execution time and cause more errors on average.

Regarding strategies I2, I1 and I0, the inequality constraints provide consistent improvement for both average and 95% error at the price of increased execution time. I2 requires more SDP calls than I1, but the improvement in estimation accuracy is very minimal.

Table 3.9: Number of anchors impact: nodes = 3969, *radius* = 0.033, *noise_factor* = 0.1, *subprob_size* = 3.

Anchors	Error			95% Error			Time			SDP's		
	I2	I1	I0	I2	I1	I0	I2	I1	I0	I2	I1	I0
5	2.71e-3	2.72e-3	3.31e-3	2.13e-3	2.14e-3	2.35e-3	32.61	30.80	21.93	1958	1920	1323
10	2.68e-3	2.68e-3	3.23e-3	2.06e-3	2.07e-3	2.28e-3	32.19	30.61	21.96	1916	1877	1321
20	2.66e-3	2.66e-3	3.27e-3	2.10e-3	2.10e-3	2.34e-3	32.09	30.42	21.93	1923	1881	1318
30	2.58e-3	2.59e-3	3.15e-3	2.01e-3	2.02e-3	2.22e-3	31.84	30.28	21.97	1885	1842	1313
40	2.61e-3	2.62e-3	3.29e-3	2.02e-3	2.03e-3	2.26e-3	32.41	30.51	22.27	1925	1862	1309
50	2.58e-3	2.60e-3	3.09e-3	2.03e-3	2.03e-3	2.21e-3	31.44	30.01	22.37	1856	1822	1307
60	2.56e-3	2.58e-3	3.18e-3	2.01e-3	2.02e-3	2.25e-3	32.04	30.42	21.90	1911	1870	1304

3.3.8 Anchors Impact with Noise and Lower *radius*

With the same randomly distributed nodes and the same noise level but lower *radius* (0.026), Table 3.10 shows the impact of the number of anchors on accuracy and performance. Increased number of anchors results in slightly better estimation accuracy with no obvious impact on algorithm speed in general. In addition, decreased radio range reduces the execution time and causes more errors on average compared with Table 3.9. At the same time we start to see outlier sensors.

The same conclusion can be drawn for I2, I1, and I0 as in section 3.3.7.

Table 3.10: Number of anchors impact: nodes = 3969, *radius* = 0.026, *noise_factor* = 0.1, *subprob_size* = 5.

Anchors	Out-liers	Error			95% Error			Time			SDP's		
		I2	I1	I0	I2	I1	I0	I2	I1	I0	I2	I1	I0
5	3	3.32e-3	3.33e-3	3.96e-3	2.44e-3	2.45e-3	2.81e-3	24.43	23.10	15.28	1437	1399	920
10	2	3.19e-3	3.19e-3	3.77e-3	2.39e-3	2.39e-3	2.75e-3	24.66	23.28	15.24	1470	1434	929
20	9	3.17e-3	3.18e-3	3.81e-3	2.30e-3	2.31e-3	2.66e-3	24.59	23.11	15.29	1452	1408	930
30	4	3.13e-3	3.14e-3	3.65e-3	2.30e-3	2.30e-3	2.61e-3	24.49	23.15	15.33	1429	1401	931
40	2	3.09e-3	3.09e-3	3.65e-3	2.30e-3	2.30e-3	2.63e-3	24.17	22.85	15.22	1389	1355	901
50	2	3.15e-3	3.16e-3	3.59e-3	2.28e-3	2.29e-3	2.56e-3	24.05	22.70	15.16	1397	1360	904
60	7	3.01e-3	3.02e-3	3.51e-3	2.22e-3	2.23e-3	2.51e-3	24.71	23.30	15.33	1429	1385	911

Chapter 4

Moving Sensor Localizations

The previous chapter explains how static sensors are being localized using SpaseLoc. In many applications, some of the sensors are dynamic. This chapter describes an algorithm for moving sensor localization. We show that SpaseLoc can be applied to a series of static localization problems to achieve the desired effect. Simulation results of this algorithm are then presented. Our experiment shows that our proposed dynamic sensor localization algorithm scales very well. For example, on a 2.4 GHz Pentium laptop the algorithm is capable of localizing 500 moving sensors within a 4000-node network every one-second time interval.

The last section discusses possible applications of the moving sensor localization algorithm, with an illustrated example simulating a bus transit arrival-time reporting system.

4.1 Moving Sensor Localization Method

The main difference between a static localization network and a dynamic one is that the distance measurements among sensors are constant in the first case, while some distance measurements are changing in the second case because of the sensor movements. The idea behind our moving sensor localization method is that at any given moment we can take a static view of the dynamic sensor network. For each snapshot of the network with all the sensors frozen in their positions and with the connection information among them, we can utilize the static localization method SpaseLoc to estimate the locations of the moving sensors at that particular instant. This provides an acceptable approximation if the computation time is less than the interval between snapshots.

4.1.1 Problem Formulation

We define *tracking instant* to be the instant of time that some sensors' locations need to be updated. There are two ways to trigger a tracking instant: either at a fixed frequency after a given time interval, or upon detection of sensor movements, which are revealed by changes in the distance measurement matrix $\widehat{d}$.

In order to track the moving sensors effectively, we need to isolate the sensors into two categories. One is called *static sensors*, the other is called *dynamic sensors*. At any given tracking instant, we assume that the static sensors are already localized by the previous iteration and can be used as anchors by this iteration. There are two situations in determining which sensors are dynamic. One situation is when the dynamic sensors are specified ahead of time. We update all of their locations at all tracking instants, regardless of whether they have moved or not since the previous instant. The other situation is when any sensor could be static or dynamic at any instant. The ones that have moved from the previous instant would be the dynamic ones. Under this situation, we find which ones are moving by searching the distance matrix $\widehat{d}$ for measurement changes (refer to section 4.1.2 for a method to do this).

As mentioned, at any given instant t we can treat the dynamic sensor localization problem as a static one and utilize SpaseLoc to localize the moving sensors at that instant. Corresponding to the SpaseLoc problem definition in section 1.1, we formulate the dynamic sensor localization problem as follows at tracking instant t.

Input

Total points: n, the total number of static and dynamic sensors, including anchors.

Unknown points: s sensors that are dynamic and whose locations $x_i \in \mathcal{R}^2$, $i = 1, \ldots, s$ are to be determined at tracking instant t.

Known points: m anchors that are static sensors and whose locations $a_k \in \mathcal{R}^2$, $k = s+1, \ldots, n$ are known at tracking instant t.

Distance measurements: The distance matrix $\widehat{d}$ consisting of $\widehat{d}_{ij}$ and $\widehat{d}_{ik}$ are the same as explained in section 1.1, except $\widehat{d}$ is partitioned according to

$$\widehat{d} = \begin{pmatrix} \text{DIST11} & m\_distance \\ m\_distance' & \text{DIST22} \end{pmatrix}, \tag{4.1}$$

where DIST11 is an s by s matrix representing the distance measurements among s dynamic sensors. In some applications, we do not use any distance measurements among moving sensors themselves. Under this condition, DIST11 will be all zeros, represented by *sparse*(s, s) in Matlab. *m_distance* is an s by m matrix representing the distance measurements among s dynamic sensors with the m static sensors. DIST22 is an m by m matrix representing the distance measurements among m static sensors themselves. They remain unchanged in between tracking instants if static sensors are continuing to be static.

Output

Locations: Estimated positions x_i for s dynamic sensors at tracking instant t.

4.1.2 Moving Sensor Identification Routine

As indicated in section 4.1.1, when the moving sensors are not known, we can identify the moving sensors by detecting the distance changes between two tracking instants $\hat{d}_t$ and $\hat{d}_{t+1}$. The following routine illustrates an approach to do this.

1. Define $D = \hat{d}_{t+1} - \hat{d}_t$.

2. Find a permutation P that sorts D's rows in descending order of the number of nonzero elements in each row. let's call the resulted matrix DR. At the same time, keep track of the corresponding row indexes.

3. Define
$$\Delta = PDP^T = \begin{pmatrix} \text{DELTA11} & \text{DELTA12} \\ \text{DELTA12}' & \mathbf{0} \end{pmatrix}. \tag{4.2}$$

4. Indexes corresponding to DELTA11 indicate all the moving sensors.

As we can see, equations (4.1) and (4.2) have one to one correspondence in matrix partitioning. The moving sensor identification routine aims to isolate the $\mathbf{0}$ matrix from Δ, that corresponds to DIST22. This is because static sensors do not move, their relative distance changes are always zero. Thus, we have DELTA11 representing the distance measurement changes among moving sensors, DELTA12 representing the distance measurement changes between moving sensors and static sensors, and DELTA22 representing the distance measurement changes among static sensors, which would be zero under no-noise condition. To allow for noise, we would use a tolerance in defining D. Elements smaller than the tolerance would be treated as zero.

Figure 4.1 shows an example with 7 sensors at time t in (a) and at time $t+1$ in (b). Let's assume distance measurements at t and $t+1$ are

$$\hat{d}_t = \begin{pmatrix} 0 & 0 & 0 & 1 & 1.5 & 0 & 0 \\ 0 & 0 & 0 & 1 & 1.5 & 1 & 0 \\ 0 & 0 & 0 & 0 & 1.5 & 0 & 0 \\ 1 & 1 & 0 & 0 & 1 & 0 & 0 \\ 1.5 & 1.5 & 1.5 & 1 & 0 & 1 & 1.5 \\ 0 & 1 & 0 & 0 & 1 & 0 & 1 \\ 0 & 0 & 0 & 0 & 1.5 & 1 & 0 \end{pmatrix}, \quad \hat{d}_{t+1} = \begin{pmatrix} 0 & 1 & 0 & 1 & 1.5 & 0 & 0 \\ 1 & 0 & 1 & 1.5 & 1 & 1.5 & 0 \\ 0 & 1 & 0 & 0 & 1.5 & 1 & 0 \\ 1 & 1.5 & 0 & 0 & 1 & 0 & 0 \\ 1.5 & 1 & 1.5 & 1 & 0 & 1 & 1.5 \\ 0 & 1.5 & 1 & 0 & 1 & 0 & 1 \\ 0 & 0 & 0 & 0 & 1.5 & 1 & 0 \end{pmatrix}.$$

We illustrate that the moving sensor identification routine should point out that sensors 2 and 6 are the moving ones. After applying the first two steps, we have

$$D = \begin{pmatrix} 0 & 1 & 0 & 0 & 0 & 0 & 0 \\ 1 & 0 & 1 & .5 & -.5 & .5 & 0 \\ 0 & 1 & 0 & 0 & 0 & 1 & 0 \\ 0 & .5 & 0 & 0 & 0 & 0 & 0 \\ 0 & -.5 & 0 & 0 & 0 & 0 & 0 \\ 0 & .5 & 1 & 0 & 0 & 0 & 0 \\ 0 & 0 & 0 & 0 & 0 & 0 & 0 \end{pmatrix}, \quad PD = \begin{pmatrix} 1 & 0 & 1 & .5 & -.5 & .5 & 0 \\ 0 & .5 & 1 & 0 & 0 & 0 & 0 \\ 0 & 1 & 0 & 0 & 0 & 1 & 0 \\ 0 & -.5 & 0 & 0 & 0 & 0 & 0 \\ 0 & .5 & 0 & 0 & 0 & 0 & 0 \\ 0 & 1 & 0 & 0 & 0 & 0 & 0 \\ 0 & 0 & 0 & 0 & 0 & 0 & 0 \end{pmatrix}.$$

After the third step, we have

$$\Delta = PDP^T = \begin{pmatrix} 0 & .5 & 1 & -.5 & .5 & 1 & 0 \\ .5 & 0 & 1 & 0 & 0 & 0 & 0 \\ 1 & 1 & 0 & 0 & 0 & 0 & 0 \\ -.5 & 0 & 0 & 0 & 0 & 0 & 0 \\ .5 & 0 & 0 & 0 & 0 & 0 & 0 \\ 1 & 0 & 0 & 0 & 0 & 0 & 0 \\ 0 & 0 & 0 & 0 & 0 & 0 & 0 \end{pmatrix}.$$

We know that DELTA11 corresponds to sensor indexes 2 and 6. From step 4, we know that these two are the moving ones, which indeed are the ones that moved from time t to time $t+1$.

There is a situation when the number of moving sensors is greater than the number of static sensors, and the moving sensors are all moving at the same direction at the same speed. In this case, the above routine won't apply. We illustrate this through an example in Figure 4.2. Sensors 2 and 6 both move diagonally with the same distance.

Let's assume distance measurements at t and $t+1$ are

$$\hat{d}_t = \begin{pmatrix} 0 & 0 & 0 & 1 & 1 & 0 & 0 \\ 0 & 0 & 0 & 1 & 0 & 1 & 0 \\ 0 & 0 & 0 & 0 & 1 & 0 & 0 \\ 1 & 1 & 0 & 0 & 1.5 & 1.5 & 0 \\ 1 & 0 & 1 & 1.5 & 0 & 0 & 0 \\ 0 & 1 & 0 & 1.5 & 0 & 0 & 1 \\ 0 & 0 & 0 & 0 & 0 & 1 & 0 \end{pmatrix}, \quad \hat{d}_{t+1} = \begin{pmatrix} 0 & 1.5 & 0 & 1 & 1 & 0 & 0 \\ 1.5 & 0 & 1.5 & 1 & 1 & 1 & 1.5 \\ 0 & 1.5 & 0 & 0 & 1 & 1 & 0 \\ 1 & 1 & 0 & 0 & 1.5 & 0 & 0 \\ 1 & 1 & 1 & 1.5 & 0 & 1.5 & 0 \\ 0 & 1 & 1 & 0 & 1.5 & 0 & 1 \\ 0 & 1.5 & 0 & 0 & 0 & 1 & 0 \end{pmatrix}.$$

After applying the moving sensor identification routine, we have

$$\Delta = \begin{pmatrix} 0 & 0 & 1 & 1.5 & 1.5 & 0 & 1.5 \\ 0 & 0 & 1.5 & 1 & 0 & -1.5 & 0 \\ 1 & 1.5 & 0 & 0 & 0 & 0 & 0 \\ 1.5 & 1 & 0 & 0 & 0 & 0 & 0 \\ 1.5 & 0 & 0 & 0 & 0 & 0 & 0 \\ 0 & -1.5 & 0 & 0 & 0 & 0 & 0 \\ 1.5 & 0 & 0 & 0 & 0 & 0 & 0 \end{pmatrix}.$$

We know that DELTA11 corresponds to sensor indexes 2 and 6, from step 4 we know that these two are the moving ones, which indeed are the ones that moved from time t to time $t+1$.

As we see, DELTA11 is also a zero matrix. This is because there is no relative movement between sensor 2 and sensor 6. Since DELTA22 has bigger dimensions than DELTA11, we are still able to identify the correct moving sensors. However, if the number of moving sensors moving at the same speed and in the same direction is bigger than the number of static sensors, the algorithm will mistakenly take the static sensors as moving ones simply because the routine will put the bigger zero partition at the lower-right part of the Δ matrix. This is not a concern for most applications because static sensors will generally outnumber the moving ones, and it is rarely the case that all moving sensors would move at the same speed in the same direction at the same time.

4.1.3 Moving Sensor Localization Procedure

The moving sensor localization procedure contains two main steps. The first initializes all sensors' positions at network startup. The second step is repetitive formulation of SDP models with updated distance measurements and then calling of SpaseLoc to localize moving sensors for the instant the new measurements were taken.

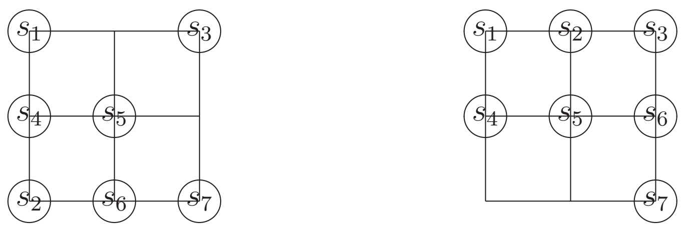

(a) At time t. (b) At time $t + 1$.

Figure 4.1: An example of moving sensors.

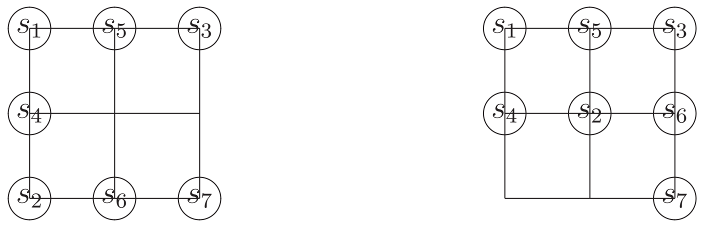

(a) At time t. (b) At time $t + 1$.

Figure 4.2: Sensors moving at same speed.

M1 Initialize all sensors' locations.

This step assumes that none of the sensors is moving. We are given the number of sensors, number of anchors, anchor locations, and the distance measurements matrix $\widehat{d}$. SpaseLoc is called to estimate the locations of all sensors.

M2 Track dynamic sensors' locations at every tracking instant.

Repeat the following steps at each tracking instant t:

- Determine moving sensors: identify s dynamic sensors and m static sensors (anchors) using moving sensor identification routine in section 4.1.2.
- Update distance matrix $\widehat{d}$: replace only the *m_distance* portion, and the DIST11 portion if distance measurements among moving sensors are used.
- Formulate new SDP model with updated sensors, anchors, and $\widehat{d}$.
- Call SpaseLoc to obtain s dynamic sensors' locations at the given tracking instant.

In most moving sensor localization applications, seeking the best estimation accuracy of the moving sensors' locations might prove costly to real-time performance of the algorithm. Our experiments in Chapter 3 show that SpaseLoc with the subsensor selection priority rules introduced in section 3.1.3 generally achieves high estimation accuracy under low connectivity and noise conditions. However, the moving sensor localization slows down by about 20% for most of our test runs when we implement the priority rules listed in Table 3.1. Hence, when there is sufficient connectivity among sensors in the network and we trust that the network is not too noisy, it may be advantageous to simplify the subsensor selection priority rules for greater real-time performance. We can achieve this by reducing the total number of priorities for sensors and the number of acting levels for acting anchors.

4.2 Moving Sensor Simulation Results

This section presents simulation results for the moving sensor localization algorithm. The simulation setup is the same as in section 3.3 using strategy I0 except with added information on dynamic sensors and distance updates at every tracking instant.

The simulation assumes a fixed number of moving sensors, and a given number of time intervals of fixed length over which the dynamic sensors are to be tracked. The movement pattern could be random or along some predefined path.

To simulate random movement of dynamic sensor i, we calculate the sensor's position at tracking instant $t+1$ to be a random step from 0 to a maximum step of $\mathit{move\_size}$. The following formula is used to generate sensor i's next position from its current position $PP^t(:,i)$:

$$PP^{t+1}(:,i) = PP^t(:,i) + \mathit{move\_size} * (2 * \mathit{rand}(2,1) - 1).$$

Any points that fall outside the simulation area are regenerated.

As an example, Figure 4.3 shows the simulation results of *one* sensor moving diagonally through a 400-node randomly uniform-distributed sensor network. A red dot represents the current position of the moving sensor, and the trail of yellow dots represents the trace of where the moving sensor has been. Following the moving sensor localization procedure in the previous section, the network with 400 total nodes and 20 anchors is first localized by SpaseLoc. Initially, the moving sensor is intentionally positioned at the bottom left corner. Then at every time interval, the sensor moves with a step of +0.1 in both x and y coordinates. The diagram shows the result of 10 movements. We see that the algorithm localizes all 400 sensors initially with virtually no errors, and

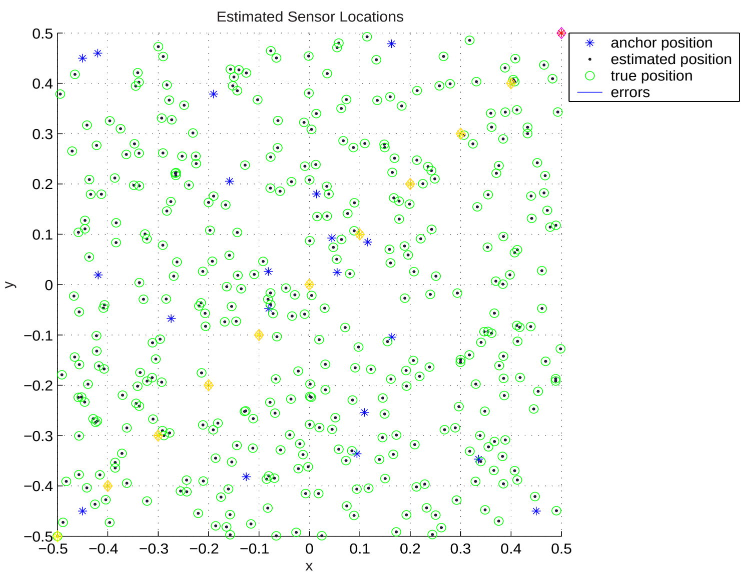

Figure 4.3: One moving sensor, 400 total points, 20 anchors, *radius* 0.1078, no noise

then tracks the moving sensor's 10 steps with the same high accuracy.

4.2.1 Moving Sensor Performance: 10% Moving Sensors

Table 4.1 shows simulation results for 10% of the sensors moving randomly with a uniform distribution among a total of 49 to about 4000 randomly uniform-distributed sensors. The number of anchors and the *radius* both change with the number of sensors being simulated in order to maintain a similar connectivity level. Noise is not included in this simulation. Error and Time in the table represent average errors and localization time per tracking instant for all moving sensors averaged over at least 20 tracking instants.

As we can see, the execution time increases only linearly with the number of dynamic sensors in the network. The Error doesn't display a pattern because it depends more on the connectivity level of all sensors.

Table 4.1: Moving sensor performance: 10% moving sensors

Nodes	Moving	Anchors	*radius*	*sub_size*	Error	Time (sec)
49	5	7	0.3412	3	1.7e-4	0.011
100	10	10	0.2275	3	2.1e-8	0.020
225	20	15	0.1462	3	1.1e-8	0.039
529	50	23	0.0931	3	2.4e-8	0.095
1089	100	33	0.0620	4	1.8e-6	0.190
2025	200	45	0.0451	4	2.8e-5	0.426
3969	400	63	0.0330	5	7.2e-6	0.778

4.2.2 Effect of Number of Moving Sensors

With a fixed total number of randomly uniform-distributed nodes (3969, of which 63 are anchors), Table 4.2 shows the direct impact of the number of randomly moving sensors on accuracy and performance. (Noise is not included.)

As we expected, Error increases with the number of moving sensors because at each tracking instant, any moving sensor cannot be used as an anchor. If the number of original anchors is held fixed at 63, the effect of more moving sensors is similar to having less available anchors, and thus lower connectivity levels. As the number of moving sensors increases to 1250 (31%) and beyond, we start to see outliers. With 50% moving, 10 sensors are unlocalizable.

Table 4.2: Effect of number of moving sensors: Anchors = 63, *radius* = 0.033, *subproblem_size* = 9, no noise

Nodes	Moving	*sub_size*	Error	Outliers	Time (sec)
3969	1	3	6.99e-8	0	0.0080
3969	5	3	4.31e-8	0	0.0185
3969	10	3	8.59e-8	0	0.0305
3969	20	3	4.70e-8	0	0.0476
3969	30	3	7.09e-8	0	0.0666
3969	40	3	1.28e-7	0	0.0872
3969	50	3	7.83e-8	0	0.1037
3969	100	4	7.26e-8	0	0.2002
3969	200	4	7.94e-8	0	0.3956
3969	300	4	8.04e-8	0	0.5758
3969	400	5	1.69e-7	0	0.7782
3969	500	5	5.53e-6	0	0.9615
3969	600	5	2.56e-5	0	1.1557
3969	700	5	1.97e-5	0	1.4315
3969	800	5	3.94e-5	0	1.6281
3969	900	5	6.51e-5	0	1.8387
3969	1000	5	8.81e-5	0	1.9545
3969	1200	7	1.61e-4	0	2.4104
3969	1250	7	3.01e-3	1	0.1357
3969	1400	7	3.01e-3	1	0.1522
3969	1500	7	3.04e-3	1	0.1628
3969	1600	7	3.06e-3	1	0.1723
3969	1800	7	3.33e-3	3	0.1974
3969	2000	7	3.54e-3	10	0.2203

The execution time displays a linear increase with the number of moving sensors until around 1200. From 1250 onwards, we see a sudden drop of execution time. This is because, at this connectivity level, the number of moving sensors connected to less than three anchors increases dramatically. As explained in Chapter 3, SpaseLoc calls the geometric subroutines instead of the SDP solver to localize sensors with less than 3 anchors connections. The geometric subroutines can localize this configuration of sensors significantly faster than the SDP solver.

4.2.3 Sensor Speed versus Number of Sensors Algorithm Can Track

As we understand, the speed of the moving sensors does not impact how quickly the algorithm can track them. The issue is the accuracy of the moving sensor's estimated position versus the time interval between the tracking instants.

For example, with a 1-second time interval, tracking a walking person who carries a sensor can be a lot more accurate than tracking a moving car that carries a sensor, because at the end of the 1-second interval, a person with a maximum walking speed of 3 miles an hour can be at most 1.4 meters away from his previous interval, but a car traveling at 60 miles an hour could be 27 meters away. In order to achieve the same estimation accuracy, we would have to reduce the tracking instant interval for sensors traveling at a higher speed. But a smaller time interval means fewer dynamic sensors that the algorithm can keep track of.

Table 4.3 lists the simulation results for tracking the maximum number of sensors with various traveling speeds at different levels of position estimation accuracy. The column under "Speed" indicates the sensors' maximum traveling speed, ranging from 2.24 mph to 600 mph. The first row of the table lists estimation accuracy, ranging from 1 meter to 100 meters, and there are two columns associated with each level of estimation accuracy:

- The column labeled "Time" represents the time interval (in milliseconds) during which a dynamic sensor moves the distance indicated by the estimation accuracy in the row above and at the speed indicated in the left-hand column. This time defines the frequency for estimating the maximum number of moving sensors.

- The column labeled "#" gives the maximum number of moving sensors; that is, the number of sensors that the algorithm can keep track of with the specified accuracy every specified number of milliseconds interval.

For example, the algorithm is capable of tracking 387 people walking at 3 miles an hour within 1 meter accuracy at 74.6 millisecond intervals, whereas only 2 trains traveling at 200 mph could be tracked with the same accuracy at 1.12 milliseconds intervals. Alternatively, the algorithm could keep up with one airliner traveling at 600 mph with

Table 4.3: Number of moving sensors that can be tracked versus speed of movement: Anchors = 63, *radius* = 0.033, *subproblem_size* = 9, no noise, speed in miles/hr, time in milliseconds

Speed	1m		2.5m		5m		10m		20m		50m		100m	
	Time	#	Time	#	Time	#	Time	#	Time	#	Time	#	Time	#
2.24	100	520	250	1200	500	-	1000	-	2000	-	5000	-	10000	-
3	74.6	387	186	900	373	-	746	-	1492	-	3729	-	7458	-
5	44.7	231	112	577	224	1100	447	-	895	-	2237	-	4475	-
10	22.4	112	55.9	287	112	577	224	1100	447	-	1119	-	2237	-
20	11.2	56	28.0	141	55.9	287	112	577	224	1100	559	-	1119	-
40	5.59	24	14.0	68	28.0	141	55.9	287	112	577	280	-	559	-
60	3.73	14	9.32	43	18.6	89	37.3	189	74.6	387	186	900	373	-
80	2.80	8	6.99	31	14.0	68	28.0	141	55.9	287	140	650	280	-
100	2.24	7	5.59	24	11.2	56	22.4	112	44.7	231	112	577	224	1100
150	1.49	4	3.73	14	7.46	33	14.9	72	29.8	151	74.6	387	149	700
200	1.12	2	2.80	8	5.59	24	11.2	56	22.4	112	55.9	287	112	577
250	0.89	1	2.24	7	4.47	18	8.95	41	17.9	88	44.7	231	89.5	463
300	0.74	0	1.86	5	3.73	14	7.46	33	14.9	72	37.3	189	74.6	387
400	0.56	0	1.40	3	2.80	8	5.59	24	11.2	56	28.0	141	55.9	287
500	0.45	0	1.12	2	2.24	7	4.47	18	8.95	41	22.4	112	44.7	231
600	0.37	0	0.93	1	1.86	5	3.73	14	7.46	33	18.6	89	37.3	189

2.5 meter accuracy at 0.93 millisecond intervals. As many as 14 airliners could be tracked with 10 meter accuracy every 3.73 milliseconds.

4.3 Applications of the Moving Sensor Localization Algorithm

Dynamic sensor networks may find applications in many areas such as battlefield intelligence, police patrol car tracking, taxi dispatching, car tracking in a car-share network, road traffic monitoring, personnel monitoring, school bus tracking, and bus transit schedule tracking. Most of these applications can be implemented using the global positioning system (GPS) [9]. However, as we discussed in Chapter 1, several drawbacks of GPS may prevent its successful use on a wide-range of real-time applications.

This section discusses how our dynamic sensor localization algorithm can be utilized in such applications, with an implemented example simulating a bus transit scheduling system. These applications all assume that the surrounding sensor network has sufficient connectivity.

4.3.1 Battlefield Tracking System

An ad hoc wireless sensor network can be used to form a battlefield tracking system. Static sensors can be spread around a battlefield by a helicopter. They may be used to track enemy forces or friendly forces (depending on the type of sensor and who is currently occupying the territory).

All soldiers could wear dynamic sensors in order to determine where their comrades are in the adjacent neighborhood. At the same time, commanders could have a real-time view of their troops' positions by using our localization algorithm in order to assess the current situation and direct the next move.

From Table 4.3, assuming soldiers run at a maximum speed of 5 miles an hour within a 4000-node sensor network, we can see that our dynamic algorithm is capable of tracking up to 231 soldiers within 1 meter accuracy in 44.7 millisecond intervals; up to 577 soldiers within 2.5 meter accuracy every 112 milliseconds; and up to 1100 soldiers within 5 meter accuracy every 224 milliseconds.

Another need in the battlefield is to track moving vehicles. In a hostile environment, it can be difficult to communicate with the vehicle directly. We can set predefined moving patterns or paths the vehicles are supposed to follow. Through the tracking traces of the moving vehicles, the command center can analyze the environment each vehicle is in, and how safe the vehicle is likely to be.

4.3.2 Police Patrol Car Monitoring and Dispatching System

If we install enough static sensors to form an ad hoc wireless network for the patrol environment, and if every police patrol car carries a sensor, the moving sensor localization algorithm could find out where each patrol car is at each given instant. These locations could be used to determine the nearest p police cars to a crime or accident scene, in order to minimize the time for the p cars to arrive at the scene.

From Table 4.3, assuming that cars drive at a maximum of 100 mph within a 4000-node sensor network, we see that our dynamic algorithm is capable of tracking up to 112 patrol cars with a 10 meter accuracy in 22.4 millisecond intervals, up to 231 cars with a 20 meter accuracy every 44.7 milliseconds, up to 577 cars with a 50 meter accuracy every 112 milliseconds, and so on.

Similar logic can be applied to taxi monitoring and dispatching. If we have all taxis carry dynamic sensors, we can easily find the idle taxi nearest to the customer requiring service.

4.3.3 Car Tracking in a Car-share Network

Car-sharing networks have been successfully deployed in Europe [14] and are becoming popular in North America [30]. In a car network, a pool of cars are scattered around the city to be shared by the network members. Ideally, a member should carry some type of wireless device such as a PDA or a cell phone to locate and reserve the nearest idle car anytime the person needs to rent it.

We can design an ad hoc wireless sensor network around the car-sharing network. Each car in the network would carry a dynamic sensor, so at any time we would be able to monitor the car's location. At the same time, we also need to know the location of the person needing the car rental in order to find the nearest available car. If we assume the future ubiquitous presence of user-portable wireless data devices (like PDAs or cell phones), we can envisage installing a dynamic sensor in the person's hand-held wireless device. For privacy reasons, the person could turn off the sensing device if he/she is not using the car-sharing service. Our dynamic sensor localization algorithm could be used in this system to track the locations of both cars and the people who are currently looking for a shared car.

A similar method could be used for bike-sharing networks. Some cities like Copenhagen already offer bicycles for free use from a public pool. The service should become more widely used if the matching of people to free bicycles can be implemented more efficiently.

4.3.4 Traffic Monitoring System

There have been many studies on the automated highway system, especially on the development of an inter-vehicle communication system [28]. Such a system could be used for dynamic traffic routing, driver assistance and navigation, co-operative driving and platooning [41]. Singh [42] presents test results for an inter-vehicle communication system based on a wireless LAN 802.11b network. The following proposes an alternative approach to traffic monitoring.

Suppose static sensors are spread around major highways to form ad hoc wireless sensor networks, and suppose cars carry dynamic sensors. We can evaluate highway traffic conditions by tracking the movement of sensors within the cars. For example, by looking at the current traces of most cars traveling on a particular highway, we can determine the average actual speed of the cars. Comparing this speed with the maximum speed of the highway, we can conclude if the highway is jammed or not. One by one, we would be able to put all highways' real-time traveling speed on a map maintained by a central computing facility. The real-time speed map could be used by police patrol officers, or by fire-fighters to predict a problem even before people could report a problem on the road. At the same time, if a car's display is connected to the central computing facility, the car driver could download any portion of the map in real-time to decide on the best option to his destination.

An even more proactive approach is to predefine the route a particular driver is to take to his destination. If there are abnormal conditions on any road along the route, the driver would be notified with a number of top alternative routes with estimated total distance and travel times computed for him/her. An alternative is to mark the actual speed on the map in real-time instants for the driver to reference while driving. We could label different traffic conditions of highways according to the speed detected by the sensors. For example, we could have 5 levels to represent traffic conditions, with level 1 being totally smooth and level 5 being totally blocked.

4.3.5 Personnel Monitoring System

Static sensors can be installed to form an ad hoc wireless sensor network in a limited area such as a university campus, a corporate complex, a retail mall, or a prison camp to monitor people's movements for different purposes.

One example application is the prisoner monitoring system. Sensors could be worn (or imbedded if permitted by law) by prisoners so that all their movements are actively monitored. Legitimate movements and locations are ignored by the system, but if any prisoner appears to be too near the fence, for example, the system could alarm relevant personnel immediately.

4.3.6 Bus Transit Arrival Reporting System

For most city's public bus transit systems, there are fixed schedules for each bus route. However, uncertainties on the road often cause the bus to be delayed, leaving new passengers waiting. In some cities with harsh climates, such as in Ottawa, Canada, there is a phone number allocated for each bus stop. Passengers can phone for the arrival times of the next coming bus and the one after that before heading to the bus stop, thus avoiding a long wait in the cold during winter times. However, the times given to the callers are mostly from a pre-recorded arrival schedule. If heavy traffic causes a certain bus to be late, the caller would still be informed about the scheduled time, not the true delayed time of arrival. It would be ideal if the schedule for each phone number and bus stop were updated with more accurate arrival times based on the current locations of the next two buses.

We propose a bus transit arrival reporting system utilizing our dynamic sensor localization algorithm. We assume each bus stop would be equipped with a static sensor, and all buses would carry a dynamic sensor. If the distance between bus stops is bigger than the sensor's sensing range, we can add more static sensors in between to form an ad hoc wireless sensor network. At each tracking instant, the algorithm would be able to estimate each bus's location in the network. We can calculate the estimated arrival times of the two buses closest to a particular stop according to average traveling speed, or if we have current road condition detection, we could use the current traveling speed to estimate the expected arrival times of the two buses. This information is fed back to the bus stop and passed on to the callers. We assume the future ubiquitous presence of user-portable wireless data device (PDA or cell phone), or a fixed LED/LCD display at each stop, to inform riders of the anticipated wait time for their current location.

Figure 4.4 shows a simulation run of a sample bus transit network. In this ad hoc network, 400 green circles represent static sensors located at all bus stops and/or in between bus stops, of which 39 are anchors with their locations known ahead of time. These anchors are positioned in the middle of the network horizontally and vertically as represented by the blue stars. Each adjacent two rows or columns of sensors represent a vertical or horizontal street. Two buses are running on each street (represented by red circles) with their initial positions at opposite ends of the street. (They are yellow in the figure because yellow represents the traces of where a bus has been.)

We can simulate the movement of different buses with different step sizes to represent different maximum traveling speeds that might be imposed on different streets.

The dynamic sensor localization algorithm initially localizes all sensors, including the static sensors at all bus stops and the dynamic sensors on all buses. Then with a given time interval, we generate random directional movements for all buses (follow a random uniform distribution), and the dynamic sensor localization algorithm tracks all dynamic sensors for a sequence of time intervals. The circles are the real positions of all sensors. The dots are estimated locations given by our algorithm (black dots represent static sensors, red dots the moving sensors, and yellow dots the traces of moving sensors). The figure shows the end result after 30 time intervals.

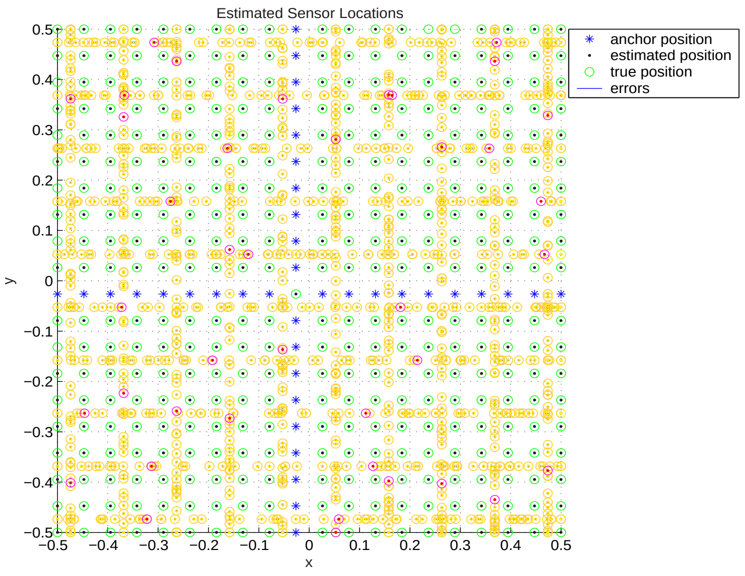

Figure 4.4: Bus transit simulation, 400 total points, 38 anchors, radius 0.0819, no noise

Chapter 5

Distributed Algorithm For Clustered Networks

As we have seen from previous discussions, existing localization methods have been practical for only moderate-sized networks (up to a few hundreds nodes), and SpaseLoc maintains efficient and accurate position estimation for networks with up to ten thousand sensors on a laptop computer with 2.4 GHz CPU and 1GB of system memory.

The variety and scale of future network applications begs for software that can fully utilize the multitude of sensor devices currently being created. We would like to achieve an *enabling technology* analogous to the device technology itself. Achieving the stated objective for sensor localization—efficient and accurate localization for networks of arbitrary size—is an *essential requirement* for tomorrow's wireless sensor networks to provide their intended services. Thus, a further quantum leap is necessary to achieve true scalability. The need is even more imperative when we recognize that the processing power for the devices that may be used to run the localization algorithm in sensor networks of the near future will be far less than the Pentium laptop that achieved our stated results. Distributed computation becomes essential, as we propose in this chapter.

In this chapter, we first discuss the need for a distributed approach to sensor localization and the intrinsic clustering architecture of large sensor networks; then we introduce a hierarchical computational platform that can utilize distributed processing. Computational results for the proposed algorithm for a particular application are presented in the last section.

5.1 The Need for Distributed Computing

It is a scientific breakthrough that SpaseLoc is able to solve such large problems with excellent speed and accuracy. Nevertheless, our experiments show that when the number of sensors reaches beyond 10000 on our particular laptop, the memory requirement becomes excessive. The single-processor environment with virtual memory is not able to proceed effectively for problems of that size.

Thus, in real network applications, SpaseLoc may face two challenges:

- The predicted explosive deployment of wireless sensor networks may involve tens of thousands of sensors per network in the future. In such large networks, centralized computing is simply not practical. Another quantum leap in algorithm performance is urgently needed.

- In some applications, there is no device in the network as powerful as even a 2GHz laptop computer to run the sensor localization algorithm (like SpaseLoc). We may have to choose multiple smaller devices, which are used as sensors at the same time, to compute the sensors' locations collectively in the network. These devices may be hand-held devices like PDAs, which currently have very limited processing speed and system memory (probably only 30MHz and 256KB RAM). This forces us to think about computing the sensors' locations distributively among multiple devices.

5.2 Clustered Sensor Network Architecture

Fortunately, large sensor networks are generally inherently clustered by design. One such network proposed by Heinzelman et al. [18] exhibits the following characteristics:

- A hierarchical adaptive clustering architecture is recommended for scalability and energy saving.

- Sensors are partitioned into clusters. Each cluster has a cluster head, and each sensor belongs to one cluster.

- Dynamic cluster head selection is adopted. All cluster heads broadcast announcements at system startup. When a sensor hears these announcements, it chooses the cluster head from which the strongest signal is received. Essentially, a sensor selects the nearest cluster head.

- Application software, for example the localization algorithm, resides in the cluster head.
- There is a multi-layer communication hierarchy. Sensors communicate only with their own cluster heads. All cluster heads communicate with a central command center. Depending on the particular implementation, cluster heads may be able to communicate directly among themselves.

The proposed distributed sensor localization algorithm makes use of the clustering architecture by adopting a hierarchical method in a distributed computing environment, in order to address networks of any size and topology.

5.3 Distributed Sensor Localization Approach

Taking advantage of the intrinsic clustering of large networks, such as the one proposed in section 5.2, we propose a hierarchical computational scheme that can utilize distributed computing for sensor localization. SpaseLoc remains a vital yet intrinsically sequential tool at a lower level. Scalability is achieved through parallelism at the cluster head level.

The proposed distributed algorithm utilizes three levels of machine devices as imposed by the clustered sensor network architecture, and three levels of software (algorithm) structure.

The top-level machine is regarded as a central command center and has relatively more computing power, like a desktop PC. The second-level machines constitute the cluster level; they are the cluster heads. These machines are generally devices that have less computing power, like a current PDA. The lowest level devices are the sensors that communicate with their own cluster heads. These devices generally don't handle any applications. They have signal communications with their neighboring sensors and with their own cluster heads to report distance information, for instance.

The three levels of software structure are as follows:

distributed algorithm,
cluster-level algorithm,
subproblem algorithm.

The top-level algorithm is the distributed algorithm that we are proposing. It is responsible for distributing a subset of anchors, sensors, and connection information to each cluster head in order for each cluster head to know when and how to conduct sensor localization at the cluster level. It is in charge of the overall sequencing and synchronization of parallel processes. Sequencing rules are created for all clusters according to their priorities; see section 5.3.2. A synchronization procedure is formulated in order to impose the sequencing rules. Typical applications can have thousands or even tens of thousands of sensors being controlled by this command center.

The second level, which is the cluster-level algorithm, utilizes SpaseLoc as a cluster-level problem solver. Typical applications can have hundreds of sensors in each cluster. SpaseLoc is very effective in terms of computational speed and accuracy at this level.

SpaseLoc further adaptively separates the problem into a sequence of smaller subproblems and calls an SDP solver iteratively as we have discussed in Chapter 3. The SDP solver in turn is effective at this much lower level.

Careful considerations need to be in place for the distributed algorithm to achieve network-wide optimal speed without compromising accuracy. For example, the sequencing and synchronization of clusters allow them to be processed in parallel in the correct order. The following subsections explain in detail how sequencing and synchronization works, and then introduce our distributed algorithm.

5.3.1 Sequencing of Parallel Processes

A sequencing rule deals with the order in which all the clusters run the localization algorithm. It is there to make sure that certain favorable clusters get localized first before some other clusters so that estimation error is minimized. At the same time it ensures that clusters in similar favorable conditions get localized in parallel to optimize computation time.

The sequencing of clusters becomes necessary because the distribution of anchors is often not uniform across the whole network. For example, in order to save cost, network designers might allocate enough anchors to localize the sensors in only some of the clusters. Other clusters might not have sufficient anchor density to localize their own sensors by themselves. In this situation, information regarding anchors and acting anchors is needed from neighboring clusters. (*Neighboring clusters* $\{c_1, c_2, \dots, c_q\}$ of a cluster c include any cluster that has a sensor within sensing range of some sensor in cluster c.) This information may become available only after the neighboring clusters' localizations run in the previous computation (iteration). Thus, if all clusters are processed in parallel without careful ordering, some of the clusters may fail to localize all their sensors, or to localize with lower accuracy than if they had waited for more information when available from their neighboring clusters.

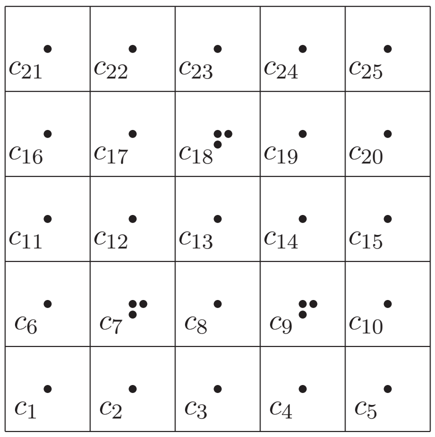

Figure 5.1: An example of a sensor network with 25 clusters.

For example, Figure 5.1 shows a sensor network of 25 squared clusters $\{c_1, c_2, \dots, c_{25}\}$. The following are assumptions for the network:

- Each cluster head is an anchor and is located in the center of each square cluster; denoted by a black dot (●) in the picture.
- Three clusters $\{c_7, c_9, c_{18}\}$ have two extra anchors (denoted by two extra black dots (●) in the picture) that are within communication range of each other and their cluster head.
- All other sensors in the network (not shown in the picture) are almost uniformly distributed around the network. (Of course, we don't know this before the localization).
- The square borders for each cluster are assumed; they don't necessarily have to follow the exact square shape. We draw them that way for easy display.

Given the above conditions, we can clearly see that at the beginning of the localization, only the three clusters $\{c_7, c_9, c_{18}\}$ with three original anchors should be localized first. And since they are in similar anchor conditions, they can all be processed in parallel. All the other clusters have only one anchor at this time (iteration); they would not achieve good estimation accuracy if they were localized before $\{c_7, c_9, c_{18}\}$ are localized. We also notice that clusters $\{c_{21}, c_{25}\}$ should wait longer than the rest of the one-anchor clusters, until after one of their neighboring clusters has been localized.

We propose a priority-driven cluster-labeling approach to address this sequencing need, as presented in the next subsection.

5.3.2 Cluster Priority

In our approach, all clusters are labeled with numerical values, called *cluster priorities*, to indicate their sequencing order. Clusters with a smaller priority value have the higher priority and are localized before clusters with a bigger priority value. Clusters with the same priority can be localized in parallel at any time.

Many factors can be considered in classifying the clusters' priorities. Here are some important ones:

1. *Original anchor density in the cluster.*

   For better accuracy, a cluster with higher anchor density within its own cluster should be considered higher priority than the one with lower anchor density. In Figure 5.1, cluster c_{18} with 3 original anchors is assigned higher priority than say clusters c_{16}, c_{17}, c_{22}, which have only one original anchor within each cluster.

2. *The cluster's neighbor-priority and the number of neighboring clusters with that priority.*

   We define the a cluster's *neighbor-priority* to be the the highest priority among all the cluster's neighboring clusters. Let's assume a cluster c has neighboring clusters $\{c_1, c_2, \ldots, c_q\}$, the highest priority among all q clusters is h, and the number of clusters with this priority h is p. We say that cluster c's neighbor-priority is h, and there are $p \leq q$ neighboring clusters with that priority.

   If cluster c has to rely on its neighboring clusters' information to localize itself, a higher neighbor-priority h will give cluster c a higher priority than that of a cluster with a lower neighbor-priority h. For example in Figure 5.1, among all of cluster c_{23}'s neighboring clusters $\{c_{17}, c_{18}, c_{19}, c_{22}, c_{24}\}$, c_{18} has the highest priority. So the cluster priority associated with c_{18} determines the neighbor-priority for c_{23}. We know from the previous factor that cluster c_{18} has a higher priority than any of c_{21}'s neighboring clusters $\{c_{16}, c_{17}, c_{22}\}$. So, cluster c_{23} will be assigned a higher priority than cluster c_{21}.

   When two clusters have the same neighbor-priority h, the one with the bigger number p will rank with higher priority. For example in Figure 5.1, clusters c_{19} and c_{13} have the same neighbor-priority, both defined by cluster c_{18}'s priority. However, we know that cluster c_{13} has 3 neighboring clusters at this priority $\{c_7, c_9, c_{18}\}$, so $p = 3$ for cluster c_{13}, while $p = 1$ for cluster c_{19}. Therefore, cluster c_{13} is assigned higher priority than c_{19}.

3. *The priority and number of anchors that are in the cluster's neighboring clusters and are within any of the cluster's sensors' radio range.*

   Let's define a cluster's *neighboring anchors* to be all the anchors in the cluster's neighboring clusters that have distance measurements with any sensor in this cluster. A cluster associated with more neighboring anchors and with more neighboring anchors at lower anchor levels will be assigned a higher priority than one with fewer neighboring anchors and with more neighboring anchors at higher anchor levels.

Depending on the applications, designers may choose to consider all these factors in determining the cluster priorities, or simply select any combination of them. Different granularity of the cluster priorities can be achieved by specifying a range of the above factors rather than specific values.

We give an example for a specific wireless sensor network application that utilizes the first two criteria in assigning a cluster's priority. A wireless sensor network may be used to detect environmental hazards over a region by using individual sensors in the network to detect smoke, chemicals or temperatures, etc. Sensors are generally spread roughly on regular square grids across the protected area according to hazard detection regulations. For example, the hazard detection rule may require that all detectors (sensors) must be within a certain distance of another detector (sensor) to guarantee coverage.

We wouldn't need localization if all sensors could be placed perfectly uniformly on the regular square grids at installation. In practice, only certain required anchors are put at known spots; the sensors are placed roughly within the regulated distance without exact knowledge of their locations. This might be caused by the fact that certain sensors have to be further apart or closer to each other because of installation barriers such as a wall. Or, it might be more efficient or convenient to install sensors on certain landmarks, such as on doors, windows, etc. At system startup, we would need to run the localization algorithm to determine all the sensors' locations.

Typically, this type of network is divided into clusters, each with a cluster head. The cluster head also acts as an original anchor. For most applications, cluster heads are too far apart from each other to be used as a group of 3 anchors to localize other sensors. For localization to function, one or more of the clusters must add at least two extra anchors that are within its cluster head's and each other's certain communication range (usually within radio range of each other would be sufficient). The example shown in Figure 5.1 represents one such network.

Combining criteria 1 and 2 for assigning cluster priority, we give the following routine designed to determine the cluster priority for such a network.

Cluster Priority Assignment Routine:

1. Find all clusters that have 3 original anchors, and assign all these clusters priority 10 (the smallest priority value but the highest priority).

   For example, in Figure 5.1, clusters $\{c_7, c_9, c_{18}\}$ all have three original anchors, so they are all assigned cluster priority 10.

   Table 5.1 tabulates partial cluster priority assignment rules for such a network. As we can see from the first row, when the cluster is a 3-anchor cluster itself, the cluster is assigned cluster priority 10.

2. If all clusters have been assigned a priority, go to Step 4. Otherwise go to Step 3.

3. For each cluster that has not been assigned a priority, find the cluster c that has the highest neighbor-priority, h. To avoid too many cluster priorities being generated in this step, we classify the neighbor-priorities that have the same first digit (say s) as one category and count them all towards the number p. Thus, we set p to be the number of neighboring clusters whose priorities have the same first digit as cluster c's neighbor-priority, h. Next, we assign cluster c's priority to be $(10(s+1)-p+9)$. (We assume that a cluster has a maximum of 8 neighboring clusters.) For most applications, the design of network would inherently limit the cluster priorities to never go beyond the 100 range. The cluster priority calculation will therefore apply.

   For example in Figure 5.1, cluster c_{13} has 3 neighboring clusters with priority 10. This cluster will be assigned priority $(10(1+1)-3+9=26)$, as listed in the 7th row in Table 5.1.

4. Report all cluster priorities and stop.

Going through the whole Cluster Priority Assignment routine for the example in Figure 5.1, we obtain the cluster priorities listed in Table 5.2.

5.3.3 Synchronization among Parallel Processes

As we discussed in section 5.3.1, after the cluster priorities are assigned, a sequence of clusters is generated from these priorities to determine the order of localization for each cluster. A cluster with a higher priority goes before a cluster with a lower priority. Clusters with the same priority go in parallel.

Table 5.1: Cluster priority: an example

Cluster priority	3-anchor cluster itself	# of neighboring clusters with priority value of 10	# of neighboring clusters with priority value of 2x	... ...
10	yes	-	-	-
21	no	8	-	-
22	no	7	-	-
23	no	6	-	-
24	no	5	-	-
25	no	4	-	-
26	no	3	-	-
27	no	2	-	-
28	no	1	-	-
31	no	0	8	-
32	no	0	7	-
33	no	0	6	-
34	no	0	5	-
35	no	0	4	-
36	no	0	3	-
37	no	0	2	-
38	no	0	1	-
...	no	0	0	...

Table 5.2: Cluster priorities for example in Figure 5.1

Cluster index	1	2	3	4	5	6	7	8	9	10	11	12	13	14	15	16	17	18	19	20	21	22	23	24	25
Cluster priority	28	28	27	28	28	28	10	27	10	28	28	27	26	27	28	35	28	10	28	35	37	28	28	28	37

For each cluster that is ready for the coming parallel iteration, a cluster-level "full" problem is formed from all reachable anchors in the neighboring clusters plus sensors and anchors belonging to this cluster. These smaller "full" problems for each cluster are solved by SpaseLoc, and are processed in parallel by the cluster heads in the network. Thus, the synchronization process involves the following two tasks:

- *Enforcing the order:* The lower priority clusters should be run after the higher priority clusters are localized, to take advantage of the newly available anchors in the neighboring clusters. Only clusters at the same priority proceed in parallel.

- *Updating the neighboring clusters with newly localized anchor information:* After the parallel clusters have been localized, their newly localized acting anchors should be fed into all their neighboring cluster heads so that the next parallel iteration will make use of the new information.

5.3.4 Distributed Sensor Localization Algorithm

After we explain how the sequencing and synchronization work under the distributed approach, this section presents our distributed sensor localization algorithm that glues these two processes together.

Distributed sensor localization algorithm:

1. Determine the cluster priority for each cluster in the network. This is done at the command center machine level by the routine given in section 5.3.2.

2. At the command center machine, sequence the cluster localization order according to cluster priorities. A cluster with a higher priority ranks before a cluster with lower priority. Clusters with the same cluster priority are put in the same rank. Hence, a list of cluster ranks is produced. Let's assume that r ranks are produced. For each rank i in the list, there is a list of cluster indexes l associated with i. The list l could include one index, or multiple indexes, which means that there are multiple clusters put in the same rank.

3. In the command center level: synchronize all cluster heads to do localizations.

    - For each rank i from 1 to r:

    - For all clusters in l of same rank i:

      Request all cluster heads in l to localize their own sensors simultaneously. For each cluster c in l, the cluster head does the following tasks in parallel:

      – Formulate cluster-level "full" problem, consisting of all the sensors, anchors, and distance measurements among them in cluster c, and all the anchor information from cluster c's neighboring clusters that are within cluster c's radio range.

      – Call SpaseLoc to solve the cluster-level "full" problem.

      – Update all cluster c's neighboring clusters with the newly localized acting anchors.

      – Report to the command center that localization is done.

    - When the command center receives reports from all clusters in l that they've finished localizing their own clusters, go to next i.

4. Report localization results. Stop.

In the following, we illustrate the distributed algorithm with the example in Figure 5.1.

- In Step 1, we generate the cluster priorities for this network as in Table 5.2.
- In Step 2, we generate a cluster rank list as shown in Table 5.3. We can see that a total of 6 ranks are produced.
- Now at Step 3,
  - $i = 1$, cluster heads {7, 9, 18} localize their clusters in parallel.
  - $i = 2$, cluster head {13} localizes its cluster alone.
  - $i = 3$, cluster heads {3, 8, 12, 14} localize their clusters in parallel.
  - $i = 4$, cluster heads {1, 2, 4, 5, 6, 10, 11, 15, 17, 19, 22, 23, 24} localize their clusters in parallel.
  - $i = 5$, cluster heads {16, 20} localize their clusters in parallel.
  - $i = 6$, cluster heads {21, 25} localize their clusters in parallel.
- All clusters are localized; report results and stop.

  Figure 5.2 shows the localization results for the above example with 625 total nodes in the network and 25 nodes in each cluster. The algorithm accurately localizes all sensors one cluster at a time with zero errors.

Table 5.3: Cluster rank list for example in Figure 5.1

Cluster priority	10	26	27	28	35	37
Cluster rank	1	2	3	4	5	6
Cluster index	7 9 18	13	3 8 12 14	1 2 4 5 6 10 11 15 17 19 22 23 24	16 20	21 25

5.4 Distributed Algorithm Simulation Results

This section explains the simulation method and the setup for experimenting with our distributed algorithm, then presents results for various parameter settings and topologies.

All assumptions made in section 3.3 (using strategy I0) regarding simulation region, *MaxAnchorReq*, radio range, measured distances, and average estimation errors are applicable here, except for the following adjustments to the clustered architecture.

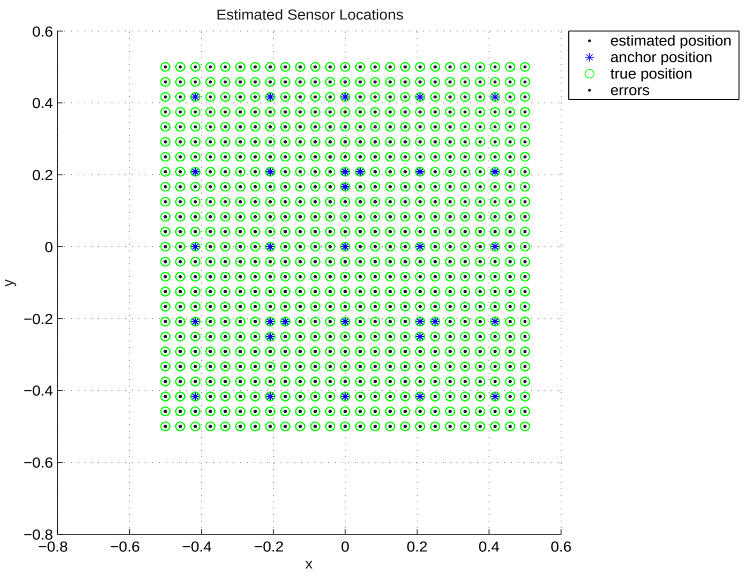

Figure 5.2: An example of distributed localization, with 625 total points, 25 clusters, 25 nodes in each cluster, radius 0.16, no noise

- The clustered network has the same characteristics as the example shown in Figure 5.1 and discussed in section 5.3.1.
- The simulation follows the cluster priority assignment routine proposed in section 5.3.2.

In the following subsections, we present simulation results (all results averaged over 10 runs) to show the accuracy and scalability of the distributed algorithm. We observe the impact of different numbers of 3-anchor clusters and different node densities, radio ranges, and noise levels on the accuracy and performance of the algorithm.

5.4.1 Number of 3-anchor Clusters Impact

As we know from section 5.3.1, in a clustered wireless sensor network, some clusters may have 3 anchors while some clusters may only have the cluster heads as anchors. This section studies the impact of the number of 3-anchor clusters on the accuracy and performance of the distributed algorithm, using simulation results from sample networks.

Figure 5.3 displays the topologies of networks with different numbers of 3-anchor clusters that our simulations are based on. Each network has 4900 nodes and 25 clusters. Each cluster contains 196 nodes that are uniformly distributed on 14×14 square grids within the cluster. All cluster heads (which are also anchors) are positioned in the middle of their clusters. They are marked as a black dot in the figure. A 3-anchor cluster also

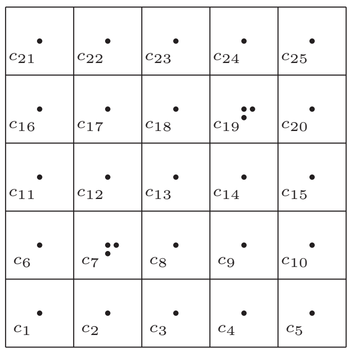
c_{21} c_{22} c_{23} c_{24} c_{25}
c_{16} c_{17} c_{18} c_{19} c_{20}
c_{11} c_{12} c_{13} c_{14} c_{15}
c_6 c_7 c_8 c_9 c_{10}
c_1 c_2 c_3 c_4 c_5

(a) Number of 3-anchor clusters = 2.

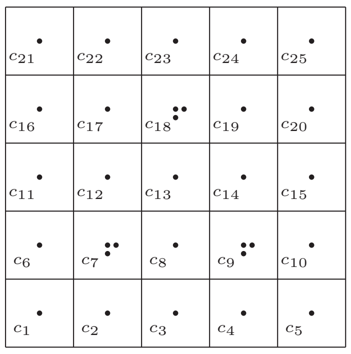
c_{21} c_{22} c_{23} c_{24} c_{25}
c_{16} c_{17} c_{18} c_{19} c_{20}
c_{11} c_{12} c_{13} c_{14} c_{15}
c_6 c_7 c_8 c_9 c_{10}
c_1 c_2 c_3 c_4 c_5

(b) Number of 3-anchor clusters = 3.

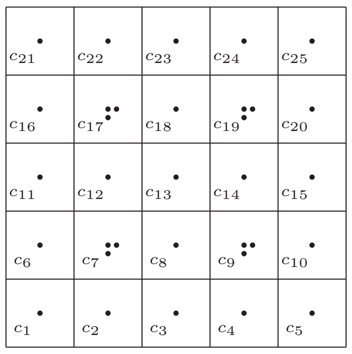
c_{21} c_{22} c_{23} c_{24} c_{25}
c_{16} c_{17} c_{18} c_{19} c_{20}
c_{11} c_{12} c_{13} c_{14} c_{15}
c_6 c_7 c_8 c_9 c_{10}
c_1 c_2 c_3 c_4 c_5

(c) Number of 3-anchor clusters = 4.

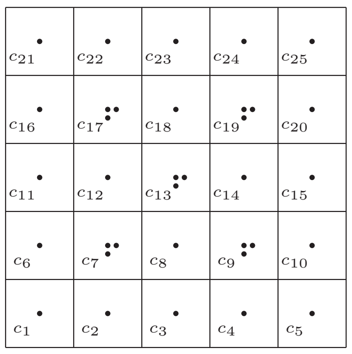
c_{21} c_{22} c_{23} c_{24} c_{25}
c_{16} c_{17} c_{18} c_{19} c_{20}
c_{11} c_{12} c_{13} c_{14} c_{15}
c_6 c_7 c_8 c_9 c_{10}
c_1 c_2 c_3 c_4 c_5

(d)Number of 3-anchor clusters = 5.

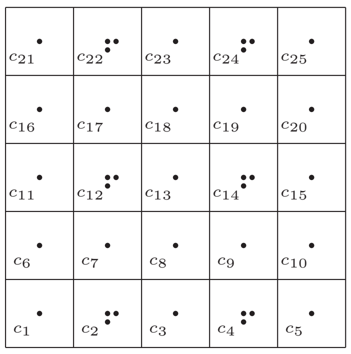
c_{21} c_{22} c_{23} c_{24} c_{25}
c_{16} c_{17} c_{18} c_{19} c_{20}
c_{11} c_{12} c_{13} c_{14} c_{15}
c_6 c_7 c_8 c_9 c_{10}
c_1 c_2 c_3 c_4 c_5

(e) Number of 3-anchor clusters = 6.

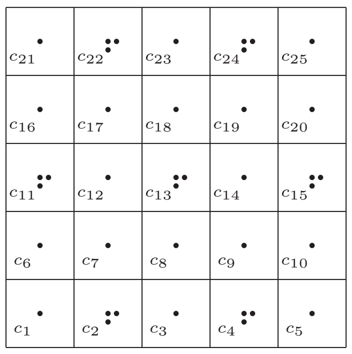
c_{21} c_{22} c_{23} c_{24} c_{25}
c_{16} c_{17} c_{18} c_{19} c_{20}
c_{11} c_{12} c_{13} c_{14} c_{15}
c_6 c_7 c_8 c_9 c_{10}
c_1 c_2 c_3 c_4 c_5

(f) Number of 3-anchor clusters = 7.

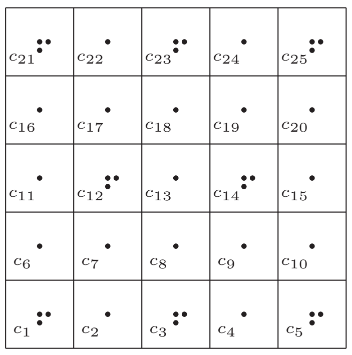
c_{21} c_{22} c_{23} c_{24} c_{25}
c_{16} c_{17} c_{18} c_{19} c_{20}
c_{11} c_{12} c_{13} c_{14} c_{15}
c_6 c_7 c_8 c_9 c_{10}
c_1 c_2 c_3 c_4 c_5

(g) Number of 3-anchor clusters = 8.

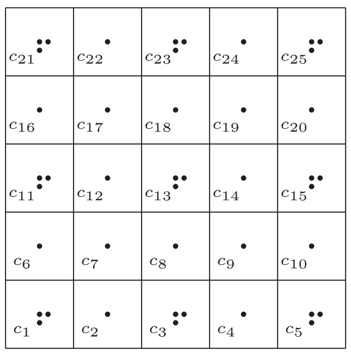
c_{21} c_{22} c_{23} c_{24} c_{25}
c_{16} c_{17} c_{18} c_{19} c_{20}
c_{11} c_{12} c_{13} c_{14} c_{15}
c_6 c_7 c_8 c_9 c_{10}
c_1 c_2 c_3 c_4 c_5

(h) Number of 3-anchor clusters = 9.

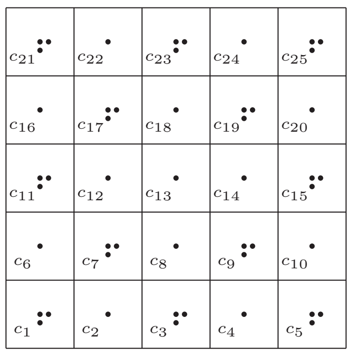
c_{21} c_{22} c_{23} c_{24} c_{25}
c_{16} c_{17} c_{18} c_{19} c_{20}
c_{11} c_{12} c_{13} c_{14} c_{15}
c_6 c_7 c_8 c_9 c_{10}
c_1 c_2 c_3 c_4 c_5

(i) Number of 3-anchor clusters = 12.

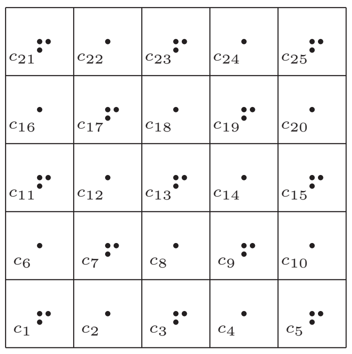
c_{21} c_{22} c_{23} c_{24} c_{25}
c_{16} c_{17} c_{18} c_{19} c_{20}
c_{11} c_{12} c_{13} c_{14} c_{15}
c_6 c_7 c_8 c_9 c_{10}
c_1 c_2 c_3 c_4 c_5

(j) Number of 3-anchor clusters = 13.

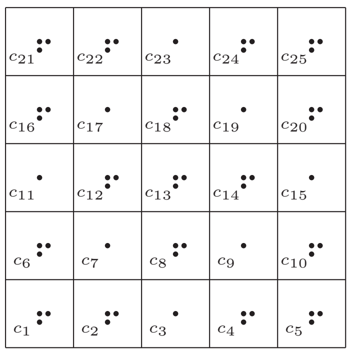
c_{21} c_{22} c_{23} c_{24} c_{25}
c_{16} c_{17} c_{18} c_{19} c_{20}
c_{11} c_{12} c_{13} c_{14} c_{15}
c_6 c_7 c_8 c_9 c_{10}
c_1 c_2 c_3 c_4 c_5

(k) Number of 3-anchor clusters = 17.

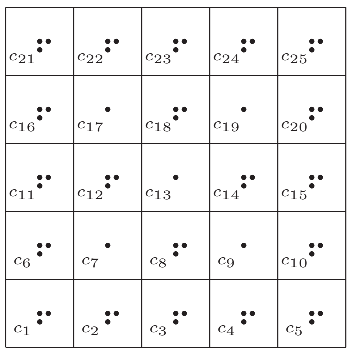
c_{21} c_{22} c_{23} c_{24} c_{25}
c_{16} c_{17} c_{18} c_{19} c_{20}
c_{11} c_{12} c_{13} c_{14} c_{15}
c_6 c_7 c_8 c_9 c_{10}
c_1 c_2 c_3 c_4 c_5

(l) Number of 3-anchor clusters = 20.

Figure 5.3: Topologies of different numbers of 3-anchor clusters.

has two extra anchors, one on the immediate right grid of the cluster head, and the other on the immediate lower grid of the cluster head. A 3-anchor cluster is marked with 3 black dots in the figure. When we make choices on the locations of the 3-anchor clusters among all 25 clusters, we try to choose their locations such that the rest of the 1-anchor clusters can achieve as high a cluster priority as possible.

Table 5.4: Number of 3-anchor clusters impact: 25 clusters, 4900 total nodes, 196 nodes in each cluster, radius 0.1, no noise

3-anchor clusters	No of anchors	Total rankings	Error	95% Error	Sequential time	Per cluster time	Parallel time
2	29	6	7.5e-9	2.4e-9	14.34	0.57	3.44
3	31	6	7.1e-9	2.3e-9	14.48	0.58	3.48
4	33	4	8.0e-9	2.5e-9	14.35	0.57	2.30
5	35	4	1.1e-8	2.5e-9	14.43	0.58	2.31
6	37	4	1.1e-8	2.8e-9	14.48	0.58	2.32
7	39	4	1.1e-8	2.9e-9	14.59	0.58	2.33
8	41	4	1.0e-8	2.2e-9	14.63	0.59	2.34
9	43	3	1.0e-8	2.3e-9	14.86	0.59	1.78
12	49	3	9.7e-9	2.1e-9	14.58	0.58	1.75
13	51	3	9.6e-9	2.1e-9	14.80	0.59	1.78
17	59	3	9.8e-9	2.1e-9	14.87	0.59	1.78
20	65	3	9.0e-9	2.0e-9	14.66	0.59	1.76

With constant *radius* (0.01) and no noise, Table 5.4 shows the impact of the number of 3-anchor clusters on accuracy and performance. Since the simulation is run on a single processor, the *sequential time* records the total time to have all clusters localized in the whole network. *Time per cluster* is a calculated average time taken to localize each cluster. *Parallel time* is given as an estimate of execution time if the computation could be done in real clustered (parallel) networks. As we can see, when the radio range is sufficiently large, the number of anchors in the network has barely any impact on estimation accuracy because all test cases show negligible errors. At the same time, we see that the per cluster execution time remains similar for all test cases. However, the execution time in a parallel computing environment reduces as the number of 3-anchor clusters increases. This analysis is beneficial for designers to gauge the performance of a given design, or to decide on a particular design with a given desired performance.

5.4.2 Number of 3-anchor Clusters Impact with Noise

Continuing from the test cases in section 5.4.1, we run the same simulation except that a *noise_factor* of 0.1 is added. Table 5.5 shows the impact of the number of 3-anchor clusters plus noise on accuracy and performance. As we can see, when the radio range is sufficiently large, the number of anchors in the network has barely any impact on estimation accuracy with 0.1 noise. Also, execution time in the parallel computing environment reduces as the number of 3-anchor clusters increases, the same as with the no-noise situation. However, compared with the no noise results in Table 5.4, the added 0.1 noise level increases both the estimation error and the execution time on average.

Table 5.5: Number of 3-anchor clusters impact with noise: 25 clusters, 4900 total nodes, 196 nodes in each cluster, radius 0.1, with *noise_factor = 0.1*

3-anchor clusters	No of anchors	Total Rankings	Error	95% Error time	Sequential time	Per cluster time	Parallel
2	29	6	6.2e-3	5.7e-3	21.12	0.84	5.07
3	31	6	6.3e-3	5.8e-3	21.48	0.86	5.16
4	33	4	6.1e-3	5.5e-3	21.78	0.87	3.49
5	35	4	6.0e-3	5.5e-3	20.76	0.83	3.32
6	37	4	5.9e-3	5.3e-3	21.10	0.84	3.38
7	39	4	6.0e-3	5.4e-3	22.35	0.89	3.58
8	41	4	5.9e-3	5.3e-3	21.07	0.84	3.37
9	43	3	5.8e-3	5.2e-3	21.28	0.85	2.55
12	49	3	5.8e-3	5.2e-3	21.56	0.86	2.59
13	51	3	5.8e-3	5.2e-3	20.49	0.82	2.46
17	59	3	6.0e-3	5.5e-3	20.50	0.82	2.46
20	65	3	6.2e-3	5.7e-3	20.32	0.81	2.44

5.4.3 Node Density Impact

In order to study the impact of node density, we choose one of the networks in section 5.4.1 with the number of 3-anchor clusters = 8. Then we vary the number of nodes in each cluster to see its impact on performance. With a fixed total number of 25 clusters and radio range of 0.1, Table 5.6 shows the direct impact of the number of nodes in each cluster on accuracy and performance. (Noise is not included.) The table shows that the algorithm can accurately position all sensors with no errors. As we expected, increasing node density increases the execution time.

Table 5.6: Node density impact with number of clusters = 25, number of 3-anchor clusters = 8, *radius* = 0.100; *noise_factor* = 0

Total nodes	Nodes per cluster	Error	95% Error	Sequential time	Per cluster time	Parallel time
400	4* 4(16)	9.4e-8	2.5e-8	0.76	0.03	0.12
625	5* 5(25)	5.0e-8	1.1e-8	1.37	0.05	0.22
1225	7* 7(49)	2.5e-8	4.7e-9	2.92	0.12	0.47
2025	9* 9(81)	1.1e-8	2.0e-9	5.07	0.20	0.81
3025	11*11(121)	8.5e-9	2.2e-9	8.22	0.33	1.32
4225	13*13(169)	8.0e-9	1.7e-9	12.86	0.51	2.06
4900	14*14(196)	1.0e-8	2.2e-9	15.13	0.61	2.42
5625	15*15(225)	5.0e-9	1.3e-9	18.78	0.75	3.00
6400	16*16(256)	8.8e-9	2.0e-9	22.79	0.91	3.65
7225	17*17(289)	6.3e-9	1.5e-9	29.01	1.16	4.64
8100	18*18(324)	5.9e-9	1.2e-9	34.45	1.38	5.51
9025	19*19(361)	8.5e-9	1.7e-9	45.47	1.82	7.27
10000	20*20(400)	7.1e-9	1.6e-9	55.03	2.20	8.80

5.4.4 Radio Range Impact

In order to study the impact of radio range, we choose one of the networks in section 5.4.1 with the number of 3-anchor clusters = 8. Then we vary the radio range to see its impact on accuracy and performance.

Table 5.7: Radio range impact with nodes = 4900, number of clusters = 25, number of 3-anchor clusters = 8, *noise_factor* = 0

Radio range	Error	95% Error	Number of outliers	Sequential time	Per cluster time	Parallel time
0.0143(1/70)	0.3847	0.360	195	0.40	0.02	0.064
0.0215(3/2/70)	9.6e-7	5.6e-7	0	15.98	0.64	2.56
0.0286(2/70)	9.6e-7	5.6e-7	0	15.78	0.63	2.53
0.0429(3/70)	1.1e-7	6.8e-8	0	14.54	0.58	2.33
0.0571(4/70)	2.5e-8	5.8e-9	0	13.63	0.55	2.18
0.0714(5/70)	1.7e-8	3.2e-9	0	13.07	0.52	2.09
0.0857(6/70)	1.4e-8	3.0e-9	0	13.36	0.53	2.14
0.1000(7/70)	1.0e-8	2.2e-9	0	14.63	0.59	2.34

With a fixed total number of 4900 nodes in 25 clusters, Table 5.7 shows the direct impact of radio range on accuracy and performance. (Noise is not included.) We can see that when the radio range is sufficiently large (no less than 0.0215), increasing radio range barely has any impact on the estimation accuracy or speed. However, when *radius* is reduced to 0.0143, none of the sensors has at least 3 connections to anchors, so the localizations totally rely on the auxiliary geometric routines, causing the execution time to be greatly reduced. In addition, the number of unreachable sensors (outliers) reaches 195, which is unacceptable. Clearly, the simulation could assist sensor network designers in selecting a radio range to achieve a desired estimation error and algorithm speed.

5.4.5 Noise Factor Impact

In order to study the impact of noise, we choose one of the networks in section 5.4.1 with the number of 3-anchor clusters = 8. Then we vary the *noise_factor* to see its impact on accuracy and performance. With a fixed total number of 4900 nodes in 25 clusters, Table 5.8 shows the impact of noise level on accuracy and performance. As we can see, more noise in the network has a direct impact on estimation accuracy. This analysis may help designers determine the sensor noise level that will give an acceptable estimation error.

Table 5.8: Noise factor impact with nodes = 4900, number of clusters = 25, number of 3-anchor clusters = 8, *radius* = 0.1

Noise_ factor	Error	95% Error	Sequential time	Per cluster time	Parallel time
0.00	1.0e-8	2.2e-9	15.50	0.62	2.48
0.05	2.7e-3	2.3e-3	20.46	0.82	3.27
0.10	6.0e-3	5.3e-3	21.51	0.86	3.44
0.20	1.4e-2	1.2e-2	23.86	0.95	3.82
0.30	2.2e-2	2.0e-2	25.30	1.01	4.05
0.40	2.9e-2	2.7e-2	23.35	0.93	3.74
0.50	3.5e-2	3.3e-2	26.95	1.08	4.31

5.4.6 Number of Clusters Impact

This section studies the impact of the number of clusters on the algorithm's performance. We run simulations for networks of 4 to 36 clusters. The number of nodes in each cluster remains the same at 256 nodes. The number of anchors and *radius* change with the number of sensors being simulated in order to maintain the same connectivity level. We assume all clusters are 3-anchor clusters, and the radio range is half the size of the cluster's square width. Noise is not included in this simulation.

Table 5.9 shows the simulation results of the number of clusters' impact on performance (all have negligible estimation errors). As we can see, with the increase of the number of clusters in the network, the parallel execution time increases. This is caused by the distributed algorithm's synchronization routine. The bigger the network, the more neighbors to search and synchronize.

Table 5.9: Number of clusters impact with 256 nodes in each cluster; all 3-anchor clusters

No of clusters	No of nodes	Radio range	Sequential time	Parallel time
4	1024	0.2500	3.17	0.79
9	2304	0.1670	7.62	0.85
16	4096	0.1250	13.91	0.87
25	6400	0.1000	22.31	0.89
36	9216	0.0833	32.97	0.92

Chapter 6

3D Extensions

Sensor localization in 3-dimensional space addresses the need to estimate sensors' locations whose distributions are beyond a plane surface in wireless sensor networks. For example, if an ad hoc wireless sensor network is used to detect fire hazard in a high-rise building, sensors may be placed on different floors. Our 3D sensor localization algorithm extends the 2D solver SpaseLoc. In this chapter, we describe modifications to the 2D implementation to permit effective 3D sensor localizations. Computational results are presented.

6.1 3D Sensor Localization Geometry

To be localizeable in 3D, a sensor needs at least 4 known distance measurements to at least 4 anchors that are not on a plane.

For example, assume a sensor at location $x \in R^3$ connects to 4 anchors whose known locations are $a, b, c, e \in R^3$. The 4 known distance measurements between the sensor and the 4 anchors are $\hat{d}_1,\ \hat{d}_2,\ \hat{d}_3,\ \hat{d}_4$.

The first two spheres centered at anchors a, b with radius $\hat{d}_1, \hat{d}_2$ put sensor x on a circle defined by the following two spheres' surfaces:

$$\begin{aligned} ||x-a||^2 &= \widehat{d_1^2}, \\ ||x-b||^2 &= \widehat{d_2^2}. \end{aligned}$$

Adding the third sphere centered at anchor c with radius $\hat{d}_3$ puts sensor x on two points

x^* or x^{**} defined by the following three spheres' surfaces:

$$\begin{aligned} ||x-a||^2 &= \widehat{d_1^2}, \\ ||x-b||^2 &= \widehat{d_2^2}, \\ ||x-c||^2 &= \widehat{d_3^2}. \end{aligned}$$

Adding the fourth sphere centered at anchor e with radius $\hat{d}_4$ puts sensor x exactly on one of the two points x^* or x^{**} defined by the following four spheres' surfaces:

$$\begin{aligned} ||x-a||^2 &= \widehat{d_1^2}, \\ ||x-b||^2 &= \widehat{d_2^2}, \\ ||x-c||^2 &= \widehat{d_3^2}, \\ ||x-e||^2 &= \widehat{d_4^2}. \end{aligned}$$

Therefore, to localize a sensor uniquely under no-noise conditions, we need a minimum of four distance measurements from at least four of the sensor's connected anchors.

6.2 3D Localization Design

The following adjustments are made to the 2D version of SpaseLoc in order for it to work in 3D space.

- In the SpaseLoc implementation, we create a parameter called DIM for dimensions. We assign DIM = 2 or 3 for the 2D or 3D case, respectively.
- All rules for subproblem creation for the 2D scenario discussed in section 3.1.2 are adjusted to work for the 3D scenario.
- The subproblem to be processed by the DSDP solver is also adjusted to accommodate the extra dimension.
- In the independent subanchor selection routine (section 3.1.5), instead of checking whether 3 points are on a line in the 2D case, the algorithm checks whether 4 points are on a plane. If so, the 4 anchors are said to be dependent.
- All the auxiliary geometric routines in sections 3.1.6 and 3.1.7 still apply to the 3D case with proper adjustment of dimensions. For example, in section 3.1.6, we developed a routine for sensors in 2D with only 2 connected anchors to localize

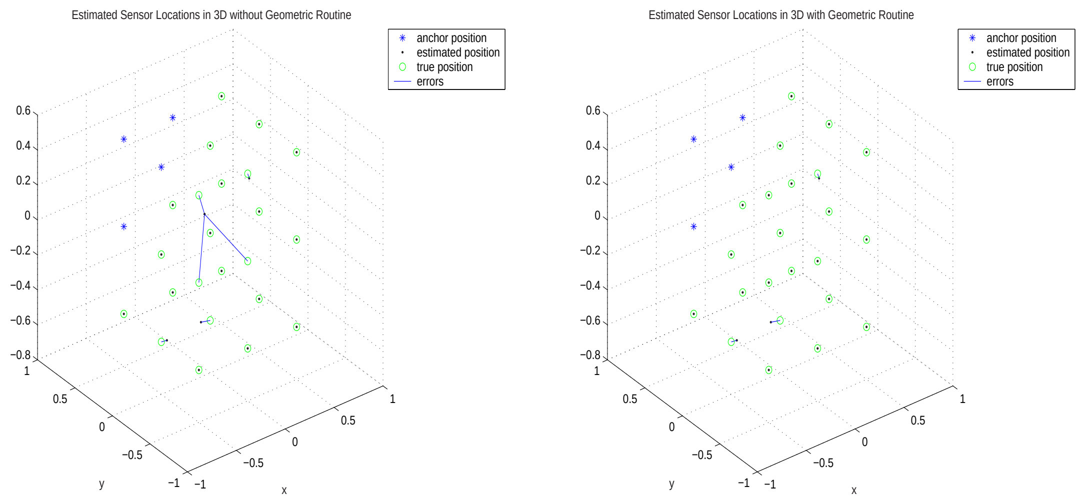

Figure 6.1: Localization errors for 3D localization with geometric routine.

with more accuracy utilizing neighboring anchors' information. We extend this heuristic to 3D space for sensors with only 3 connected anchors. We use the same technique first to calculate the two possible points where the sensor could be using three distance equations. Then, we eliminate one of the two possible points by the sensor's anchors' neighboring anchors. Figure 6.1 shows the results of localization accuracy with or without the auxiliary geometric routine. 27 sensor nodes are purposely placed on square grids within a $1 \times 1 \times 1$ volume in 3D, within which 4 of the nodes are anchors. With a radio range of 1, some of the sensors do not have at least 4 independent connected anchors (original or acting) to localize them. We can see from Figure 6.1 that our geometric subroutine is very effective in reducing error under this condition. The average error without the geometric routine is 0.0689, but with the geometric routine, the average error is reduced to 0.0124.

6.3 3D Localization Simulation Results

This section presents some simulation results in order to compare the performance of the 3D algorithm with the 2D version.

The simulation setup is the same as for the 2D case as discussed in section 3.3 using strategy I0, except the area is confined within $1 \times 1 \times 1$ in 3D. Figure 6.2 shows 100 randomly uniform-distributed nodes being localized by 3D SpaseLoc. As we can see, all nodes are localized accurately with essentially no error.

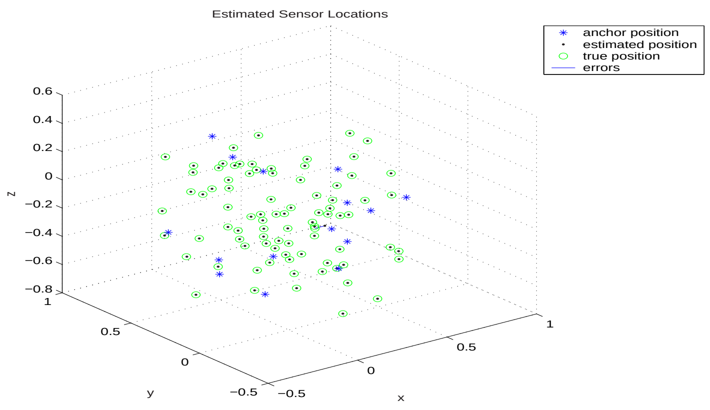

Figure 6.2: 3D sensor localization, 100 total points, 15 anchors, radius 0.5, no noise

6.3.1 Scalability

Table 6.1 shows scalability results for 27 to 10000 randomly uniform-distributed sensors being localized using the 3D localization algorithm. All sensors' positions are randomly generated with a uniform random distribution in the $1 \times 1 \times 1$ volume with anchors also randomly chosen. The number of anchors and *radius* change with the number of sensors being simulated in order to maintain the same connectivity level. Noise is not included in this simulation.

Not unexpectedly, comparing with the 2D case in Table 3.5, we see that the execution times increase steadily with increasing sizes of the networks.

Table 6.1: 3D algorithm scalability.

Nodes	Anchors	*radius*	*sub_size*	Error	Trace	95% Error	95% Trace	Time	SDP's
27	9	1.0000	2	2.7e-10	1.9e-10	1.9e-10	1.5e-10	0.04	9
64	16	0.6667	2	9.1e-9	7.8e-9	2.0e-9	9.9e-10	0.20	24
125	25	0.5000	2	8.1e-9	1.9e-9	4.4e-9	8.4e-10	0.42	50
216	36	0.4000	2	3.9e-8	5.9e-9	1.9e-8	3.8e-9	0.76	90
512	64	0.2858	2	5.4e-4	1.1e-8	2.7e-8	4.8e-9	2.09	225
1000	100	0.2223	3	2.3e-4	1.1e-8	3.6e-8	6.1e-9	4.71	301
2197	169	0.1667	4	1.2e-7	3.2e-8	5.2e-8	8.7e-9	11.88	508
2744	196	0.1539	5	9.6e-5	1.7e-8	6.3e-8	1.1e-8	15.73	512
3375	225	0.1429	5	1.1e-4	1.6e-8	5.9e-8	9.2e-9	20.34	631
4096	256	0.1334	6	1.1e-4	2.5e-5	6.6e-8	9.8e-9	26.52	642
4913	289	0.1250	6	1.2e-7	1.7e-7	7.3e-8	1.1e-8	33.71	772
5832	324	0.1177	7	1.4e-5	4.6e-6	8.3e-8	1.2e-8	42.34	788
6859	361	0.1112	7	2.2e-5	2.6e-8	9.5e-8	1.4e-8	52.85	930
8000	400	0.1053	7	3.4e-5	2.6e-8	1.1e-7	1.7e-8	65.42	1087
9261	441	0.1010	7	4.8e-5	3.6e-8	1.2e-7	2.0e-8	81.61	1263
10648	484	0.0960	7	4.9e-5	1.2e-6	1.4e-7	2.2e-8	99.80	1455

6.3.2 Radio Range Impact

With a fixed total number of randomly uniform-distributed nodes (4096, of which 256 are anchors), Table 6.2 shows the impact of radio range on accuracy and performance. (Noise is not included.) As we can see from the table, increasing the radius generally produces better estimation accuracy but increases execution time slightly. Bigger radio range normally results in more connections among nodes, which may lead to more constraints for the subproblem.

Table 6.2: Radio-range impact: nodes = 4096, anchors = 256, no noise.

radius	*sub_size*	Error	95% Error	Outliers	Time	SDP's
0.1250	6	7.2e-5	8.3e-8	0	25.43	641
0.1300	6	5.9e-5	7.7e-8	0	25.97	641
0.1334	6	1.1e-4	6.6e-8	0	26.52	642
0.1400	6	2.1e-5	5.8e-8	0	27.62	641
0.1450	6	8.8e-5	4.8e-8	0	28.72	641
0.1500	6	6.4e-8	3.9e-8	0	29.53	640

6.3.3 Noise Factor Impact

With constant *radius* (0.1500) and the same randomly uniform-distributed nodes (4096), Table 6.3 shows the impact of noise conditions on accuracy and performance. As we can see, more noise in the network has a direct impact on estimation accuracy. Higher noise level also increases execution time.

Table 6.3: Noise factor impact: nodes = 4096, anchors = 256, *radius* = 0.15.

noise_factor	*sub_size*	Error	95% Error	Time	SDP's
0.0	6	6.4e-8	3.9e-8	29.53	640
0.1	6	0.042	0.037	37.65	680
0.2	6	0.092	0.083	41.70	746
0.3	6	0.151	0.140	42.30	725
0.4	6	0.219	0.205	43.47	703
0.5	6	0.290	0.275	45.37	663

6.3.4 Number of Anchors Impact

With constant *radius* (0.15) and the same randomly uniform-distributed nodes (4096), Table 6.4 shows the impact of the number of anchors on accuracy and performance. (Noise is not included.) As we can see, bigger radio range generally improves estimation accuracy and algorithm speed. This is because more anchors mean less sensors to be localized and more accurate anchor references are available for localizing sensors other than relying on acting anchors.

Table 6.4: Number of anchors impact: nodes = 4096, *radius* = 0.15, no noise.

Anchors	*sub_size*	Error	95% Error	Time	SDP's
16	6	4.6e-4	6.1e-8	31.81	681
32	6	4.3e-5	5.1e-8	31.68	679
64	6	7.7e-8	4.9e-8	31.41	673
128	6	8.1e-8	4.7e-8	30.88	662
256	6	6.4e-8	3.9e-8	29.53	640
384	6	6.1e-8	3.7e-8	28.34	619
768	6	4.9e-8	3.3e-8	24.71	555

6.3.5 Number of Anchors Impact with Noise

With the same *radius* (0.150) and the same randomly uniform-distributed nodes (4096), Table 6.5 shows the impact of the number of anchors on accuracy and performance when a *noise_factor* of 0.1 is included in the simulation. With this radio range, more anchors give slightly better estimation accuracy and a lot greater algorithm speed in general. Also, the presence of noise does add execution time and cause more errors on average compared with Table 6.4.

Table 6.5: Number of anchors impact: nodes = 4096, *radius* = 0.150, *noise_factor* = 0.1.

Anchors	*sub_size*	Error	95% Error	Time	SDP's
16	6	4.8e-2	4.0e-2	51.37	889
32	6	4.4e-2	3.9e-2	47.15	833
64	6	4.6e-2	4.0e-2	45.51	799
128	6	4.3e-2	3.9e-2	40.74	731
256	6	4.2e-2	3.7e-2	37.65	680
384	6	4.1e-2	3.7e-2	35.36	636
768	6	4.0e-2	3.6e-2	30.22	555

6.3.6 Number of Anchors Impact with Noise and Lower *radius*

With the same randomly uniform-distributed nodes and the same noise level but lower *radius* (0.125), Table 6.6 shows the impact of the number of anchors on accuracy and performance. The increase in the number of anchors results in better estimation accuracy and algorithm speed in general. In addition, decreased radio range reduces slightly the execution time and causes more errors on average compared with Table 6.5.

Table 6.6: Number of anchors impact: nodes = 4096, *radius* = 0.125, *noise_factor* = 0.1

Anchors	*sub_size*	Error	95% Error	Time	SDP's
16	6	5.9e-2	4.6e-2	50.40	961
32	6	5.2e-2	4.2e-2	45.45	865
128	6	4.8e-2	4.0e-2	41.28	807
256	6	4.4e-2	3.9e-2	35.08	704
384	6	4.4e-2	3.8e-2	32.60	672
768	6	4.2e-2	3.7e-2	26.43	558

Chapter 7

Sensor Localization in Anchorless Networks

We have been assuming in the previous chapters that the network contains sufficient original anchors for the sensors to be localized by our algorithms. This chapter presents a preprocessor for SpaseLoc called *Surrogate Anchor Selection* to localize a network where no absolute locations are known for any node in the network. We call such cases anchorless networks.

7.1 Anchorless Networks

In an anchorless network, each node can estimate the distance to each of its neighbors, but no absolute position references such as GPS or fixed anchor nodes are available. Localization of sensors in this type of network becomes: given pairwise distance measurements between sensors, recover the relative positions of each sensor up to a global rotation and translation.

Sensor localization without absolute position information is important for homogeneous networks, where any node may become mobile.

Niculescu and Nath [34] and Moore, et al. [31] propose anchorless sensor localization based on a trilateration primitive. Moore's method uses a notion of robust quadrilaterals to minimize the probability of realizing a flip ambiguity incorrectly because of measurement noise. The localization problem is formulated as a 2D graph realization problem: given a planar graph with edges of known length, recover the position of each vertex up to a global rotation and translation.

Paper [31] reports results from using the method on a network of nodes using MIT's

Crickets, which are hardware-compatible with the Mica2 Motes developed at Berkeley with the addition of an ultrasonic transmitter and receiver on each device. This hardware enables the sensor nodes to measure inter-node ranges using the time difference of arrival (TDoA) between ultrasonic and RF signals. Although the Crickets can achieve ranging precision of around 1cm on the lab bench, the ranging error in practice can be as large as 5cm because of off-axis alignment of the sending and receiving transducers.

The paper reports experimental results for 16-sensor network localization using the proposed algorithm. When the measurement errors are averaged at 5.18cm, the algorithm's localization error is averaged at 7.02cm. The paper also reports simulation results for bigger networks, and the results of tracking a mobile sensor. There is no report on the algorithm's speed.

7.2 Surrogate Anchor Selection

With pairwise distance measurements among sensors and without reference to any absolute positions, we would only be able to determine relative locations of all nodes. The idea behind our approach is to choose some sensors as reference points (we name these *surrogate anchors*), such that the rest of the sensors can be localized relative to these positions.

We need three surrogate anchors that are not on a line in order to localize the rest of the sensors uniquely on the plane that the three surrogate anchors are on. (We assume the network is on a plane. The method can be intuitively expanded to 3D space.)

We define surrogate anchors $SA = \{a_1, a_2, a_3\}$ in a network to be a subset of sensors in the same network. Suppose the subset happens to be sensors $\{s_1, s_2, s_3\}$ with pairwise distance measurements $\widehat{d}_{12}$, $\widehat{d}_{13}$, $\widehat{d}_{23}$. These surrogate sensors satisfy the following properties:

- The first surrogate anchor a_1 corresponding to s_1 is artificially set to a position of $(0, 0)$.
- The second surrogate anchor a_2 corresponding to s_2 is set to a position of $(\widehat{d}_{12}, 0)$.
- The third surrogate anchor a_3 corresponding to s_3 is set to a position of (x_x^*, x_y^*), an intersection of the following two circles:

$$\begin{aligned} x_x^2 + x_y^2 &= (\widehat{d}_{13})^2, \\ (x_x - \widehat{d}_{12})^2 + x_y^2 &= (\widehat{d}_{23})^2. \end{aligned}$$

Generally there would be two solutions to the above equations. Either one can be chosen as (x_x^*, x_y^*).

In this section, we propose a preprocessor to select three sensors to act as surrogate anchors in the network. SpaseLoc can then be applied to localize the remaining sensor nodes relative to the surrogate anchors' positions.

In choosing the surrogate anchors, we give priority to sensors with the highest connectivity to other nodes in the network, in order to reduce transitive errors.

Here are the main steps in the preprocessor for selecting three surrogate anchors.

SA1 Initialize sensor_list to include all sensors in the network, and assign sensor_list1 = sensor_list.

SA2 For surrogate_anchor1, choose the sensor connected to most other sensors in sensor_list1, say sensor1.

SA3 For surrogate_anchor2, choose sensor2 such that:

- It is connected to surrogate_anchor1.
- It is connected to some node sensor$k$ that is also connected to surrogate_anchor1.
- sensor1, sensor2, and sensor$k$ are not on the same line.

If more than one candidate satisfies the above three items, choose the one that has the most connections to other sensors in sensor_list, and set surrogate_anchor3 to be sensor$k$. Go to step SA4.

If there is no candidate satisfying the first three items, delete sensor1 from sensor_list1 and return to step SA2.

SA4 Stop.

$$
dist = \left[\begin{array}{cccccccccccccccc}
0 & 1 & 0 & 0 & 1 & \sigma & 0 & 0 & 0 & 0 & 0 & 0 & 0 & 0 & 0 & 0 \\
1 & 0 & 1 & 0 & \sigma & 1 & \sigma & 0 & 0 & 0 & 0 & 0 & 0 & 0 & 0 & 0 \\
0 & 1 & 0 & 1 & 0 & \sigma & 1 & \sigma & 0 & 0 & 0 & 0 & 0 & 0 & 0 & 0 \\
0 & 0 & 1 & 0 & 0 & 0 & \sigma & 1 & 0 & 0 & 0 & 0 & 0 & 0 & 0 & 0 \\
1 & \sigma & 0 & 0 & 0 & 1 & 0 & 0 & 1 & \sigma & 0 & 0 & 0 & 0 & 0 & 0 \\
\sigma & 1 & \sigma & 0 & 1 & 0 & 1 & 0 & \sigma & 1 & \sigma & 0 & 0 & 0 & 0 & 0 \\
0 & \sigma & 1 & \sigma & 0 & 1 & 0 & 1 & 0 & \sigma & 1 & \sigma & 0 & 0 & 0 & 0 \\
0 & 0 & \sigma & 1 & 0 & 0 & 1 & 0 & 0 & 0 & \sigma & 1 & 0 & 0 & 0 & 0 \\
0 & 0 & 0 & 0 & 1 & \sigma & 0 & 0 & 0 & 1 & 0 & 0 & 1 & \sigma & 0 & 0 \\
0 & 0 & 0 & 0 & \sigma & 1 & \sigma & 0 & 1 & 0 & 1 & 0 & \sigma & 1 & \sigma & 0 \\
0 & 0 & 0 & 0 & 0 & \sigma & 1 & \sigma & 0 & 1 & 0 & 1 & 0 & \sigma & 1 & \sigma \\
0 & 0 & 0 & 0 & 0 & 0 & \sigma & 1 & 0 & 0 & 1 & 0 & 0 & 0 & \sigma & 1 \\
0 & 0 & 0 & 0 & 0 & 0 & 0 & 0 & 1 & \sigma & 0 & 0 & 0 & 1 & 0 & 0 \\
0 & 0 & 0 & 0 & 0 & 0 & 0 & 0 & \sigma & 1 & \sigma & 0 & 1 & 0 & 1 & 0 \\
0 & 0 & 0 & 0 & 0 & 0 & 0 & 0 & 0 & \sigma & 1 & \sigma & 0 & 1 & 0 & 1 \\
0 & 0 & 0 & 0 & 0 & 0 & 0 & 0 & 0 & 0 & \sigma & 1 & 0 & 0 & 1 & 0
\end{array}\right]
$$

Figure 7.1: Example anchorless network. The entry σ is $\sqrt{2}$.

7.3 An Example

This section illustrates through an example our approach for sensor localization of anchorless networks using the surrogate anchor preprocessor.

Suppose a network has 16 sensors, and we are given the table of pair-wise distance measurements shown as *dist* in Figure 7.1.

In Step SA2, the surrogate anchor selection procedure finds surrogate_anchor1 to be sensor 11 because that sensor has the most connections to other sensors. In Step SA3, sensor 10 is chosen to be surrogate_anchor2 because it connects to sensor 11 and to sensor 7 (this is sensor$k$, which is also connected to 11) and it has the most connections to other sensors. Thus, surrogate_anchor3 is determined to be sensor 7.

Now we have three surrogate anchors s_{11}, s_{10}, s_7. We now give the first surrogate anchor s_{11} point position $(0,0)$, and the second surrogate anchor s_{10} point position $(1,0)$ because the distance between s_{11} and s_{10} is 1. For surrogate anchor 3's position, we solve the following equations:

$$
\begin{aligned}
x_x^2 + x_y^2 &= 1, \\
(x_x - 1)^2 + x_y^2 &= 2.
\end{aligned}
$$

The roots of these equations give two points: $(0,1)$ and $(0,-1)$. Out of habit, we choose the one with a positive coordinate, namely $(0,1)$.

With the distance matrix and three surrogate anchors and their reference positions, we now call SpaseLoc to localize the remaining sensors. The relative positions of all sensors output by SpaseLoc are given in Figure 7.2. As we can see, the figure recovers the relative positions of all 16 nodes satisfying all the distance measurements in *dist*.

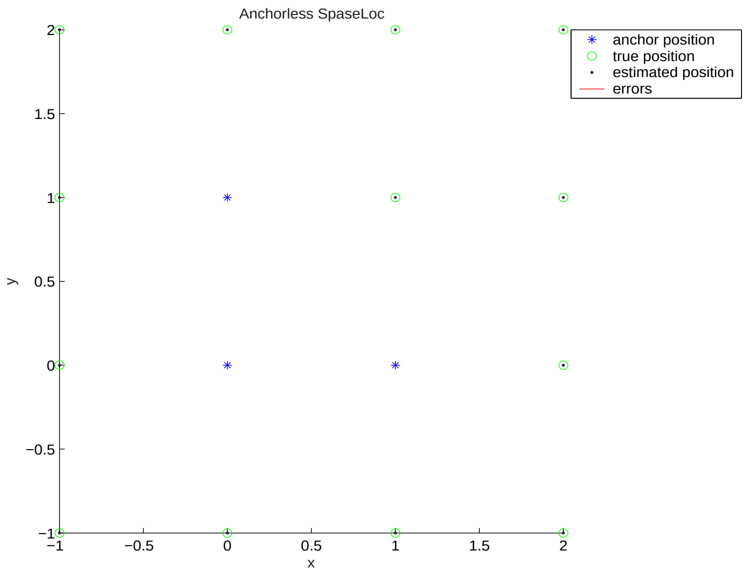

Figure 7.2: An example of anchorless localization, radius $\sqrt{2}$, no noise

Chapter 8

Conclusions and Future Research

In this dissertation research, we have developed a range of algorithms to estimate sensor positions in static, dynamic, distributed, 2D and 3D wireless sensor networks. This chapter summarizes the proposed approaches and discusses future research directions.

8.1 Contributions

The proposed algorithms achieve a breakthrough in scalability and accuracy compared with existing methods. The advances were recognized when this research project tied for first prize in the 2005 Stanford-Berkeley Innovators' Challenge competition. All entries were judged in the categories of Technical Innovation, Execution, and Future Impact [25].

Existing localization methods have been applicable for only moderate-sized networks. The recent optimization approach by Biswas and Ye [4] uses semidefinite programming (SDP) to find an approximate solution. This is a vital tool, but its speed and accuracy deteriorate rapidly with network size. The computational complexity of this approach is $O(n^p)$, where p is between 3 and 4.

The complexity of our SpaseLoc algorithm is $O(n)$. On a 2.4GHz laptop with 1GB memory, the algorithm maintains efficiency and provides accurate position estimation for networks with 10000 sensors and beyond.

SpaseLoc is further utilized as a vital tool for more general localization algorithms. A dynamic version can estimate moving sensors' locations in real-time, and a 3D version extends its utility. We also deploy SpaseLoc in clustered and distributed environments, permitting application to arbitrarily large networks.

Figure 8.1 compares the localization results between our SpaseLoc algorithm and the pure SDP approach for various size networks. The left-hand figure shows a comparison

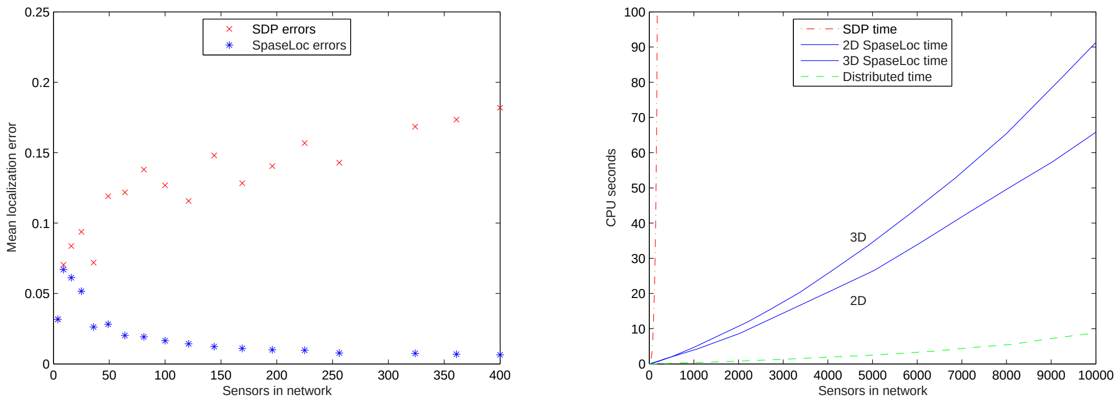

Figure 8.1: Accuracy and performance comparison.

in terms of estimation accuracy for localizing various sizes of networks when sensors are placed at the vertices of an equilateral triangle grid with 0.1 *noise_factor* added to distance measurements (refer to section 3.3.2). It shows clearly that SpaseLoc provides much better positioning accuracy.

The right-hand graph summarizes the localization results in terms of execution time for various sizes of networks. Data for SDP is taken from Table 3.4; data for 2D is taken from Table 3.5; data for 3D is taken from Table 6.1; and data for distributed time is taken from Table 5.6. The figure displays remarkable performance improvement of the proposed algorithms.

The following summarizes our proposed suite of algorithms for various sensor localization applications. Please also refer to Figure 8.2 for the hierarchical algorithm structure.

1. The basic SDP relaxation approach is adopted for solving the subproblems generated by SpaseLoc.

2. SpaseLoc proceeds iteratively by estimating only a portion of the total sensors' locations at each iteration.

   Some anchors and sensors are chosen according to a set of rules to form a (very small) localization *subproblem*. This is solved by the SDP approach, or by auxiliary geometric subroutines.

   The subproblem solution is then returned to the *full problem* and the algorithm iterates again until all sensors are localized.

3. With SpaseLoc in hand, we are able to develop a dynamic sensor localization algorithm to track hundreds or thousands of sensors moving within a larger network

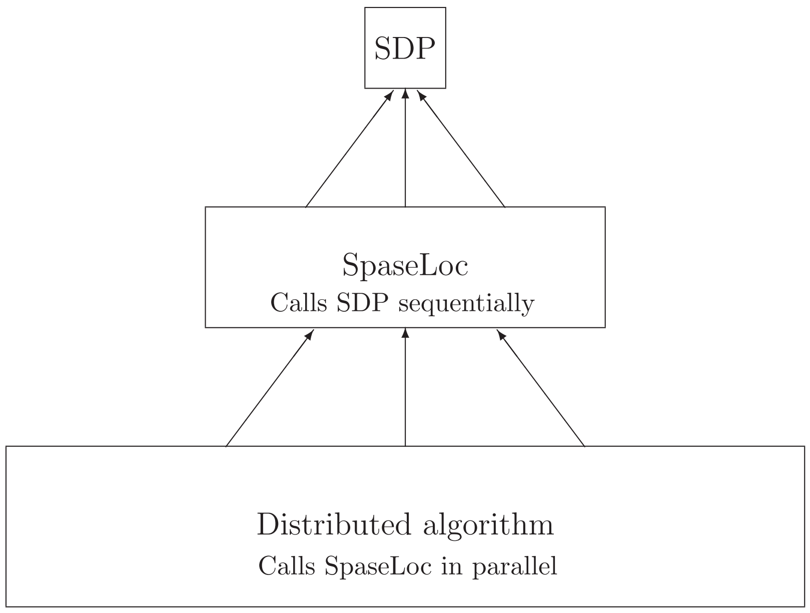

Figure 8.2: Hierarchical algorithm structure.

in real-time. This algorithm utilizes SpaseLoc with extracted data sets that only affect the moving sensors.

4. A priority-driven hierarchical scheme that utilizes distributed computing is developed for large clustered networks. SpaseLoc remains a vital yet intrinsically sequential tool at a lower level. Scalability is achieved through parallelism at the cluster level.

5. A preprocessor for SpaseLoc is developed to localize sensors in anchorless networks.

8.2 Impact of the Research

The proposed sensor localization algorithms (research) transform academic research in the area into usable software deployable in practical sensor networks.

The variety and scale of future network applications begs for software that can fully utilize the multitude of sensor devices currently being created. The broad impact of the research is that it has produced an *enabling technology* analogous to the device technology itself. Efficient and accurate localization for networks of arbitrary size is an *essential requirement* for tomorrow's wireless sensor networks to provide their intended services.

The need is even more imperative when we recognize that the processing power in sensor devices of the near future will be far less than a current Pentium laptop. SpaseLoc is already a major advance for networks up to ten thousands nodes. The distributed algorithm takes a further quantum leap by attaining true scalability and deployability.

8.3 Future Research

We are actively pursuing extensions of the sensor localization algorithms. The following are some promising directions.

Molecular structure identification

In biotechnology, there exist ways to obtain clustered pairwise distance measurements between atoms inside a molecule. The problem then is how to deduce the molecular structure utilizing these known distance measurements, so the molecule's characteristics can be further analyzed. This molecular structure identification problem [47, 48] is very similar in form to the geometric distance model for sensor localization. The protein folding problem [1, 10, 32, 35] and the Euclidean Distance Matrix problem [49, 50] are also closely related. We plan to expand our method to be applicable to these areas.

Cartography

A classical paper by Gauss [16] describes a least-squares approach to constructing a map of Holland using pairwise distance measurements between neighboring villages. This is closely related to the sensor localization problem. The distance matrix is sparse, and the required solution is in 3D (to allow for curvature of the earth). We plan to explore applying our method to this problem.

General version of distributed algorithm

We are currently working on generalizing our distributed approach to arbitrary topologies. In the future, we plan to utilize Stanford's Sweet Hall computer clusters to implement our distributed algorithm to achieve true parallel computing.

Objective function with ℓ_2 norm

This thesis reports results from formulating the sensor localization problem as in (2.1): minimizing the ℓ_1 norm of the squared-distance errors α_{ij} and α_{ik}. The localization problem can also be formulated as a least-squares problem, minimizing the ℓ_2 norm of the errors α_{ij} and α_{ik} subject to the same equality and inequality constraints as in (2.1):

$$\begin{array}{llcll}
\underset{x_i,x_j,\alpha_{ij},\alpha_{ik}}{\text{minimize}} & \displaystyle\sum_{(i,j)\in N_1} \alpha_{ij}^2 + \sum_{(i,k)\in N_2} \alpha_{ik}^2 & & & \\
\text{subject to} & \|x_i - x_j\|^2 - \alpha_{ij} & = & (\widehat{d}_{ij})^2, & \forall\ (i,j) \in N_1, \\
 & \|x_i - a_k\|^2 - \alpha_{ik} & = & (\widehat{d}_{ik})^2, & \forall\ (i,k) \in N_2, \\
 & \|x_i - x_j\|^2 & \geq & r_{ij}^2, & \forall\ (i,j) \in \overline{N}_1, \\
 & \|x_i - a_k\|^2 & \geq & r_{ik}^2, & \forall\ (i,k) \in \overline{N}_2, \\
 & x_i,\ x_j \in \mathcal{R}^2, & & \alpha_{ij},\ \alpha_{ik} \in \mathcal{R}, & \\
 & i,j = 1,\ldots,s, & & k = s+1,\ldots,n. &
\end{array} \tag{8.1}$$

The ℓ_2 norm formulation increases the nonlinearity of the problem. SeDuMi [44] is capable of handling this objective function directly. For DSDP5.0 [3] we could include additional variables and semidefinite constraints of the form $\begin{pmatrix} 1 & \beta_{ij} \\ \beta_{ij} & \alpha_{ij} \end{pmatrix} \succeq 0$.

Lian, Wang, and Ye [26] have studied the least-squares form of the localization problem and its SDP relaxation. They show that the ℓ_2 objective gives a weighted maximum likelihood estimation. This formulation could be used for all of the subproblems solved by SpaseLoc in Chapter 3. A future comparison of the formulations would be of interest.

Porting codes to C

Our localization algorithms are currently implemented in Matlab, with a Mex interface to the SDP solver DSDP5.0 [3] (which is implemented in C). The next step is to convert the Matlab codes to C to facilitate their application to real network implementations.

Conversions between absolute locations and digital map

We use coordinates to represent sensors' locations in our localization algorithms. Some applications may prefer to use a landmark (called a spot) to pinpoint where the sensors are. A spot fitting interface will need to be developed for network applications of this nature. Also, many applications would simply provide a digital map for identifying sensor locations. Conversion of sensors' coordinates into a corresponding spot in the digital map needs further development.

Deployment to real-world applications

We are currently developing collaborations with several companies with the aim of applying our algorithms to real-world applications.

Bibliography

[1] A. Alfakih, A. Khandani, and H. Wolkowicz. *Solving Euclidean distance matrix completion problems via semidefinite programming*, Comput. Optim. Appl., 12(1–3) (1999), pp. 13–30. Computational optimization—a tribute to Olvi Mangasarian, Part I.

[2] P. Bahl and V. N. Padmanabhan. *RADAR: An In-Building RF-Based User Location and Tracking System*, Proceedings of IEEE INFOCOM 2000, Vol. 2, Tel-Aviv, Israel, March 2000, pp. 775–784

[3] S. J. Benson, Y. Ye, and X. Zhang. *DSDP*, http://www-unix.mcs.anl.gov/~benson/ or http://www.stanford.edu/~yyye/Col.html, 1998–2005.

[4] P. Biswas and Y. Ye. *Semidefinite programming for ad hoc wireless sensor network localization*, IPSN 2004, Berkeley, CA, April 26–27, 2004.

[5] P. Biswas and Y. Ye. *A distributed method for solving semidefinite programs arising from ad hoc wireless sensor network localization*, Working Paper, Departments of EE and MS&E, Stanford University, CA, October 30, 2003.

[6] S. Boyd, L. El Ghaoui, E. Feron, and V. Balakrishnan. *Linear Matrix Inequalities in System and Control Theory*, SIAM, Philadelphia, 1994.

[7] N. Bulusu, J. Heidemann, and D. Estrin. *GPS-less low cost outdoor localization for very small devices*, Technical Report 00-729, Computer Science Department, University of Southern California, CA, April 2000.

[8] S. Capkun, M. Hamdi, and J. P. Hubaux. *GPS-free positioning in mobile ad-hoc networks.* Procedings of the 34th Hawaii International Conference on System Sciences, 2001.

[9] A. Cha. *Electronic tracking is finding new uses*, San Jose Mercury News, Sunday, Jan. 16, 2005.

[10] G. M. Crippen and T. F. Havel, *Distance Geometry and Molecular Conformation*, Wiley, New York, 1988.

[11] D. Culler and W. Hong. *Wireless sensor networks.* Communications of the ACM, 47(6), June 2004, pp. 30–33.

[12] L. Doherty, L. El Ghaoui, and K. Pister. *Convex position estimation in wireless sensor networks.* Proc. IEEE Infocom 2001, Anchorage, AK, April 2001, pp. 1655–1663.

[13] A. Dragoon. *Small wonders.* CIO Magazine, January 15, 2005.

[14] W. Drozdiak. *Automotive alternative: In German Port City, cheap, efficient car rentals catch on*, Washington Post, September 20, 1999, p. A09.

[15] D. Ganesan, B. Krishnamachari, A. Woo, D. Culler, D. Estrin, and S. Wicker. *An empirical study of epidemic algorithms in large-scale multihop wireless networks.* Report UCLA/CSD-TR-02-0013, Computer Science Department, UCLA, CA, 2002.

[16] C. F. Gauss. *Gauss's work (1803–1826) on the theory of least squares: an English translation by Hale F. Trotter*, QA 275.G3, 1957.

[17] G. H. Golub and C. F. Van Loan. *Matrix Computations*, The Johns Hopkins University Press, Baltimore, MD, 3rd edition, 1996.

[18] W. B. Heinzelman, A. P. Chandrakasan, and H. Balakrishnan. *An application-specific protocol architecture for wireless microsensor networks*, IEEE Transactions on Wireless Communications, 1(4) (October 2002).

[19] J. Hightower and G. Boriello. *Location systems for ubiquitous computing*, IEEE Computer, 34(8) (2001), pp. 57–66.

[20] A. Howard, M. J. Mataric, and G. S. Sukhatme. *Relaxation on a mesh: a formalism for generalized localization*, in Proc. IEEE/RSJ International Conf. on Intelligent Robots and Systems (IROS01), 2001, pp. 1055–1060.

[21] H. H. Jin, M. W. Carter, M. A. Saunders, and Y. Ye. *SpaseLoc: An adaptive subproblem algorithm for scalable wireless sensor network localization*, SIAM J. on Optimization, submitted December 2004.

[22] H. H. Jin, M. W. Carter, and M. A. Saunders. *Moving sensors localizations*, presented at INFORMS Annual Meeting, Denver, October 23–27, 2004.

[23] H. H. Jin, M. W. Carter, and M. A. Saunders. *Sensors localization in 3D*, presented at SIAM Conference on Optimization, Stockholm, Sweden, May 15–19, 2005.

[24] H. H. Jin, M. W. Carter, and M. A. Saunders. *Distributed algorithm for sensor localization*, presented at IFORS Triennial International Conf., Hawaii, July 11–15, 2005.

[25] H. H. Jin, M. W. Carter, M. A. Saunders, and Y. Ye. *Scalable algorithms for sensor localization*, first-equal prize winner at the Stanford-Berkeley Innovators' Challenge competition, Stanford University, April 19, 2005.

[26] T.-C. Liang, T.-C. Wang, and Y. Ye. *Semidefinite programming relaxation solution for ad hoc wireless sensor network localization*, Technical Report, Stanford University, October 1, 2004.

[27] M. Lawlor. *Small systems, big business*, Signal Magazine, January 2005.

[28] X. Y. Lu. *Coordination layer control and decision making for automated ground vehicles*, Proceedings of the American Control Conf., Anchorage, May 8–10, 2002, pp. 3034–3039.

[29] Matlab 6.5, Release 13 with Service Pack 1. The MathWorks, Inc., Natick, MA, 2003.

[30] A. F. McMillan. *Car sharing's time comes*, CNN Money, July 19, 2000.

[31] D. Moore, J. Leonard, D. Rus, and Seth Teller. *Robust Distributed Network Localization with Noisy Range Measurements*, SenSys04, November 3–5, 2004, Baltimore, Maryland, USA.

[32] J. J. Moré and Z. Wu. *Distance geometry optimization for protein structures*, J. Global Optim., 15(3) (1999), pp. 219–234.

[33] D. Niculescu and B. Nath. *Ad hoc positioning system*, IEEE GlobeCom, November 2001, pp. 2926–2931.

[34] D. Niculescu and B. Nath. *DV based positioning in ad hoc networks*, Kluwer Journal of Telecommunicaton Systems, 2003, pp. 267–280.

[35] R. Reams, G. Chatham, W. Glunt, D. McDonald, and T. Hayden. *Determining protein structure using the distance geometry program apa*, Computers and Chemistry, 23 (1999), pp. 153–163.

[36] A. Ricadela. *Sensors everywhere*, Information Week, January 24, 2005.

[37] C. Savarese, J. Rabaey, and K. Langendoen. *Robust positioning algorithm for distributed ad hoc wireless sensor networks*, in USENIX Technical Annual Conf., Monterey, CA, June 2002.

[38] A. Savvides, C.-C. Han, and M. B. Srivastava. *Dynamic fine-grained localization in ad hoc networks of sensors*, in ACM/IEEE International Conf. on Mobile Computing and Networking (MOBICON), July 2001, pp. 166–179.

[39] A. Savvides, H. Park, and M. B. Srivastava. *The bits and flops of the n-hop multilateration primitive for node localization problems*, in 1st ACM International Workshop on Wireless Sensor Networks and Applications (WSNA'02), Atlanta, GA, 2002, ACM Press, pp. 112–121.

[40] Y. Shang, W. Ruml, Y. Zhang, and M. Fromherz. *Localization from mere connectivity*, MobiHoc 2003, Anapolis, MD, June 2003, ACM Press.

[41] S. Shladover, and P. Ioannou. *Reasons for operating AHS vehicles in platoons*, Automated Highway Systems, Klumer Academic/Plenum Publishers, New York, 1997, pp. 11–28.

[42] J. P. Singh, N. Bambos, B. Srinivasan, and D. Clawin. *Wireless LAN performance under varied stress conditions in vehicular traffic scenarios*, Technical Report, Department of Electrical Engineering, Stanford University, CA, and Robert Bosch Coorporation, Research and Technology Center, Palo Alto, CA.

[43] A. So and Y. Ye. *Theory of semidefinite programming for sensor network localization*, Stanford University, CA, 2004, to appear in SODA 2005.

[44] J. F. Sturm. *Let SeDuMi seduce you*, http://fewcal.kub.nl/sturm/software/sedumi.html, October 2001.

[45] R. Szewczyk, E. Osterweil, J. Polastre, M. Hamilton, A. Mainwaring, and D. Estrin. *Habitat monitoring with sensor networks.* Communications of the ACM, 47(6), June 2004, pp. 34–44.

[46] P. Tseng. *SOCP relaxation for nonconvex optimization*, presented at ICCOPT 1, RPI, Troy, NY, August 2–5, 2004.

[47] G. A. Williams, J. M. Dugan, and R. B. Altman, *Constrained global optimization for estimating molecular structure from atomic distances*, J. Computational Biology, 8 (2001), pp. 523-547.

[48] D. Wu and Z. Wu, *An updated geometric build-up algorithm for molecular distance geometry problems with sparse distance data*, preprint, University of Iowa, 2005.

[49] F. Z. Zhang. *On the best Euclidean fit to a distance matrix*, Beijing Shifan Daxue Xuebao, 4 (1987), pp. 21–24.

[50] Z. Zou, R. H. Byrd, and R. B. Schnabel. *A stochastic/perturbation global optimization algorithm for distance geometry problems*, Technical Report, Dept. of Computer Science, University of Colorado, Boulder, CO, 1996.